

AD-A082 360

ITT ELECTRO-OPTICAL PRODUCTS DIV ROANOKE VA
FIBER OPTIC COUPLERS.(U)

F/G 20/6

JUL 79 G W BICKEL, L E FOLTZER, G A RINES

F33615-78-C-1448

UNCLASSIFIED

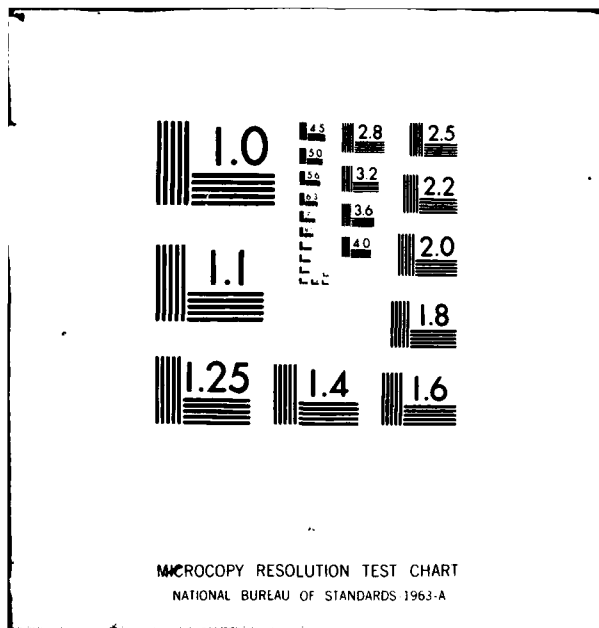
AFAL-TR-79-1140

NL

1-3

20/6







UNCLASSIFIED

SECURITY CLASSIFICATION OF THIS PAGE (When Data Entered)

REPORT DOCUMENTATION PAGE		READ INSTRUCTIONS BEFORE COMPLETING FORM
1. REPORT NUMBER (18) AFAL-TR-79-1149	2. GOVT ACCESSION NO.	3. RECIPIENT'S CATALOG NUMBER
4. TITLE (and Subtitle) (6) FIBER OPTIC COUPLERS		5. TYPE OF REPORT & PERIOD COVERED (9) Final Report, 17 Apr 78-14 May 79 April 17, 1978-May 16, 1979
7. AUTHOR(s) (10) G.W. Bickel, L.E. Foltzer, G.A. Rines, J. A.R. Nelson		6. PERFORMING ORG. REPORT NUMBER
8. PERFORMING ORGANIZATION NAME AND ADDRESS (ART) ITT ELECTRO-OPTICAL PRODUCTS DIVISION 7635 Plantation Road Roanoke, VA 24019		8. CONTRACT OR GRANT NUMBER(s) (15) F33615-78-C-1448
11. CONTROLLING OFFICE NAME AND ADDRESS Avionics Laboratory (AFWAL/AADO) Wright Aeronautical Laboratories Wright-Patterson AFB, Ohio 45433		10. PROGRAM ELEMENT, PROJECT, TASK AREA & WORK UNIT NUMBERS 62204F; 2001 02 64 (11) 02
14. MONITORING AGENCY NAME & ADDRESS (if different from Controlling Office)		12. REPORT DATE (11) July 1979 (12) 208
		13. NUMBER OF PAGES 207
		15. SECURITY CLASS. (of this report) UNCLASSIFIED
		15a. DECLASSIFICATION/DOWNGRADING SCHEDULE
16. DISTRIBUTION STATEMENT (of this Report) Approved for public release; distribution unlimited.		
17. DISTRIBUTION STATEMENT (of the abstract entered in Block 20, if different from Report) G		
18. SUPPLEMENTARY NOTES		
19. KEY WORDS (Continue on reverse side if necessary and identify by block number) Optical Fiber Couplers Multimode Coupler Fiber Optic Data Bus Plastic Clad Silica Directional Couplers Acoustic-Optic Direct Fiber Fusion "T" Couplers Electro-Optic Area Ration Splitters Transmission Stars Electro-Absorption Active Couplers Reflection Stars Franz-Keldysh Modulators Switches		
20. ABSTRACT (Continue on reverse side if necessary and identify by block number) This report is the final report on a one-year technology development program for active and passive fiber optic coupler components. The passive coupler effort consisted primarily of the development of packaging method for coupler type developed previously under contract #F33615-77-C-1058. The active coupler effort explored techniques of obtaining active switching and modulation for multimode data bus applications.		

DD FORM 1 JAN 73 1473

EDITION OF 1 NOV 65 IS OBSOLETE

UNCLASSIFIED

SECURITY CLASSIFICATION OF THIS PAGE (When Data Entered)

189750

JOL

Block 20 (Continued)

The packages developed for the directional and "T" couplers incorporated a "v" groove connector concept as part of the package. The packaging technique used for the star couplers consisted of a subpackage, that housed the coupler, that was mounted in an external package to provide the mounting surface for the multiway connectors.

Packaged couplers were successfully subjected to environmental stresses in accordance with the requirements of MIL-E-5400.

In order to support the devices adequately with their packages, special cladding techniques were used to preserve the waveguiding properties of the couplers. These techniques did, however, have an affect on the optical performance of the packaged devices.

The active coupler tasks examined a variety of concepts that appeared promising for switching and modulation of multimode light. Three techniques, Acousto-optic (A-O), Electro-optic (E-O), and the Electro-absorption (Franz-Keldysh, FK) effects were selected for further investigation. Experiments with the A-O and F-K effects were conducted and conclusions drawn from the results.

It was determined that the E-O and A-O techniques are reasonable candidates for multimode switches and modulators. The F-K effect, however, appears suitable primarily for single mode applications.

Accession For	
NTIS	<input checked="" type="checkbox"/>
DDC TAB	<input type="checkbox"/>
Unannounced	<input type="checkbox"/>
Justification	<input type="checkbox"/>
By _____	
Distribution/	
Availability Codes	
Dist	Avail and/or special
A	

FOREWORD

This final report summarizes the twelve months of work performed on Air Force Contract F33615-78-C-1448 entitled, "Fiber Optic Couplers." This work was performed from April 17, 1978 to May 16, 1979. This report was prepared by the Electro-Optical Products Division of ITT and describes work performed by Mr. Lawrence Foltzer, Dr. Art Nelson and Mr. Glen Rines.

The work performed under this contract is administered by the Air Force Avionics Laboratory, Air Force Systems Command, Wright-Patterson Air Force Base, Ohio. Mr. E.R. Nichols (AFAL/DHO) is the technical representative for the Avionics Laboratory. This report was submitted by the authors in August 1979.

"Preferentially Etched Diffraction Gratings in Silicon" by Won-Tien Tsang and Shyh Wang from the Journal of Applied Physics, Vol. 45 No. 5 and "Accurate Silicon Spacer Chips for an Optical Fiber Connector" by C.M. Schroeder, Bell System Technical Journal are reprinted as references in Appendix C. Permission to reprint these articles from the American Inst. of Physics, copyright 1975, and the Bell System Technical Journal, copyright 1978, the American Telephone and Telegraph Co., are gratefully acknowledged.

TABLE OF CONTENTS

<u>SECTION</u>	<u>TITLE</u>	<u>PAGE</u>
I	INTRODUCTION AND BACKGROUND	1
1.0	Background	4
II	ENVIRONMENTAL REQUIREMENTS AND TESTING	10
1.0	Requirements	10
2.0	Tests and Results	11
III	PACKAGING CONCEPTS	22
1.0	Coupler Strain Relief	22
2.0	Integral Connector Design	28
3.0	Vibrational Package Design Considerations	43
IV	PACKAGING MATERIALS	46
V	PACKAGE AND COUPLER INTEGRATION	51
1.0	Coupler to Package Bonding and Package Sealing	52
1.1	Metallic Sealing Approaches	52
1.2	Epoxy Bonding Agents	55
2.0	Refinement of Silvering Process	57
2.1	Approach 1	58
2.2	Approach 2	59
2.3	Approach 3	60
3.0	Plastic Cladding Considerations	63
VI	DIRECTIONAL COUPLERS	64
1.0	Technique Improvement	64
2.0	Coupling Designs	68
3.0	Brassboard Directional Coupler Data	68
VII	"T" COUPLERS	75
1.0	Package Design	83
2.0	Special Considerations for Tap-off Designs	85
3.0	Brassboard "T" Coupler Data	87

TABLE OF CONTENTS (Continued)

<u>SECTION</u>	<u>TITLE</u>	<u>PAGE</u>
VIII	TRANSMISSION STAR COUPLERS	91
1.0	Fusion Technique Improvement	91
2.0	Star Coupler Fabrication Procedure	93
3.0	External Packaging	102
4.0	Brassboard Models	105
IX	ACTIVE COUPLERS	113
1.0	Acousto-optic Interaction	115
1.1	Theory	115
1.2	Predicted Performance	121
1.2.1	Static Insertion Loss	127
1.2.2	Loss in Switched State	129
1.2.3	Contrast Ratio	131
1.2.4	Speed	131
1.2.5	Operating Wavelength	132
1.2.6	Size	132
1.3	Experimental Results	132
2.0	Franz-Keldysh Effect	140
2.1	Theory	140
2.2	Experimental Results	148
3.0	Electro-optic Devices	153
3.1	Electro-optic Coupler No. 1	154
3.2	Electro-optic Coupler No. 2	158
X	CONCLUSIONS AND RECOMMENDATIONS	162
1.0	Passive Couplers - Conclusions	162
2.0	Passive Couplers - Recommendations	166
3.0	Active Couplers - Conclusions	169
4.0	Active Couplers - Recommendations	172
APPENDIXES		
A	MODIFIED FIBER SILVERING PROCESS	173
B	TERMINATION OF PCS FIBERS USING PLASTIC CLADDING MATERIALS	183
C	REFERENCES ON V-GROOVE ETCHING	188

LIST OF ILLUSTRATIONS

<u>FIGURE</u>	<u>TITLE</u>	<u>PAGE</u>
1	MIL-E-5400 Vibration Graph	12
2	Vibration Test With Optical Monitoring	17
3	Temperature Test of Seven-port Star Coupler	20
4	Directional Coupler With Detachable Pigtailed	26
5	"T" Coupler with Detachable Pigtailed	27
6	Directional Coupler Package Mechanical Drawing	30
7	"T" Coupler Package Mechanical Drawing	32
8	Preferred Star Coupler Package Approach	34
9	Oxide Growth Apparatus	37
10	First Mask Design on Silicon	38
11	Edge on Views of Assembled "V" Groove Connector	40
12	Hughes Multiway Connector	42
13	Fused Biconical Taper Coupler	66
14	"T" Configuration	76
15	"T" Coupler Performance	79
16	Photograph of "T" Coupler	81
17	Throughput vs Bend Radius	84
18	Stacking Block for Star Couplers	95
19	Lid for Star Couplers	96
20	Main Channel of Internal Star Coupler Package	97
21	Star Coupler Fabrication Steps	99
22	Cross-sectional View of Fiber Stacks	100
23	Hughes Ferrule Modification	104
24	Photograph of Completed Star Couplers	106
25	Geometry of Input and Output of Acoustic-optic (A-O) Device	118
26	Variation of Intensity in A-O Modulator	120
27	Intensity Variation vs Bragg Angle Error	122
28	Configuration of Switch or Modulator	123
29	Modulator/detector For "Bit Deletion" Data Bus	144
30	Franz-Keldysh Results	151
31	Electro-optic Coupler No. 1	155
32	Electro-optic Coupler No. 2	159

LIST OF TABLES

<u>TABLE</u>	<u>TITLE</u>	<u>PAGE</u>
1	Summary of Previous Program Results	6
2	Coupler Performance Predictions	7
3	Environmental Conditions	13
4	Environmental Tests Performed on Couplers	15
5	Thermal Expansion Properties of Packaging Material Candidates	47
6	Masking Materials	61
7	Fiber Size Requirements for Directional Couplers	69
8	-3 dB Directional Coupler	71
9	Directional Coupler Performance - (10 dB)	72
10	Directional Coupler Performance - (20 dB)	73
11	Fiber Size Requirements for "T" Couplers	77
12	Three dB "T" Performance	88
13	Five dB "T" Performance	89
14	Ten dB "T" Performance	90
15	Elongated Seven-port Star Coupler Data	94
16	Seven-port Star Coupler Performance Output Ports	107
17	Nineteen-port Star Coupler Performance	108
18	Backscatter Data Seven-port Star (Delivered Device)	111
19	Model 1206-1 Specification Sheet	125
20	Performance of Modulator with He-Ne Laser	133
21	Results of A-O Device	139
22	Broadening of GaAs Band Edge	142

SECTION I

INTRODUCTION AND BACKGROUND

This report is the final report of a one year technology development effort on coupling devices for fiber optic data bus systems. Specifically, the work reported on here was an extension of the effort previously funded under Contract Number F33615-77-C-1058. The present program effort was to further improve device performance and to develop packaging methods for coupler components suitable for aircraft applications. In addition, this program also investigated active coupling mechanisms to determine their potential for use in multimode fiber applications. This work was performed under Contract Number F33615-78-C-1448 from the Air Force Avionics Laboratory at Wright-Patterson Air Force Base.

The packaging techniques developed under this program were for three types of plastic clad silica (PCS) single fiber couplers. These are (1) directional couplers, (2) "T" couplers, and (3) transmission star couplers. These couplers were fabricated by direct fiber fusion. The packaging

concepts investigated were designed to aid in the fabrication of the devices, provide mechanical support to the coupler elements, and isolate the devices from externally applied mechanical and environmental stresses.

The active coupler portion of this program consisted of three phases. These were (1) a study phase to determine potentially useful coupling mechanisms, (2) an experimental phase to verify the concepts, and (3) a fabrication phase in which a device with promising characteristics will be fabricated and evaluated.

Sections II through VII of this report deal with the passive data bus couplers while Section IX reports on the active coupler work. These sections are outlined in further detail below.

In Section II of this report, the environmental performance requirements for data bus couplers are outlined. Section II also describes the measurement apparatus and techniques used to test the couplers under various environmental conditions.

Sections III and IV discuss the packaging issues with reference to the particular requirements of the coupler types developed under the previous program. Section III deals specifically with the packaging concepts and form factors, and Section IV deals with the materials issues and environmental and process compatibility.

Section V describes in detail the various methods that were investigated to preserve the low loss transmission characteristics of the terminated PCS fiber ends. Although basically this is a problem of materials compatibility, it is treated in a separate section to highlight its importance and influence on the couplers optical performance.

Sections VI, VII and VIII deal with the three (3) specific coupler types developed during this program, the directional, "T," and transmission stars respectively. The performance data for each of the brassboard deliverables is included in the appropriate sections.

Section IX describes the active coupler effort and results obtained. This effort was primarily one of studying potential multimode active coupler principles, selecting a few with the greatest potential of performance, and conducting experiments to determine the pertinent performance data.

1.0 Background

The general background leading to the present program for the development of data bus couplers and active couplers is presented in this section on data bus couplers. The results of the previous program to develop data bus couplers are summarized here to provide the general background behind the approaches and concepts investigated during this program.

The previous program (Contract No F33615-77-C-1058) demonstrated that the direct fusion approach to coupler fabrication was capable of producing directional and transmissive star couplers with excess loss equal to or less than that achieved with competing technologies. In addition, certain limitations of the technology and

special handling requirements were determined. Table 1 indicates the results of the previous program. As the program progressed, and the fabrication techniques were refined, the sources of the coupler excess loss were understood, coupler performance improved and performance predictions for some of the coupler types were possible. Table 2 summarizes the predictions of coupler loss made after the program was completed.

As indicated in Table 1, with the possible exception of the "T" couplers, the issues of mechanical strength and thermal limitations needed to be addressed for these devices to be used in systems with reliability.

The overall structural weakness of the fused couplers was seen as the overriding problem to be solved prior to implementing the fused PCS coupler technology in real systems. In addition, the problems seemed to be inherent to the fusion process and no successful method was found to prevent its occurrence. However, the potential benefits

Table 1

Summary of Previous Program Results.

	Coupler Type			
	Directional	"T"	Star	
	-3 dB	High Tap-offs	3 dB	High Tap-offs
	7	19	32	
<u>Optical</u>				
Excess Loss	<- .5 dB	<-1.0 dB	>-5 dB	<3 <6 <8
Backscatter	<-28 dB	<-28 dB		
<u>Mechanical Strength</u>				
Isolation from External Forces	Weak			
	Poor			
Thermal				
	Susceptible to breakage due to package expansion coefficient.			
<u>Other</u>				
	Severe sensitivity of excess loss due to preferential mode coupling	Very difficult to achieve low loss reflection devices		

Table 2
Coupler Performance Predictions.

Directional -3 dB	High Tap-offs	"T"	Star (Xmissive)	
			7 Ports	19 Ports
Excess Loss			Excess Loss	
-0.2 to -0.5 dB	- .5 dB	Unknown	-2.0 dB	-4.0 dB
Backscatter			Uniformity	
<-30 dB	<-30 dB		±1 dB	±1.5 dB

of this technology, low loss and relative immunity to radiation, warranted investigation of alternative methods of protecting the coupler elements from mechanical or environmental damage.

The differential thermal expansion between the coupler element and the package was one of the areas where it was felt that considerable improvement could be made with the appropriate selection of materials.

Couplers developed during the first program were also subject to failure from tensile and shear stresses that were transferred to the fragile coupler element due to the highly compliant nature of the cladding materials used for PCS fibers. The proposed solution to this problem was to develop a method of restricting stress transfer from the coupler fiber pigtails to the coupler element or to provide some other method of isolation.

Sections II, III, IV and V of this report describe in detail the packaging concepts investigated and developed during this program.

Section IX of this report covers the active coupler portion of the program. In general, the availability of active couplers as a component would greatly increase the versatility of data bus systems through more flexible architectural configurations and protocol. One of the more commonly known forms of bus structures that could take advantage of active coupler devices is the bit-deletion type of ring bus. Potential advantages of this approach include (1) reduction in power loss at the nodes of the ring (coupler in off-state) with respect to a passive device that would always tap-off a portion of the incident power, (2) improved bus reliability since only a single source of optical power would be required in some architectures, and (3) it also appears feasible that some active coupler forms could serve dual roles as both detectors and modulators.

SECTION II

ENVIRONMENTAL REQUIREMENTS AND TESTING

The use of optical fiber data bus systems in airborne applications places severe environmental requirements on the data bus coupler components. This section discusses first the requirements placed on the couplers fabricated under this program and second the specific tests performed and their results.

1.0 Requirements

In order to establish a set of reasonable requirements for the optical hardware to be produced in this program, the MIL-E-5400 standards were used as a reference. The environmental conditions addressed were vibration, temperature and humidity. These tests were considered to be the most demanding with respect to potential weaknesses of packaged PCS optical couplers.

The vibration requirement was drawn from the MIL-E-5400 specification for equipment designed for installation in jet

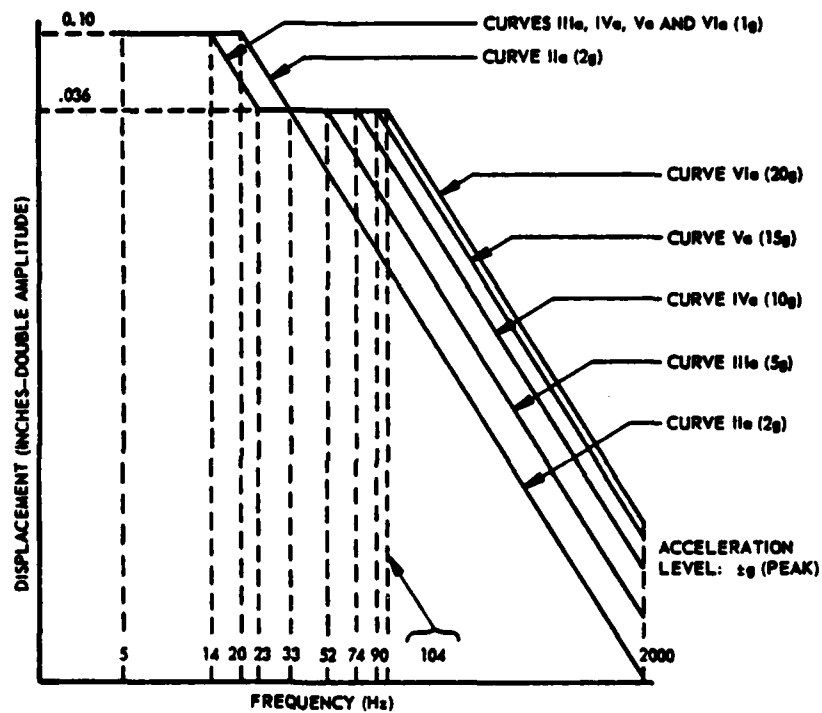
airplanes as shown in Figure 1. As optical components would be normally mounted with vibration isolators, Curve IIa of the graph must be satisfied. This was the first test requirement imposed on the couplers vibrationally. In order to demonstrate a greater margin of operation, a more severe test was also imposed. This test corresponded to Curve IIIa of Figure 1.

The temperature environment requirements were drawn from the Class 2 specifications as shown in Table 3.

The humidity requirement was imposed to demonstrate the package sealing integrity during exposure to moisture. The specific test conducted and its results are described in the tests and results subsection.

2.0 Tests and Results

The tests performed under this program are outlined in Table 2. This discussion will address each type of test separately.



CURVE Ie (OF PREVIOUS ISSUES) - REPLACED BY CURVE IVe
 CURVE IIe - EQUIPMENT DESIGNED FOR OPERATION ON ISOLATORS WITH ISOLATORS REMOVED
 CURVE IIIe - EQUIPMENT MOUNTED IN FORWARD HALF OF FUSELAGE OR IN WING AREA WITH ENGINES AT REAR OF FUSELAGE
 CURVE IVe - EQUIPMENT MOUNTED IN REAR HALF OF FUSELAGE OR IN WING AREA WITH WING OR FRONT MOUNTED ENGINES
 CURVE Ve - EQUIPMENT MOUNTED IN ENGINE COMPARTMENT OR ENGINE PYLON
 CURVE VIe - EQUIPMENT MOUNTED DIRECTLY ON ENGINE

Figure 1. MIL-E-5400 Vibration Graph.

Table 3
Environmental Conditions.

Equipment operating										Equipment nonoperating	
Temperature extremes for the chamber (without external cooling provisions)				Combined temperature-altitude			Temperature shock	Altitude	Temperature extremes	Temperature shock	
Equipment class	Column I continuous	Column II intermittent	Column III short-time	Column IV	Column V	Column VI	Column VII	Column VIII	Column IX	Column X	
Class 1	-44° C +55° C	30 min. +71° C	---	Defined by curve A, figure 3, (sheet 1)	Defined by curve B, figure 3, (sheet 1)	---	-44° C to +71° C	Sea level (30.0 in. Hg.) to 30,000 ft. (9.33 in. Hg.)	-42° C to +85° C	-42° C to +85° C	
Class 1A	-44° C +65° C	30 min. +71° C	---	Defined by curve A, figure 3, (sheet 1)	Defined by curve B, figure 3, (sheet 1)	---	-44° C to +71° C	Sea level (30.0 in. Hg.) to 30,000 ft. (9.33 in. Hg.)	-42° C to +85° C	-42° C to +85° C	
Class 1B	-40° C +65° C	30 min. +71° C	---	Defined by curve A, figure 3, (sheet 1)	Defined by curve B, figure 3, (sheet 1)	---	-40° C to +71° C	Sea level (30.0 in. Hg.) to 15,000 ft. (16.00 in. Hg.)	-42° C to +85° C	-42° C to +85° C	
Class 2	-44° C +71° C	30 min. +95° C	---	Defined by curve A, figure 3, (sheet 2)	Defined by curve B, figure 3, (sheet 2)	---	-44° C to +95° C	Sea level (30.0 in. Hg.) to 70,000 ft. (1.32 in. Hg.)	-42° C to +95° C	-42° C to +95° C	
Class 3	-44° C +95° C	30 min. +125° C	10 min. +150° C	Defined by curve A, figure 3, (sheet 3)	Defined by curve B, figure 3, (sheet 3)	Defined by curve C, figure 3, (sheet 3)	-44° C to +125° C	Sea level (30.0 in. Hg.) to 100,000 ft. (0.32 in. Hg.)	-42° C to +125° C	-42° C to +125° C	
Class 4	-44° C +125° C	30 min. +150° C	10 min. +200° C	Defined by curve A, figure 3, (sheet 4)	Defined by curve B, figure 3, (sheet 4)	Defined by curve C, figure 3, (sheet 4)	-44° C to +150° C	Sea level (30.0 in. Hg.) to 100,000 ft. (0.32 in. Hg.)	-42° C to +150° C	-42° C to +150° C	

* 1/ Altitude range shown is for operation only.
Classes 1A and 1B equipment shall withstand a nonoperating altitude of 40,000 feet (5.5 in. Hg.).

The vibration testing was conducted in two phases. Early in the program a packaged 3 dB directional coupler and a packaged seven-port star coupler were vibrated without optical monitoring as a preliminary analysis of the soundness of the package design. Later, the more fragile 10 dB "T" coupler and a seven-port star coupler were vibrated with optical monitoring to demonstrate their operational ability in a vibration environment.

For the preliminary test, the couplers were examined before and after the test under a microscope with 40X magnification. There was no observable degradation of either the directional or the star coupler after either test. These results confirmed the soundness of the package design and allowed continuation of the package integration phase.

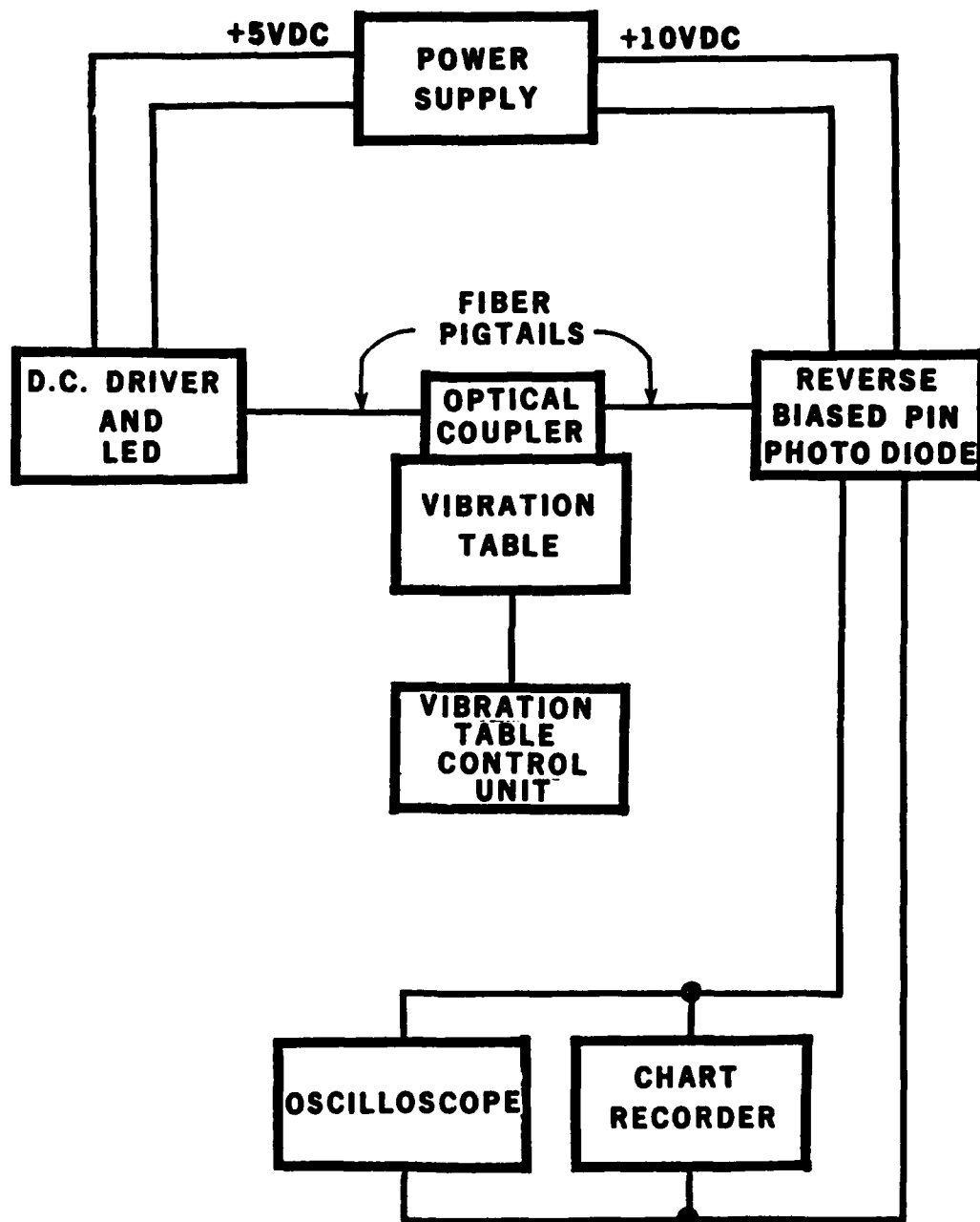
At the end of the package integration phase, two sample packages were vibrated at the same levels (Table 4) and were optically monitored during the test. The test apparatus used is diagrammed in Figure 2. An oscilloscope and a chart recorder

Table 4
Environmental Tests Performed on Couplers.

Type of Test	Test Conditions		Measurement Conditions	Results
Preliminary vibration test on directional and star couplers	5-2000-5 Hz 20 min log cycle, 5-20 Hz .1" double amplitude constant displacement, 20-2000 Hz 2 g constant acceleration		Visual inspection before and after test using 40X magnification	Both 3 dB directional and seven-port star survived
Preliminary vibration test on directional and star couplers	5-2000-5 Hz 6 min log cycle, 5-20 Hz .2" double amplitude constant displacement, 20-2000 Hz 5 g constant acceleration		Visual inspection before and after test using 40X magnification	Both 3 dB directional and seven-port star survived
Temperature test to ensure compatibility of materials in package design for directional and star couplers	TEMPERATURE CHANGE	ELAPSED TIME	Visual inspection before and after test using 40X magnification	Both 3 dB directional and seven-port star survived
	25° to -62°C const. -62°C -62°C to +95°C const. +95°C +95°C to -25°C	45 min 30 min 30 min 30 min 30 min		

Table 4
Environmental Tests Performed on Couplers (Continued).

Type of Test	Test Conditions	Measurement Conditions		Results
		TEMPERATURE CHANGE	TIME ELAPSED	
Operational vibration test on "T" and star coupler designs	Two complete cycles: (5-2000-5 Hz 8 min log cycle) 5-18 Hz .2" double amplitude, constant displacement 18-2000 Hz 5 g constant acceleration			No measurable degradation at any point during or after test cycles
Humidity test for Invar/Torr-seal package (seven-port star coupler tested)	Coupler confined to glass container with water reservoir	25°C to 95°C +95°C to -10°C 95°C 95°C to -10°C	20 min 60 min 18 h 60 min	Optical monitoring throughout test cycle (See Figure 2).



302 12129

Figure 2. Vibration Test With Optical Monitoring.

were connected in parallel to the output of the receiver module. The chart recorder provided a hard copy of the average optical power while the oscilloscope provided visual monitoring of any dynamic fluctuations at the vibration frequency or its harmonics.

These couplers survived both the 2 g (Figure 1 Curve IIa) and the 5 g (Figure 1 Curve IIIa) test cycle without any measurable degradation in optical performance with respect to both the average and the dynamic monitoring.

There have been a number of vibration tests performed on optical components at EOPD for other programs. The results of these tests support the results of the testing under this program. Specifically, they indicate that couplers of these designs will withstand the vibrations level specified in Figure 1 Curve IVa (10 g).

At the 15 g level (Figure 1 Curve Va) dynamic modulation is seen in the optical signal if the connecting fiber pigtails are not restrained.

The temperature testing was divided into two phases along with the vibration testing as described above. The same two couplers, a 3 dB directional and a seven-port star coupler, were temperature cycled as described in Table 4. These couplers were visually examined before and after the testing using a microscope with 40X magnification. Both survived the test without incurring physical damage. This demonstrated the compatibility of the Invar package and the silica coupler with respect to thermal expansion and allowed continuation of the package integration phase without further package design modification.

After the completion of the package integration phase, more temperature testing was conducted and optical monitoring was employed in this phase. Figure 3 shows the results of this test which took place over a period of about six hours. The attenuation of the optical signal as a function of decreasing temperature can be clearly attributed to the PCS pigtailed rather than to the coupler package itself. The optical signal returned to its original level as the coupler and pigtailed returned to room temperature.

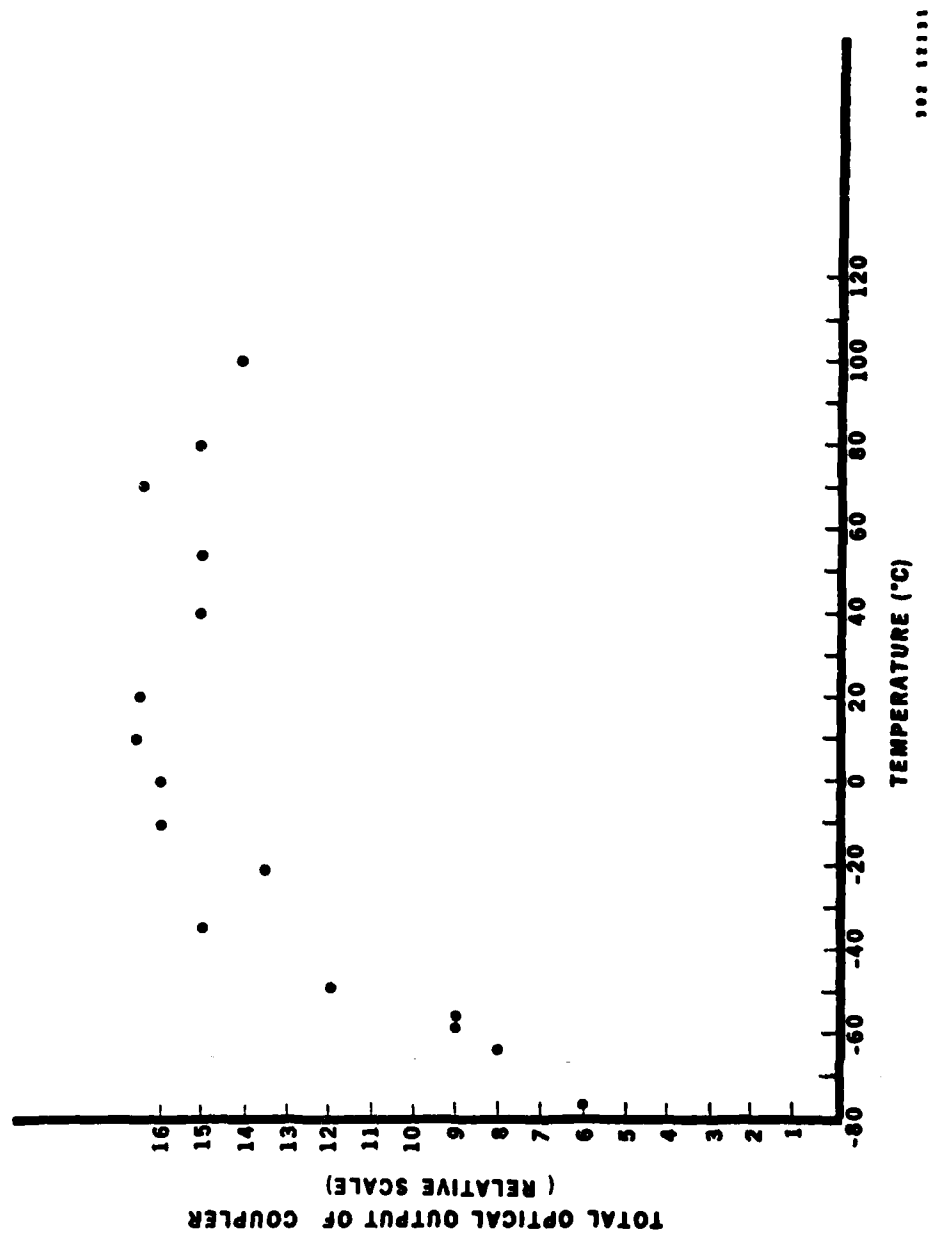


Figure 3. Temperature Test of Seven-port Star Coupler.

The coupler did not fracture during the temperature cycling. The attenuation seen is due to the change of the refractive index of the plastic cladding on the pigtails with temperature. As the temperature decreases, the refractive index of the cladding increases, thus restricting the numerical aperture of the fiber pigtail. When the refractive index increases to and beyond that of the silica core, the waveguide properties are completely lost. This is an inherent limitation of PCS fibers clad with silicone rubber.

The final test performed was a humidity test. The coupler tested was optically monitored and quantitative results were recorded. The actual humidity conditions imposed were of a more qualitative nature. The coupler experienced a temperature range of -10°C to $+95^{\circ}\text{C}$ with a high enough moisture level to maintain condensation (water droplets or ice) on the coupler package throughout the temperature range. Under these conditions, no measurable change in optical performance was seen.

SECTION III

PACKAGING CONCEPTS

The most important objective of this program was to explore and develop packaging concepts for the couplers developed on the previous program. Due to the fragile nature of the coupler structures, resulting from the fusion process, the package designs were required to provide mechanical support to the couplers, isolation from externally derived forces that could be transmitted to the coupler via the pigtail lead, and provide a good thermal expansion coefficient match between the package and coupler. These requirements were determined as a result of the previous program efforts which isolated the coupler failure mechanisms and causes.

This section deals with the selection of the most appropriate packaging concepts for the different coupler types. Section IV of this report covers the material selection issues.

1.0 Coupler Strain Relief

Section I highlighted the primary coupler failure mechanisms. One of these was due to stress transfer to the coupler element from the connecting pigtail fiber by which optical access to the device is gained. It was found that coupler

failure resulted when only moderate tensile loads were applied to the pigtails and that these forces were representative of normal handling condition loads. In addition, failure would also occur simply by displacing the fiber pigtails from side to side close to the coupler package.

The coupler mounting techniques that were employed for these devices was one of bonding the cladded and jacketed fibers to mounting platforms at each end of the package using an epoxy adhesive. Although the actual bonding length was approximately 1.5 cm, and the total diameter of the jacketed fiber was $\frac{1}{2}$ mm, sufficient strain relief was not obtained.

The basic problem with this approach was due to the essentially nonelastic properties (or stiffness) of the optical fiber, relative to the highly compliant nature of the cladding and jacketing materials used. Close inspection, under a microscope, indicated substantial movement of the fibers leading to the coupler on the inside of the package as a result of moderate external forces. In almost all cases, the fragile coupler transition regions would break as a result of external forces on the pigtails. From this experience, it was evident that a technique must be developed

to allow the fibers to be hard bonded to the package structure to prevent or minimize external stress transfer, and thus have reasonable assurance that the devices will survive normal handling conditions.

As a secondary issue, it is also apparent if one is to bond to the fibers either directly or indirectly to achieve stress relief, that a question of materials compatibility exists with respect to the preservation of the waveguiding characteristics of the fibers. Section V of this report, "Waveguide Preservation," covers this topic in detail.

There are two potential forms that the coupler can take, each with its own particular merits and both providing stress isolation. The first of these is a pigtailed device. One of the desirable features of the pigtailed coupler is that one can either splice the unit directly into a system, eliminating the need for connectors or install connectors if desired. In all likelihood, however, if connectors are installed, the coupler will be repackaged to protect the pigtails and to provide a mounting surface for the connectors. One disadvantage of the pigtailed coupler

approach is that if one of the pigtails is broken close to the coupler package, the device may not be recoverable and have to be discarded. The pigtailed coupler has other disadvantages, a stand-alone coupler with connectors and external package not only impacts the cost of the device but substantially increases the size and weight of the device, an undesirable feature for aircraft applications.

The primary packaging concept that was explored and developed during this program can be characterized as a hybrid form of the pigtailed coupler, however, it has also been referred to as the integral connector/package concept. Devices of this type are shown in Figures 4 and 5. The pigtail fibers interfacing to the coupler in this design are detachable and may be repaired by retermination if damaged. It is also feasible to mount the small coupler package as a stand-alone device within a piece of hardware, terminate the attachment fibers from a cable, another piece of hardware or device and plug-in to the coupler. This approach eliminates the need for splices or connectors and keeps the package size within reason. External stress isolation is also inherent to this design concept.

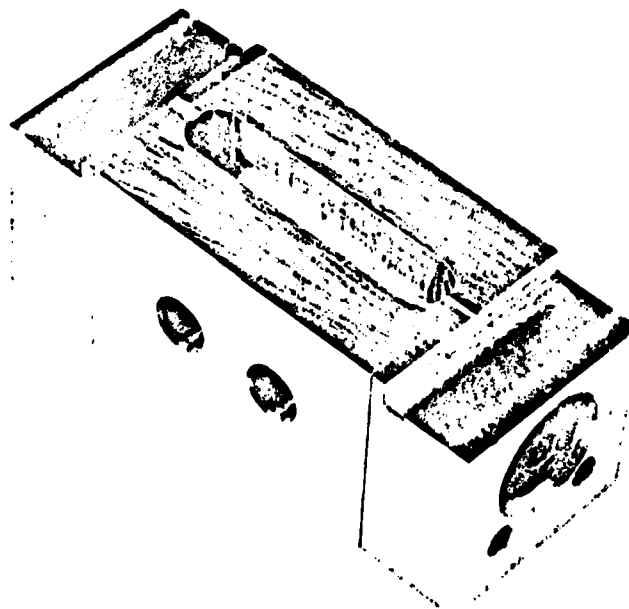


Figure 4. Directional Coupler With Detachable Pigtails.



Figure 5. "T" Coupler with Detachable Pigtails.

Another advantage of this approach is in the actual fabrication of the coupler elements. The design of fixturing required to hold the fibers during fusion process is less complicated since the lengths of the fibers involved is only about 10 to 15 centimeters. With short fiber lengths, the fibers could be easily mounted without the torsional loads that result when using long fiber lengths as required to fabricate a pigtailed coupler.

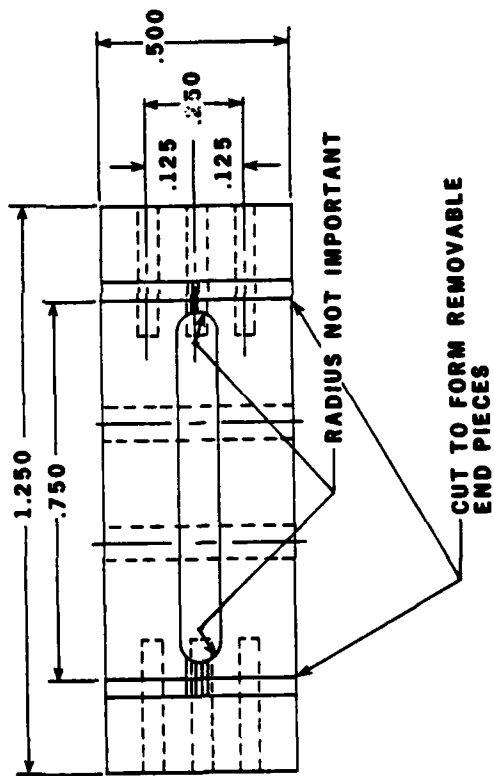
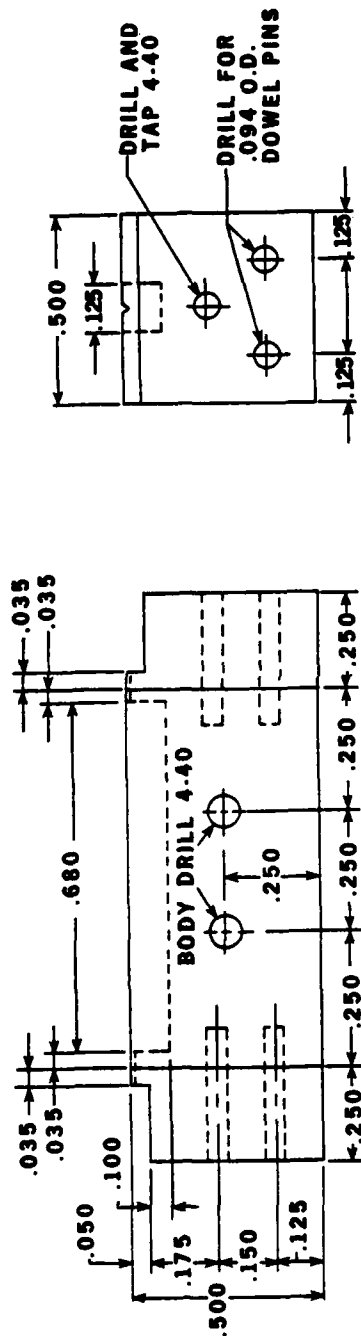
2.0 Integral Connector Design

The package designs shown in Figures 4 and 5 represent those used in this program for the brassboard models of the directional and "T" couplers. For these coupler types, the design of the integral connector is straightforward. The fabrication approach selected was to machine "V" groove for the fibers in the pigtail attachment pieces and coupler package as a single-assembled unit. Alignment pins in the ends of the packages ensure that the alignment between the pigtail attachment pieces and coupler package are maintained during and after the machining of the grooves. To achieve a small radius of curvature in the bottom of the groove, a sharp milling tool is required, cobalt-tipped tools are capable of maintaining their edge

sharpness very well even though the package materials used are very hard and normally difficult to machine.

Although the integral connector/package concept worked very well, there is one drawback to this approach, at least in the way it was implemented during this program. The package and connecting pieces for the pigtails were not interchangeable, although it is quite probable that such designs can be made to be interchangeable. Figures 6 and 7 are the mechanical drawings of the directional and "T" coupler packages used for the brassboard models.

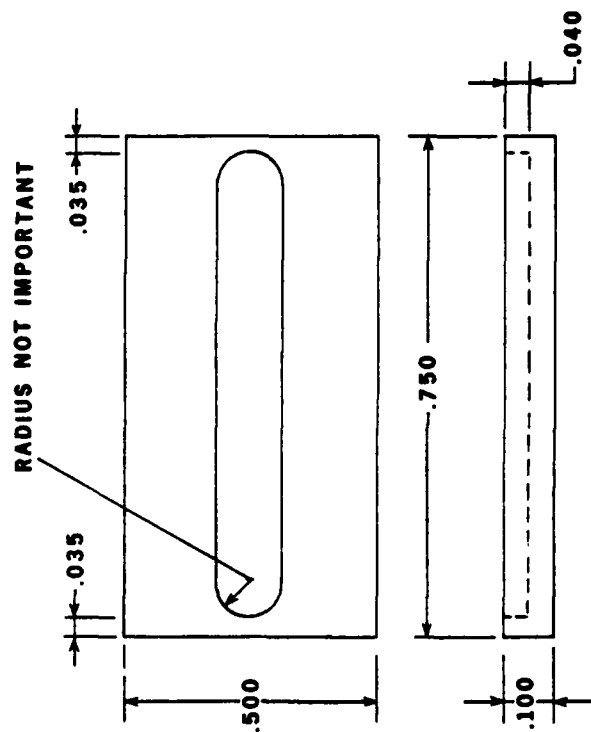
Because of the multiplicity of fibers involved, the package design for the transmission star couplers was more complicated than for the three-port couplers. The primary approach that was selected was to pursue an integral connector/package concept, but the design of the connector required a considerable amount of developmental effort in itself. Figure 8 illustrates the design concept that was preferred for the star couplers. In this design, the fibers were to be stacked in layers using a series of



ALL DIMENSIONS
IN INCHES
ALL TOLERANCES
±.002 INCHES
UNLESS OTHERWISE
STATED.

902 12150

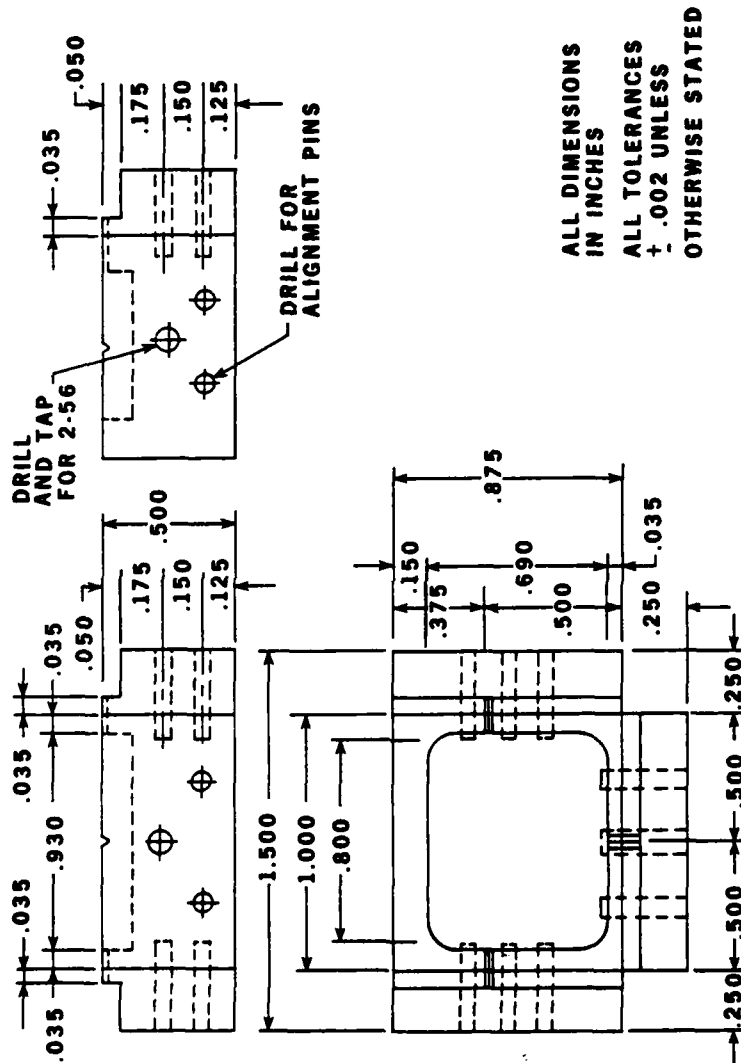
Figure 6. Directional Coupler Package Mechanical Drawing.



ALL DIMENSIONS IN INCHES
 ALL TOLERANCES $\pm .002$
 UNLESS OTHERWISE STATED.

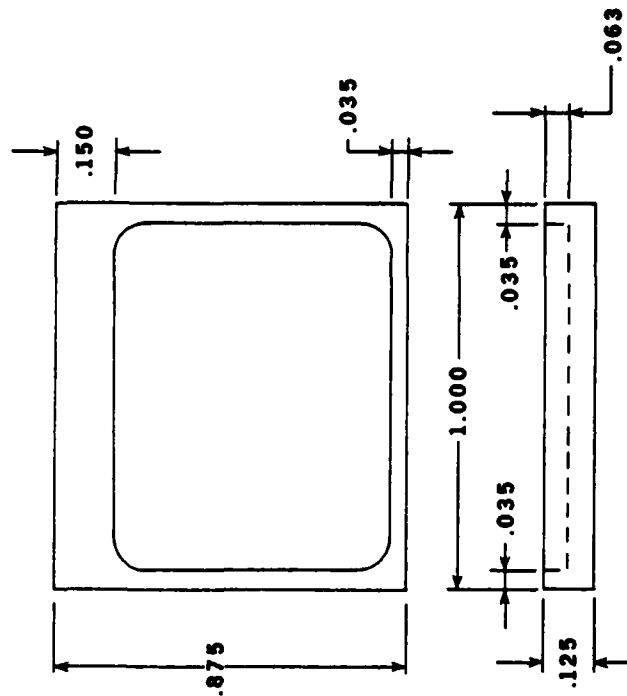
302 12153

Figure 6. Directional Coupler Package Mechanical Drawing (continued).



302 12151

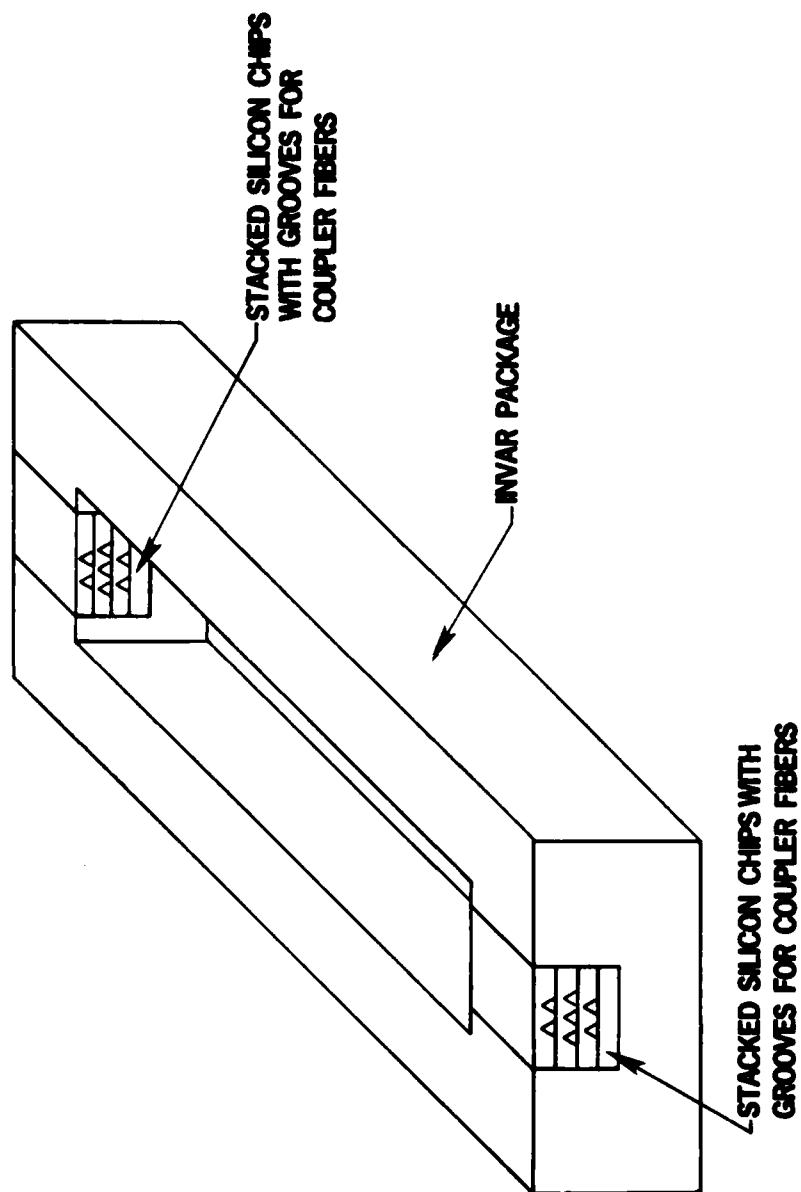
Figure 7. "T" Coupler Package Mechanical Drawing.



DIMENSIONS IN INCHES
TOLERANCES $\pm .002$

302 12160

Figure 7. "T" Coupler Package Mechanical Drawing (continued).



302 10624

Figure 8. Preferred Star Coupler Package Approach.

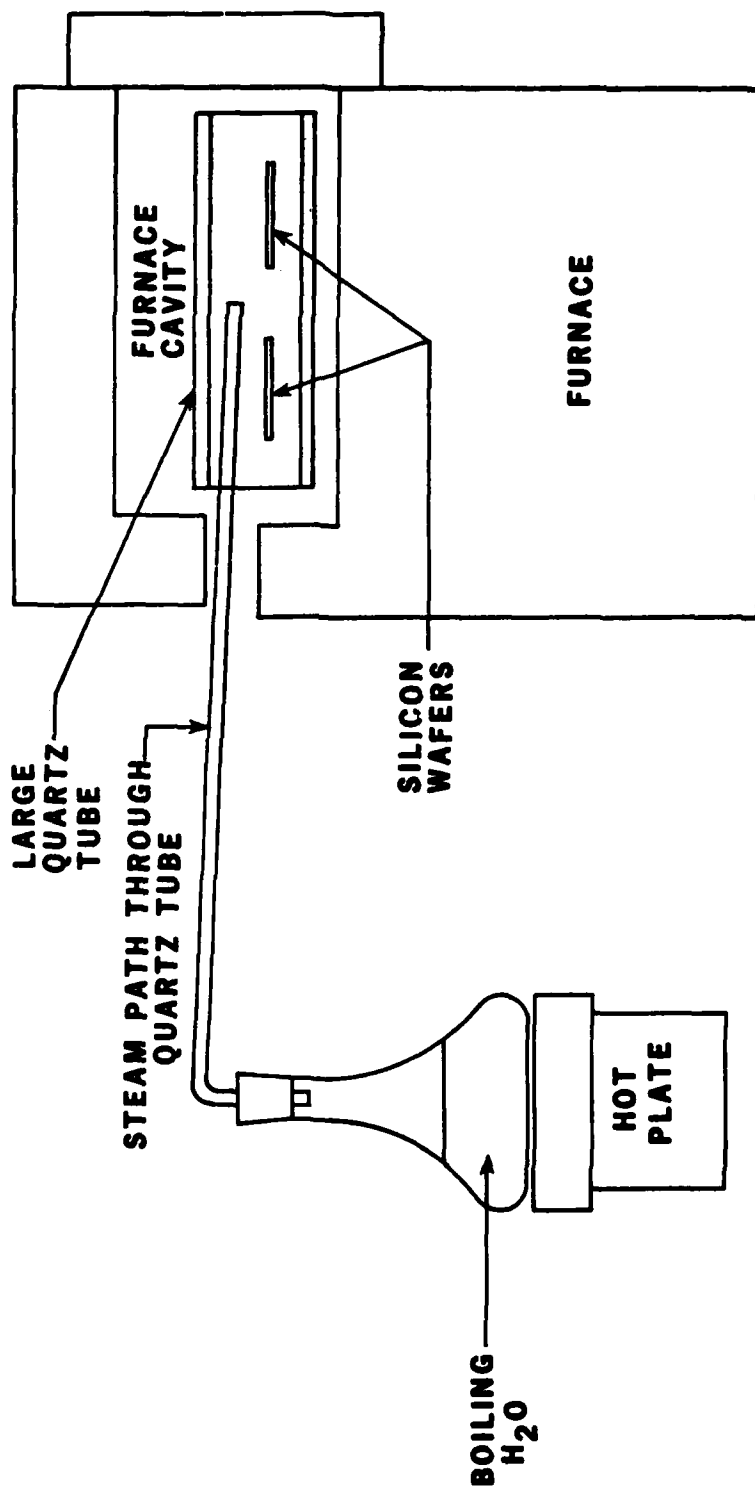
spacer chips with the fiber positions for each layer defined by grooves in the chips. As seen in the figure, the geometry formed by the fibers is that of a hex pack. For this design to perform well, a common reference surface is required to register the individual chips in the layers. This requires well-defined edges on the package and chip in relation to the grooves. Two methods were investigated for forming the grooves: (1) the grooving of the chip substrate using a precision diamond saw, and (2) a preferential etching process on a properly-oriented silicon wafer (see Appendix C).

For groove formation using a precision diamond saw, the saw that was investigated is manufactured by Tempres Micro-electronics. This saw is used widely in the semiconductor industry for dicing up wafers into individual chips. Although this device is capable of making many successive cuts without accumulative error, Tempres was incapable of controlling the depth of cut, the width of cut and blade wander sufficiently to achieve the alignment required to achieve low loss fiber interconnections.

The second alternative available for forming the fiber alignment grooves was that of preferentially etching grooves in silicon. The silicon wafer processing requirements, in terms of crystallographic orientation masking techniques, and etching solutions are covered in Appendix C.

In this application, however, a thicker oxide growth required in the semiconductor industry was needed to withstand the effects of the long (three to four hours) groove etching process. Figure 9 shows schematically the oxide growth apparatus used for this program. With this apparatus, oxides ranging from 1 to 2 micrometers were produced in two hours @ 1200°C.

The quality of the etched "V" groove made steady improvement with time, however, it also became evident that a basic flaw existed in the design of the photolithograph mask. Figure 10 is a photograph of the mask design pattern as transferred to an oxidized silicon wafer that has been etched to remove all but the desired oxide mask pattern. In this mask



302 12152

Figure 9. Oxide Growth Apparatus.

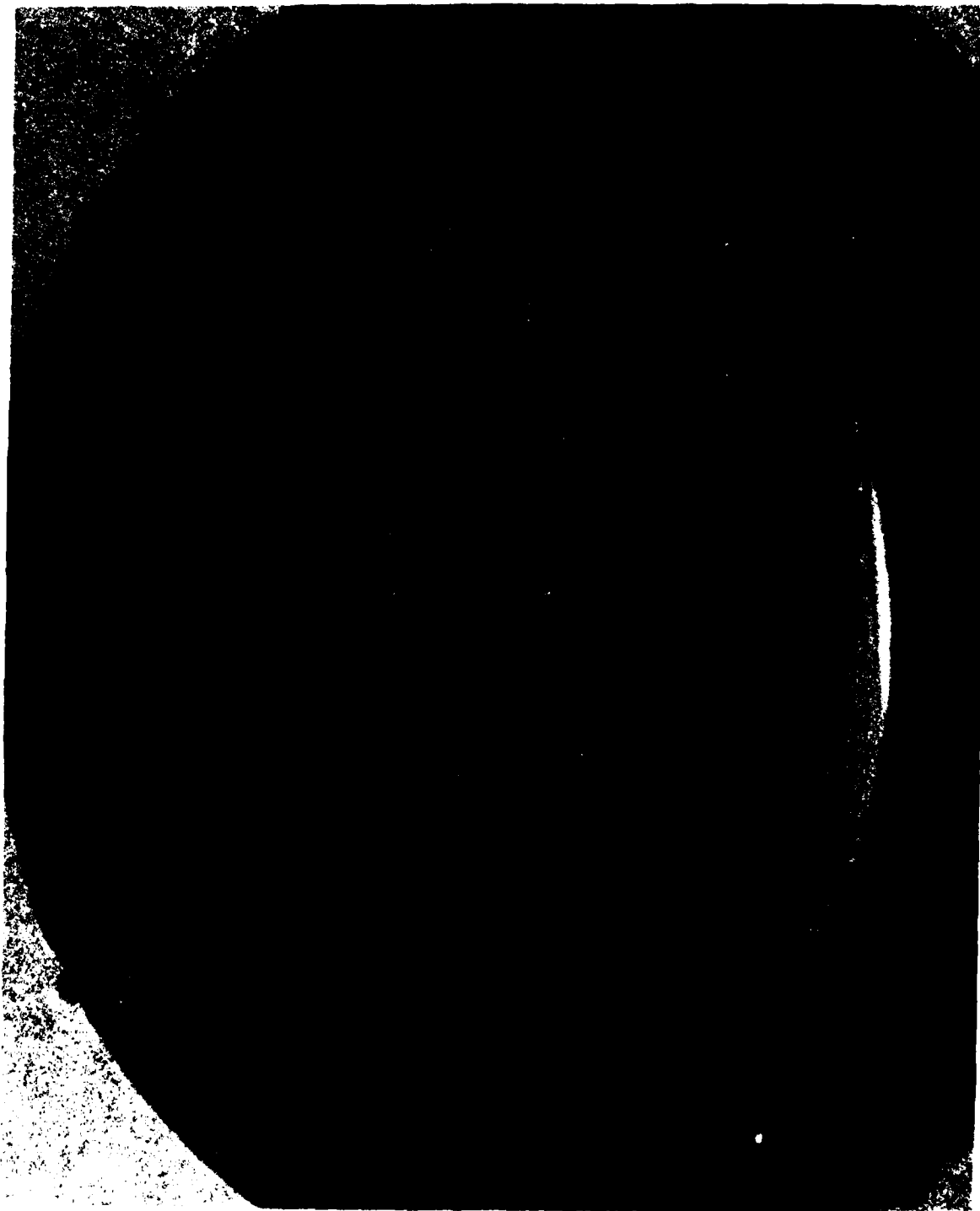


Figure 10. First Mask Design on Silicon.

design, each row contained only one or two of the specific chip patterns required to build up the hexagonally packed fiber array. This, in itself, would not have been a problem, had the diamond saw been able to dice the wafer with sufficient accuracy to permit the saw cut edges of the chips to be used as a reference for stacking. Attempts were made at lapping the edges of the rows of chips to obtain a reference, however, this proved to be very time consuming. A new mask design was generated in which all of the chips required for one end of a device were in the same row of the mask. This approach to the mask design would allow all of the chip edges to be processed simultaneously, thus creating a common reference surface. A mask of this type could, in principle, eliminate the problem of a common reference surface for chip alignment. The decision was made, however, to abandon the integral connector approach for the star couplers because of the available time left in the program and the mask delivery time. Figure 11 shows edge on views of the "V" groove integral connectors developed for the seven-port transmission stars. At this point, the approach to be pursued was changed to the pigtailed star using commercially available connectors.



Figure 11. Edge on Views of Assembled "V" Groove Connector.

The following vendors were considered as sources for the connectors to be used for the stars: (1) Amphenol RF[®], (2) Hughes, and (3) ITT Leeds. At present, these are the only vendors providing multiway, single fiber connectors. The Amphenol RF[®] and ITT Leeds connectors are quite similar in design except for the ferrule design and the method of primary fiber alignment. In both cases, the maximum number of contacts available per connector is eight.

The Hughes connector was the connector selected for use on the stars. The primary reason for this selection was because of the contact density of this design. The physical size of the Hughes is essentially the same as for the other connector candidates, however, 20 contacts are provided for as contrasted to eight for the other candidates. Figure 12 is a representative data sheet for the Hughes Multiway Connector. Section V of this report describes the details of the termination of the PCS fibers for this connector.

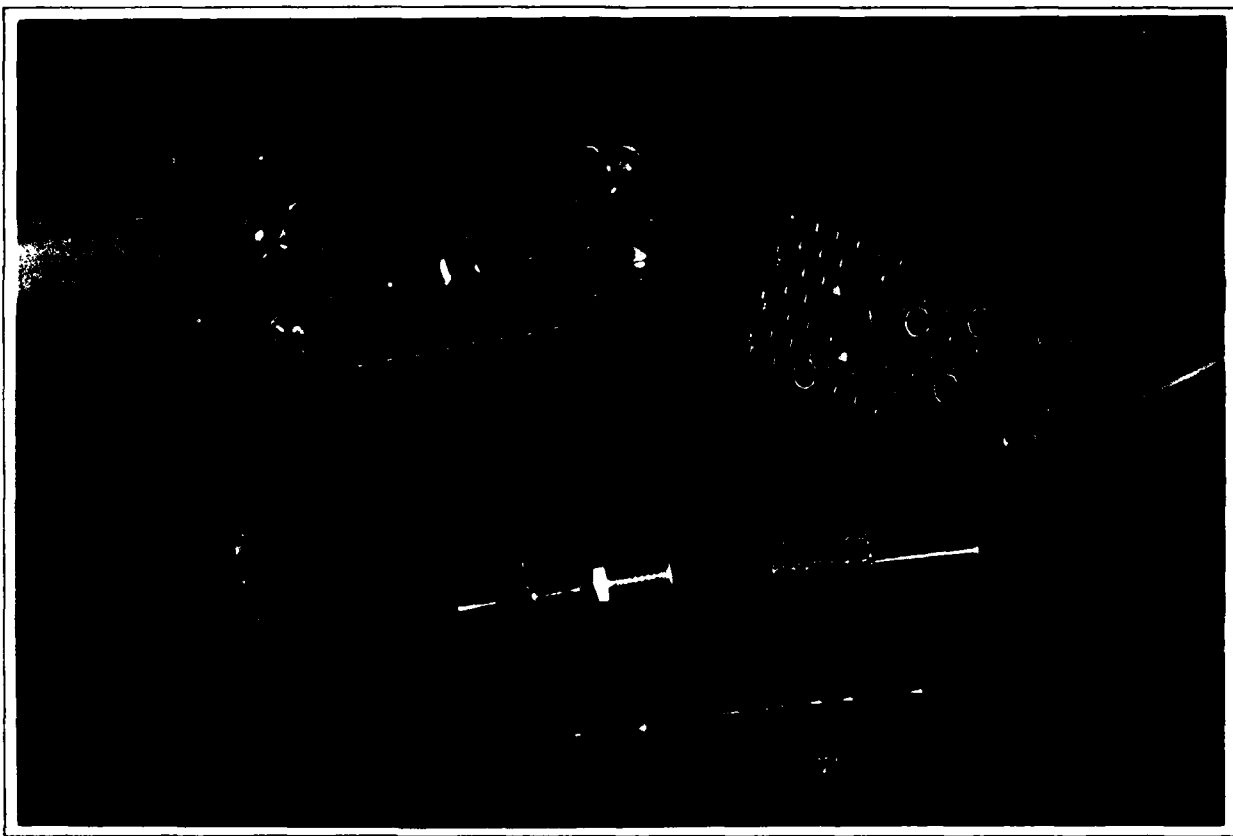


Figure 12. Hughes Multiway Connector.

3.0 Vibrational Package Design Considerations

This subsection deals with the coupler and package design as a single entity and describes the model used to aid in their design to obtain immunity from potential damage caused by vibration. Section II deals with the specific environmental requirements and testing methods used.

One of the mechanical design methods used to eliminate potential damage due to vibration is to ensure that the mechanical resonant frequency of a device is well above the range of the vibration spectrum anticipated in the use environment. Should resonances lie within the environmental spectrum, mechanical damping methods are used to limit the vibrational amplitudes to acceptable levels. In the case of the coupler designs however, the use of damping materials would in all probability result in reduced optical performance and impact the thermal design. The preferred approach was therefore, to try to raise the mechanical resonance of the coupler and package above 2 kHz.

The model that was used in the design was that of a rigid beam, fixed at its end points. For this model, the following equation defines the maximum displacement, Δy , that can be experienced without exceeding the elastic properties of the silica.

$$\Delta y(\max) = \frac{-5Wl^3}{384 EI_0} @ X = \frac{l}{2}$$

where, W = weight of beam

l = length of beam

E = elastic modulus of silica

I_0 = moment of inertia of beam

$X = \frac{l}{2}$ = center point of beam

Since the cross-sectional geometry changes with length in a coupler, an approximation of the moment of inertia was made in calculating $\Delta y(\max)$.

For the case of a .005" fiber of circular cross section this equation yields,

$$\begin{aligned} \Delta y(\max) &= \frac{-5(2.3 \times 10^{-4} \text{ lb})(.93'')^3}{384(10.4 \times 10^6 \text{ psi})(3.07 \times 10^{-11} \text{ in}^4)} \\ &= .0075'' \end{aligned} \quad (1)$$

The fundamental resonant frequency, F_n , for this model is given by

$$F_n = \frac{1}{2\pi} \sqrt{\frac{386}{\Delta y(\max)}}$$

Substitution of the maximum displacement, $\Delta y(\max)$, found from Equation (1) above yields a fundamental resonant frequency of 36 hertz. Reducing the fiber diameter to .0035" and the internal package length by one-half raises the resonant frequency to approximately 215 hertz, still an order of magnitude below the design goal.

Although it was not considered practical, according to the model, to achieve the design goal, each of the package designs was minimized in length to increase the vibrational stability. Actual vibration testing of the couplers and packages developed during this program has shown that the designs were more than adequate for use in aircraft applications. All of the couplers tested survived with no degradation; and in addition, no modulation of the optical throughput was detected during the tests.

SECTION IV

PACKAGING MATERIALS

One of the problem areas encountered with the couplers fabricated for the previous program was failure due to the differential thermal expansion between the coupler and the substrate or package that was used to support the device. The previous program was more of a developmental nature and, as such, little consideration was given to the packaging material issue. It is also important to note that there was no requirement for the couplers to be capable of surviving over temperature and as a result, the couplers were exposed to only small temperature ranges primarily around room temperature. In spite of the limited exposure range, however, there were numerous failures that were identified as being temperature related. From this experience, it was evident that the fiber and package thermal coefficient of expansion would have to be addressed if the devices were to survive the temperature requirements set forth in MIL-E-5400.

At the beginning of the program, several materials were identified as having desirable or potentially desirable thermal expansion coefficients. Table 5 presents data on the physical properties of a few of the candidates.

Table 5
Thermal Expansion Properties of
Packaging Material Candidates.

Material	Thermal Expansion Coefficient	Thermal Expansion Coefficient Norma- lized to Fused Silica
"MACOR" [®] Glass-Ceramic	94×10^{-7} in./in./°C	17.1
"KOVAR" Fe-Ni-Co Alloy	2×10^{-6} in./in./°C	3.64
"INVAR" (Nilvar) Ni-Fe Alloy	-.5 to +1.5 $\times 10^{-6}$ in./in./°C	-.91 to 2.73
"Super Nilvar" 31% 4-6% Fe-Ni-Co Alloy Hot-rolled	0	-
Fused Silica	5.5×10^{-7} in./in./°C	1

These materials are of two types, metallic and dielectric. The dielectric material that was considered is known by its trade name as "MACOR." Basically this material is a glass, ceramic composite material with excellent machinability properties. The metallic materials considered were special steel alloys that are used commonly in applications where glass to metal seals are required. These materials are known for their low expansion coefficients and, in some cases, their difficult machining properties. The machining properties are of importance in holding the level of tolerances required for the integral package/connector approach.

A simple calculation of the total change in package length over the temperature range specified in MIL-E-5400 is shown below.

$$\Delta L = L \times \Delta T \times K_T$$

where ΔL = length change over ΔT

L is the nominal length of the package

ΔT = operating temperature range required

and K_T = thermal coefficient of linear expansion

Inserting the values

$$L = 1 \text{ inch}$$

$$\Delta T = 157^{\circ}\text{C} = (95^{\circ}\text{C}) - (-62^{\circ}\text{C})$$

and $K_T = 2 \times 10^{-6} \text{ in./in./}^{\circ}\text{C}$ ("KOVAR")

A ΔL of $3 \times 10^{-4} \text{ in./in.}$ change in package length can be expected for a KOVAR package.

The worst case stress on the coupler that would be expected to result from package expansion is determined from the following relationships:

$$\text{Stress (psi)} = Y \times (\Delta L/L/^{\circ}\text{C} \times \Delta T)$$

where $\Delta L/L/^{\circ}\text{C} \times \Delta T$ over the maximum temperature range from -62°C to $95^{\circ}\text{C} \approx 3 \times 10^{-4} \text{ inches/W.}$ and $Y = 9 \times 10^6 \text{ psi}$
Young's Modulus

$$\therefore \text{Stress} \approx 2.7 \text{ kpsi}$$

This level of package expansion is reasonable because the resulting stress is approximately 40 times below the fiber proof test level and 300 times below the break strength levels measured for PCS fibers in one meter gauge lengths.

Although the Glass-Ceramic material at first appeared suitable for this application, it was ruled out because of its relative softness (the property that contributes to its machinability) and fragility. Its ability to be machined, although good, was not sufficient to obtain the accuracy required for the small fiber alignment grooves.

The selection of the best metallic packaging material was the free-cut, "Invar 36" alloy. This decision was made primarily based on its machinability. Although the "Super Nilvar" alloy is superior in terms of its thermal expansion properties, the alloy contains cobalt which seriously impairs its ability to be worked. The "Invar 36" alloy, however, when doped slightly (<1%) with selenium and manganese has substantially improved machining characteristics and is compensated to maintain the low thermal expansion properties of the undoped alloy.

SECTION V

PACKAGE AND COUPLER INTEGRATION

The discussion of package integration is divided into three subsections. The first portion describes the evolution of the bonding system. It deals with materials selection and its restrictions in terms of bonding, strength, waveguide preservation, and environmental soundness. The conclusion of this phase of the development led to the need for refinement of the silver application procedure. This is discussed in detail in Section V.2.0. The final section discusses the consideration given to plastic cladding materials.

1.0 Coupler to Package Bonding and Package Sealing

The aspect of package integration discussed here involves the selection of a bonding agent and an application method that will provide good bonding to both the Invar package and the fused silica coupler and at the same time provide an adequate degree of environmental sealing. Both metallic and epoxy sealants were explored in the attempt to achieve the best overall combination of desirable qualities in the final product. In addition to good bonding characteristics, there must be good waveguide properties over the bonded region and the processing required must not damage or contaminate the optical core material. The preservation of the waveguide quality was a very important consideration in the ultimate selection of an acceptable process. The following paragraphs described the evolution of this bonding and sealing technique from the original approach of metallic sealing to the final epoxy techniques employed.

1.1 Metallic Sealing Approaches

The silver electroless plating process used in the termination of PCS fibers is well established and provides a good reflective surface. It was, therefore, a primary approach for providing waveguiding in the bonded region; however, two other optical interface materials were considered namely, indium and aluminum.

Indium was considered because of its potential soldering properties.

The intended procedure with indium was to electroplate the appropriate surfaces of the Invar package and its lid with pure indium and sandwich the coupler in the "V" grooves between the two indium plated surfaces. The entire package would then be heated and the two surfaces would be soldered together. This would minimize handling of the coupler itself and greatly reduce problems of breakage and surface contamination. However, it was found that the fiber surface had to be prepared for this soldering by rubbing the surface with hot indium to produce an indium oxide layer on the surface. This was necessary to achieve a true bond to the silica.

It became apparent that there were three serious problems with this approach. The first problem was the handling of couplers for producing the oxide layer; coupler breakage generally occurred. Secondly, the bonding was found to be weak even with the surface preparation. (A 5 mil fiber bonded over a one-quarter inch length would rarely hold to a tensile load of 100 grams.) Thirdly, the reflective properties of indium determined by experimentation were found to be very poor in comparison to silver, resulting in significant additional loss.

At this point, some experimentation was done with vacuum deposition of aluminum on the fibers. The reflectivity of aluminum is nearly as high as that of silver in the wavelength region of interest and, therefore, it could be considered as an optical interface. There was a significant problem with the deposition process with respect to uniform thickness of the coating around the entire fiber circumference. "Shadowing" of some sections of the fibers occurred causing thin spots in the coating. Although many of the problems with the aluminum coating could be eliminated with proper fixturing, the process complexity, and turn around time versus the relative optical performance relative to the silvering method, eliminated this approach from further consideration.

As a result of the experimental investigations with the various metallic coating procedures, it was determined that the silver coating process has the best set of attributes in terms of process complexity, reproducibility, compatibility with other fabrication processes, and preservation of the optical waveguide characteristics.

1.2 Epoxy Bonding Agents

Having defined the silvering process as the preferred method of coating the fiber to preserve the optical waveguide, the selection of a suitable bonding material compatible with the silver coated fiber and Invar package was addressed. The desirable characteristics of the adhesive material are as follows:

- o Low thermal coefficient of expansion
- o High bonding strength to coated fiber and
Invar package
- o High viscosity
- o Low outgassing properties
- o Hardness over the desired temperature range
- o Ability to be polished

Although many materials were investigated, only one of these will be described here because it alone was found to have all of the desirable characteristics. This material is known as "Torr-Seal", and is distributed exclusively by Varian, Inc., Vacuum Products Division. The cured "Torr-Seal" epoxy was found to be stable over the temperature range (-62°C to $+95^{\circ}\text{C}$) specified in MIL-E-5400. Since this material is normally used in high

vacuum applications, it was reasonable to expect that it would provide reasonable environmental sealing properties.

The bonding of the coupler into the package was accomplished as a two (2) step process. First, the coupler element was bonded to the package by positioning the fibers into their respective "V" grooves and applying a small quantity of "Torr-Seal". This process was performed at $+60^{\circ}\text{C}$ to reduce the viscosity in order to facilitate wetting, and the collapse of air pockets introduced during mixing and also to achieve short cure cycles (1/2 h). The final packaging step was the bonding of the package lid to the main package body. This, too, was accomplished at 60°C using as small an amount of adhesive as required.

In the following subsections, the techniques that were used to (1) coat the fibers at the appropriate points with silver, and (2) prevent coupler surface contamination during fabrication steps that follow the actual coupler fusion process are described. In addition, experiments conducted with plastic cladding materials on the fibers as opposed to the metallic coatings is also discussed.

2.0 Refinement of Silvering Process

The primary approach selected to permit indirect bonding of the fiber ends of the couplers to the package and also to bond the pigtails to the attachment pieces was to use an electroless silver plating on the fibers. Some modifications were implemented in the fiber precleaning steps (see Appendix A) to obtain consistent film density, however, the actual plating process remains as described in the technical report AFAL-TR-78-199 and repeated with modifications in Appendix A.

Due to the finite reflection coefficient of the glass-metallic interface, it is necessary to limit the coated length of the fiber to an absolute minimum (for a .005" diameter fiber, -0.25 dB of loss can be expected for a 1 mm coating length assuming a 98% reflection coefficient).

The couplers fabricated for this program were fabricated using short lengths (<6 inches) of bare fused silica fiber core material. The order in which the coupler fabrication steps are implemented is an important consideration in terms of preserving the optical properties of the coupler element.

In any case, the finished coupler element will be fused in the central region with the fiber ends coated with silver (or other appropriate material) in the regions where it is bonded to the package. Many process order experiments were carried out throughout the course of the program in order to improve upon the performance of the couplers. Independent of the process order, however, the processing steps involved were silvering of the fibers, masking of various regions of the fiber of coupler, etching, removal of the masking material and coupler fusion. The following paragraphs describe some of the process orders investigated.

2.1 Approach 1

In this approach, after the fibers were stripped of their jacket and cladding and thoroughly cleaned, the coupler element was formed by fusion and the entire coupler coated with silver. At this point the coupler was bonded into the package with a suitable material and a protective coating (Blackwax) or mask applied over the coupler ends to protect the silver and bonding material from attack by the subsequent etching process to follow. Two problems were inherent to this procedure. First of all, the coupler element could be easily damaged when install-

ing the device in the package either by breakage or scarring of the silver film and secondly, the etching of the silver film from the coupler region left some surface contamination when etched with nitric acid. The contaminated surface had the appearance of being frosted, although nonsilvered fibers, when similarly etched did not show this appearance. At times this affect seemed to go away, however, its disappearance was only optical and due to the fibers being wet. Other acids and or solvents were less effective removing the silver and were abandoned.

2.2 Approach 2

In this approach, after the fusion of the couplers has been performed, the coupler is masked over a carefully controlled length of the central region of the coupler. The actual masked length was slightly less than the internal package length such that after the application of the silver, the silvered regions would correspond to the bonding points in the package. After the device was bonded in place the masking material was removed by an appropriate solvent. This approach, in general worked well, however, the positional accuracy required to align the bonding points of the package and the silvered regions was objectionable. The following paragraph describes a modified form of this approach that was implemented in the construction of the brassboard models.

2.3 Approach 3

The primary difference between this approach and the previously described approach is the final etching step, and the length of the coupler that was masked off in preparation for the silvering process.

In order to reduce the coupler positional accuracy required to install the coupler in the package, the masked region was shortened. The reduction of the masked length, therefore, caused a larger portion of the silvered ends to overhang the mounting points on the inside of the package. In the interest of minimizing loss contributed by the increased silver length due to the finite reflection coefficient, a final step of etching back the silver was used. Although there always seemed to be some evidence of surface contamination in the etched silver region, this was limited to only a millimeter or so of length rather than the total length of the coupler as described in paragraph V.1.1.

Table 6 lists the materials investigated for the masking function, suitable solvents for removal and the results of their application. One of the most important experiences gained in this program became apparent during the search for a suitable masking material, and the ultimate

Table 6
Masking Materials.

<u>Material</u>	<u>Primary Solvent*</u>	<u>Results</u>
Crystallbond 509 (Glycol Phthalate)	Acetone	Some surface contaminants remained
Blackwax	Trichloroethylene	Clean Removal
Kynar	Acetone	Porous mask unless consolidated with heat, difficult to obtain consistent results
Shipley AZ-1350J (+) photoresist	AZ-351 Developer (after UV exposure) or Acetone (without exposure)	Some surface contaminated

*In all cases, after primary solvent was used, a final rinse with Dupont TP-35 (FREON TF[®] and ISOPROPYL ALCOHOL[®]) was used.

performance of the PCS couplers appears to be keyed to solving this problem, at least in relation to the fused coupler approach. The necessity of removing the cladding material and performing a multitude of processing steps (fusion, masking, recladding and mounting), creates many opportunities for the irreversible contamination of the fiber core material. As seen in Table 6 and described in this section, this problem persisted throughout the program and additional effort is required to solve this problem in order to realize the full potential of the direct fusion approach for PCS fibers.

3.0 Plastic Cladding Considerations

In the last subsections, the fabrication processes that were based on the use of silver depositions on the fiber ends was described. An alternate technique, that of using a low index plastic recladding process over the coupler ends for waveguide preservations after bonding, was also investigated. Appendix B presents the results of a program in which several cladding materials were investigated. As described in the appendix, the most suitable material was the Kynar[®]-TFE-Copolymer. This material was purchased and tried as an alternative to the silvering process and found to be of little use for this program when used alone as a cladding material to enable bonding. For this material to work well, the following parameters must be very well controlled: (1) fluid viscosity, (2) coating thickness, (3) consolidation time and temperature. The results obtained as a result of using this material varied widely. Later in the program, however, and described in detail in Section IX, a way was found of using this material that greatly improved the fiber terminations in the connectors for the star couplers.

SECTION VI

DIRECTIONAL COUPLERS

Previous sections of this report have described in detail the evolution of the package designs, the integral connector/package design approach, the integration of the package and coupler element, and the environmental performance of these designs. This section will deal with actual coupler fabrication techniques and improvements leading to the fabrication of the -3, -10, and -20 dB brassboard coupler models at the end of the program.

1.0 Technique Improvement

The most significant improvement in the coupler fabrication technique was achieved by the elongation and tapering of the coupler transition regions. This technique was the result of knowledge obtained from the fabrication of couplers from fibers made by the chemical vapor deposition (CVD) process funded internally at ITT. The CVD fiber couplers were also formed by a direct fiber fusion approach as is the case here for the plastic clad silica (PCS) coupler devices, but in the CVD couplers, the power splitting mechanism is referred to as "diffusion

coupling", whereas in the PCS couplers, the coupling mechanism is referred to as area ratio splitting.

In order to understand why the elongation and tapering procedure is beneficial to the area ratio coupling mechanism, some background into the diffusion coupling mechanism is provided in the paragraphs to follow.

The basic diffusion coupler type that is discussed here is known as the "Fused Biconical Taper Coupler". A four-port biconical coupler is shown in Figure 13. In order to couple energy from one of the fiber cores to the adjacent fiber core, the fibers are heated and drawn to create a down taper at one end of the coupler and an up taper on the opposite side as seen by the propagating wavefront incident from one end of the coupler. Based on a ray tracing analysis, each ray is converted to a higher order mode upon encountering the boundary between the core and cladding in the region of the down taper (down taper causes a modal up-conversion). If the original ray represented the highest order ray that could propagate in the core, up-conversion at the taper means that the angle of incidence of the ray is therefore

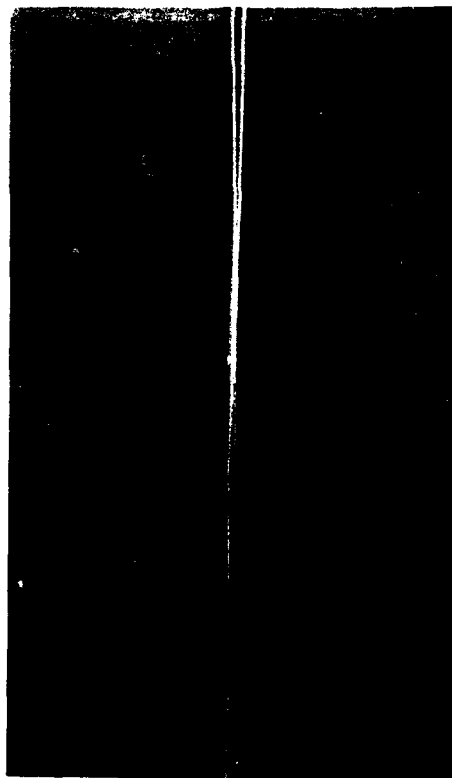


Figure 13. Fused Biconical Taper Coupler.

less than the critical angle and the ray escapes from the core into the cladding. This energy that escapes from the core, however, is not necessarily lost from the total fiber structure as long as the effective numerical aperture (NA) of the total fiber, as determined by the cladding index and the surrounding boundary index, is large enough such that the ray is incident on that boundary at an angle greater than the critical angle of the interface.

In the case where tapering is employed in the structure of the PCS coupler however, there is only a single core; but the NA of the original cladded fiber is less than that of an air bound pure silica core; some amount of tapering, therefore, will only force the light into higher order modes that remain bound to the air-clad-core and, if accomplished in a smooth manner, substantially reduces the peak mode conversion below that obtained with a smooth but untapered transition region. It can also be shown that a modal down-conversion process takes place in the expanding taper region of the coupler and that this process can take place efficiently.

Although most of the evidence supporting the improvement gained by the elongation process is easily detected in the more complicated coupler structures ("T" and star), this process was used for the directional couplers as well.

2.0 Coupling Designs

Table 7 summarizes the fiber size requirements for each of the coupler designs developed during the program. The fabrication of the -3 dB and -10 dB coupler designs was straight forward; however, the fabrication of the -20 dB design was complicated due to the fact that a 13 μm diameter fiber could not be produced using normal fiber drawing equipment. As a result, the approach that was taken was that of only partially fusing a 30 μm fiber to the side of a 125 μm fiber that formed the main throughput arms of the coupler. The remainder of the coupler fabrication is as described in the previous sections.

3.0 Brassboard Directional Coupler Data

The performance data presented here is that taken on the hardware delivered to AFAL as the brassboard directional

Table 7
Fiber Size Requirements for
Directional Couplers.

Coupling Ratio (dB)	Through-put Fiber Dia. (μm)	Tap-off Fiber Dia. (μm)
-3 dB	90	90
-10 dB	120	40
-20 dB	126	13

coupler models. The data presented in Tables 8, 9 and 10 reflect the total performance of the devices including the integral connectors of the packages. The following paragraphs describe the performance of each of these devices specifically.

-3 dB Directional Coupler

The measurements on this coupler represent its use in a power splitting configuration. The short length measurement values represent the total loss, geometric and excess, for the coupler and the integral connector measurements result from measuring the power available at the input connector on the left of the coupler as shown in the diagram. The diagram also shows the other isolated components of the total coupler loss. Note that the loss at the output connector interface is greater than at the input. This is due to the difference in fiber sizes used at these locations. This is described further in the final report.

-10 dB Directional Coupler

For this device, the throughput loss refers to the total of the coupler loss and the integral connector losses.

Table 8
-3 dB Directional Coupler.

Port Coupling (dB)			
Reference	Port 1	Port 2	Excess Loss
Short Length	-6.49	-6.82	-3.64 dB
Input Connector	- 6.02	-6.35	-3.17 dB

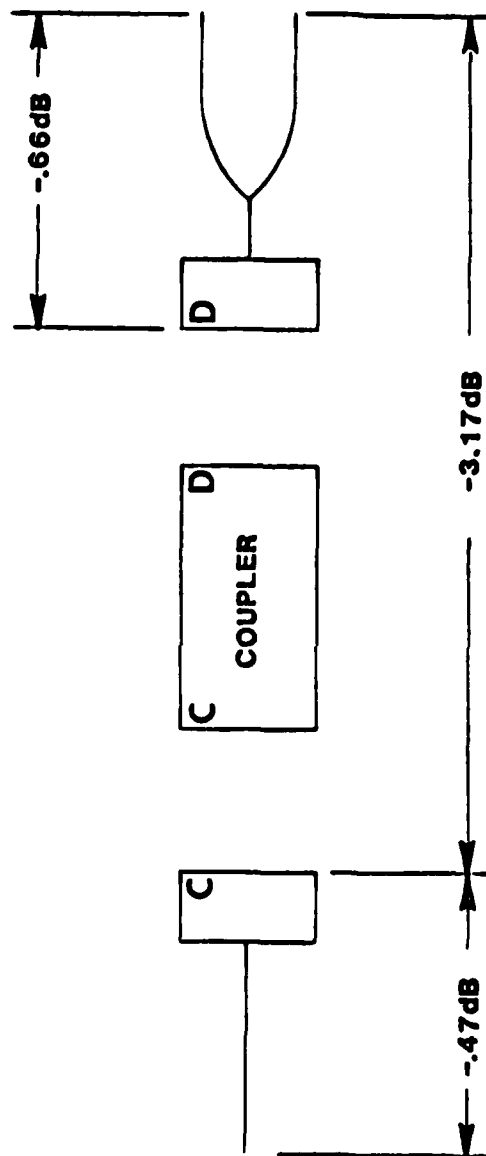


Table 9

Directional Coupler Performance - (10 dB).

<u>Package ID</u>	<u>Throughput Loss</u>	<u>Tap-off Level</u>	<u>Total Excess Loss</u>
#AB	-8.15 dB	-13.8 dB	-7.1 dB

Loss due to termination of output pigtail: -.3 dB

Tap-off level with respect to throughput signal: -5.7 dB

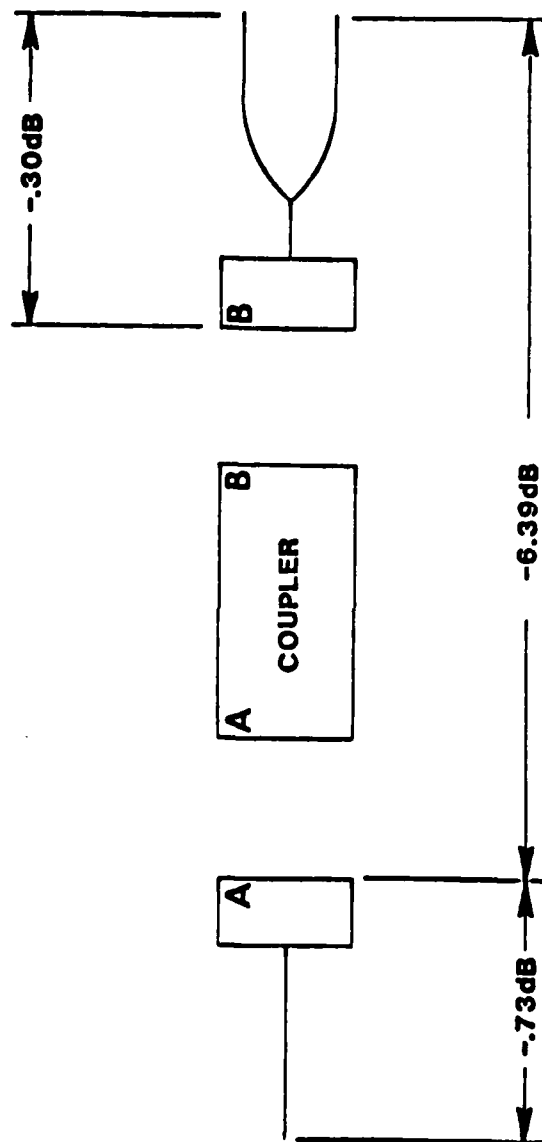


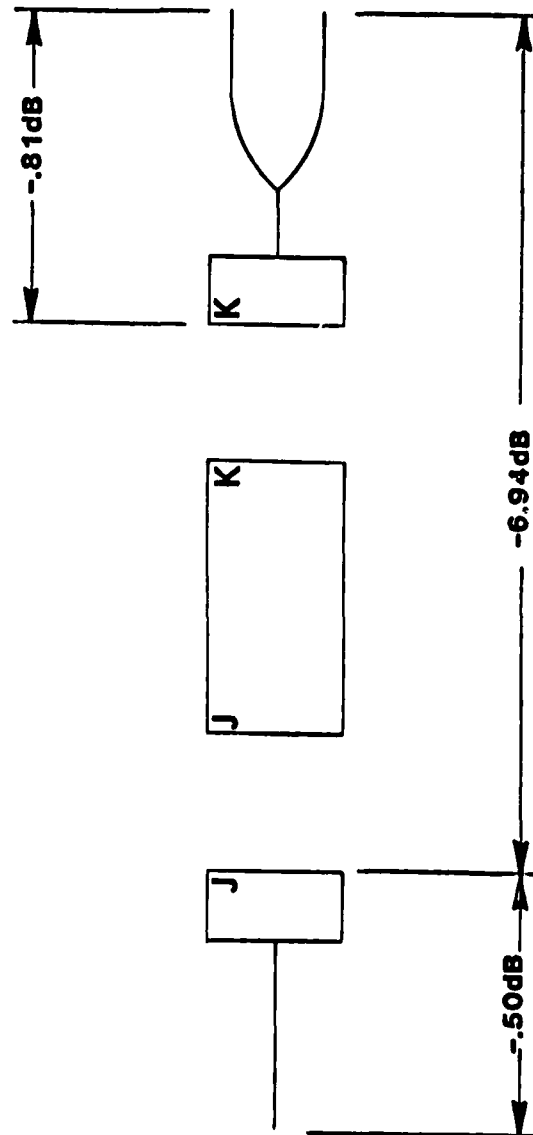
Table 10

Directional Coupler Performance - (20 dB).

<u>Package ID</u>	<u>Throughput Loss</u>	<u>Tap-off Level</u>	<u>Total Excess Loss</u>
#JK	-7.1 dB	-22.0 dB	-6.9 dB

Loss due to termination of output pigtail: -.81 dB

Tap-off level with respect to throughput signal: -15.0 dB



The tap-off level is with reference to the input to the coupler on the left of the drawing. The -0.3 dB loss shown to the right of the diagram represents the average of the two output port losses at this interface point. Due to the proximity of the output fibers on the coupler, it was not possible to determine the power available from each of these ports to further define the losses. The -5.7 dB level represents the difference in power available at the output pigtails of the unit.

-20 dB Directional Coupler

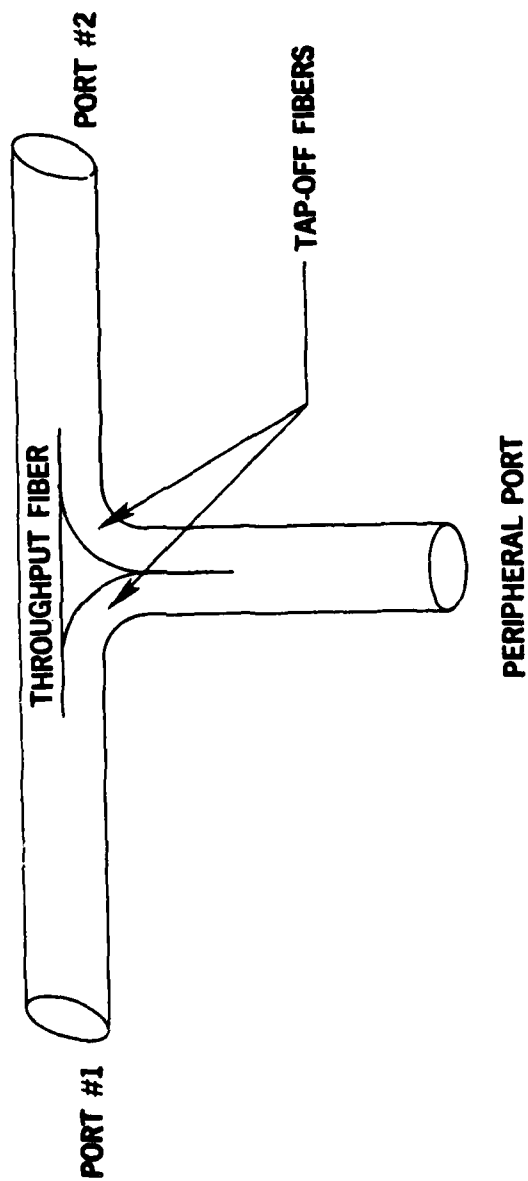
The same definitions given for the -10 dB Directional Coupler applies to this coupler also.

SECTION VII

"T" COUPLERS

Three "T" coupler designs were fabricated as part of this program. These designs were to have tap-off power levels, relative to the power injected into either of the main throughput arms of the coupler (Figure 14) of -3 dB, -5 dB and -10 dB. Table 11 summarizes the fiber sizes required for each of these designs to achieve the desired coupling coefficients assuming that the main throughput arms of the coupler are to be .005" diameter.

As in the case of the directional couplers, an integral connector/package concept was selected as the primary approach to solving the environmental problems associated with previous designs. The details of the package design have been covered in a previous section and will not be repeated here, however, the package design concept did prove to be sound for this coupler type as well as for the directional couplers.



302 10333

Figure 14. "T" Configuration.

Table 11
Fiber Size Requirements for "T" Couplers.

<u>Coupling Ratio (dB)</u>	<u>Throughput Fiber Dia (μm)</u>	<u>Tap-off Fiber Dia (μm)</u>
-3	90	90
-5	105	71
-10	120	40

As a result of the previous program, and described in the final report for that program, there is a special problem highlighted that arises in the optical performance of "Ts." This problem is due to the method of construction of such devices and the ability to control the modal distribution of the energy divided among each arm of the coupler and the ability to capture this energy (within the NA of the fiber) efficiently at the output arms of the device. It is also important to note that the modal power distribution problem was more severe for the -3 dB coupler design, due to the greater amount of constituent fiber deformation required to fabricate this design.

As part of the technique improvement phase of this program, the technique of elongating the transition regions was implemented and resulted in a substantial improvement in the "T" coupler performance level for a device constructed from three (3) directional coupler elements. Figure 15 shows the results obtained for such a device. It is important to note that the "T" coupler

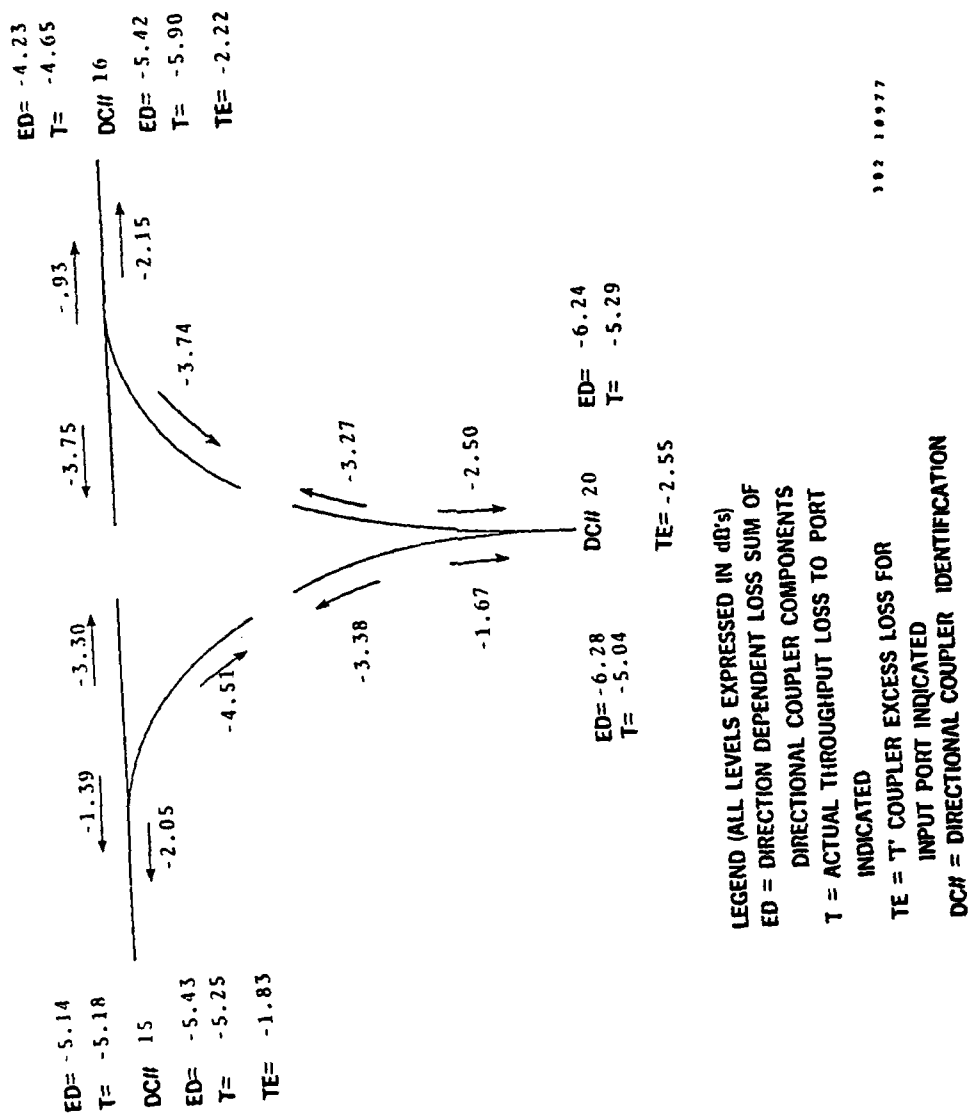


Figure 15. "T" Coupler Performance.

excess loss levels indicated are approximately equivalent to the sum of the losses in the directional coupler elements, indicating reasonable control of the modal power distribution in each arm and efficient recapture of this power at the output ports of the device.

In this program, however, it was not practical to assemble "T" couplers from directional coupler elements and keep the size of the device within reason and also provide environmental protection for the device. The approach that was selected, was to fabricate the devices using three (3) short fiber lengths in which two of the fibers that would ultimately form the tap-off port would be bent (prior to assembly) at 90° (see Figure 16), and the adjacent fiber ends would be subsequently fused together to form the coupler ports.

The use of the elongated transitions was incorporated as part of the fabrication procedure for all of the "T" couplers produced. However, due to the fact that



Figure 16. Photograph of "T" Coupler.

short fiber lengths (10-15 cm) were used in the fabrication, it was not possible to monitor the coupler performance during formation. In actuality, the couplers had to undergo complete fabrication, packaging, and pigtail attachment before the first measurements could be made. Although this procedure is handleable for a device as simple as a directional coupler, it proved to be unacceptable in the case of the "Ts." This approach did not allow for any reliable method of diagnosing specific fabrication errors and substantial yield problems resulted.

1.0 Package Design

The package design for the "T" is shown in Figure 7.

This design was a direct outgrowth of the directional coupler design. The integral connector approach had been refined for directional package and was easily used in the "T" design. The overall size was kept as small as possible for vibrational stability as well as weight considerations. The lower limit of the size was determined by the amount of excess loss introduced as a function of the fiber bend radius. Figure 17 shows the results of an experiment to determine the loss introduced as a function of bend radius. In the package design for the "Ts," a bend radius of approximately 0.3" was easily obtained thus contributing less than 0.5 dB loss to the coupler tap-off ports.

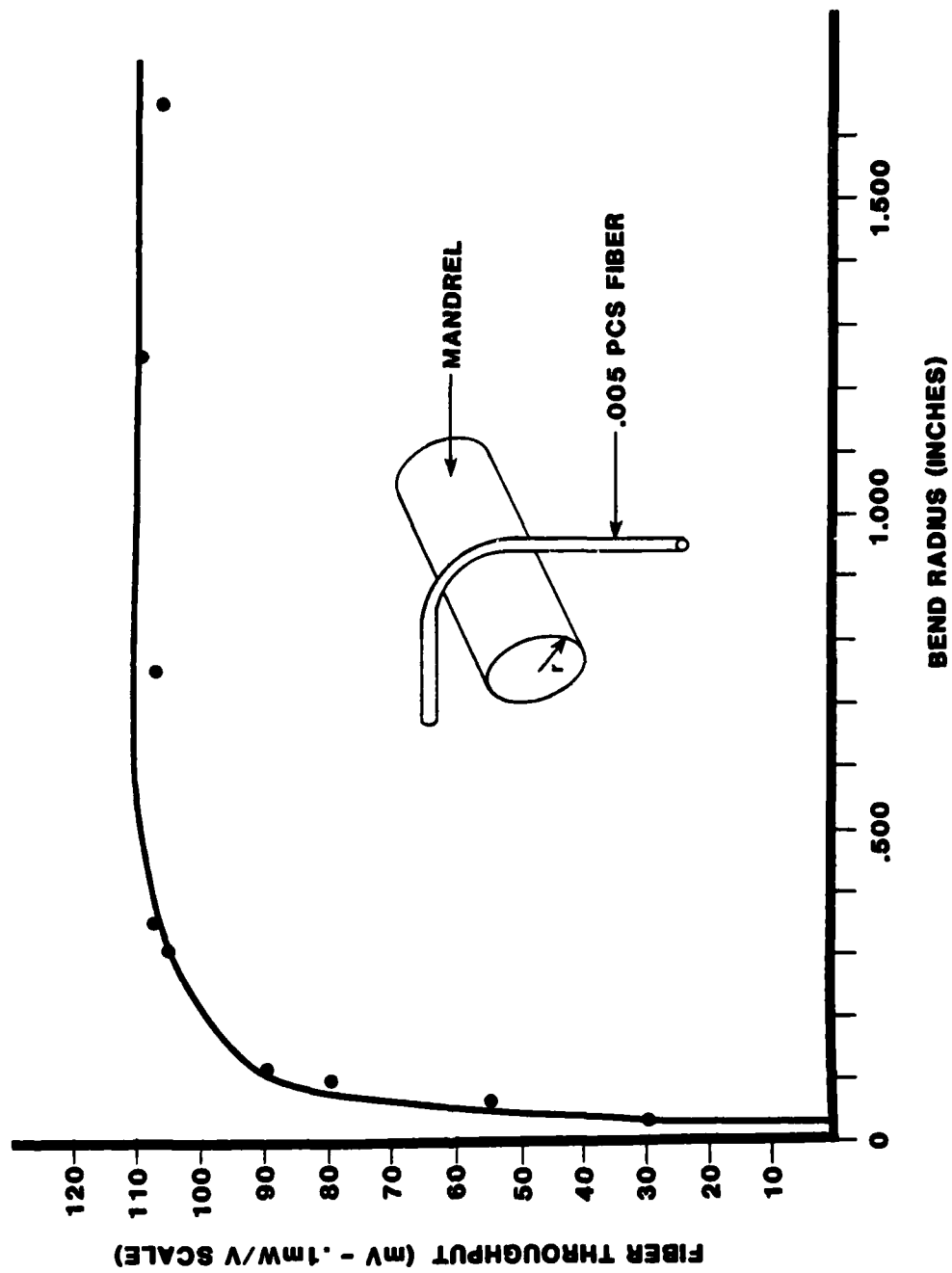


Figure 17. Throughput vs Bend Radius.

2.0 Special Considerations for Tap-off Designs

The 5 dB design has the modal redistribution problems to the same degree of severity as the 3 dB design, however, the problem is not as severe in the 10 dB case. This is most likely due to the fact that the primary (larger) internal throughput fiber is relatively undisturbed by the fusion of the small tap-off fibers.

The 10 dB design has a separate problem, however, in the mating of the two small fibers that form the internal tap-off arm to the large fiber which matches the transmission fiber size. Achieving a good low loss fusion between these two fiber sizes is difficult to complete and package without causing breakage in the other fusion areas. Due to this difficulty the small fibers were silvered and terminated in the internal package "V" groove and the 5 mil fiber was terminated in the demountable connector half. The mating was achieved best with this approach. A drawback that is inherent to this approach, however, is that the smaller diameter

fiber experiences more reflections per unit length than a larger fiber would. The finite reflection of the silver becomes more significant and an additional excess loss is seen in the tap-off arm.

3.0 Brassboard "T" Coupler Data

The performance data presented here is that taken on the brassboard models supplied as hardware for this program. This data, presented in Tables 12, 13, and 14 reflect the total device performance data, that is, the combination of the coupler, packaging, and connector losses. The package identification numbers refer to the stampings on the bottom of the packages which indicates the proper mating of the main coupler package and connector pieces.

AD-A082 360

ITT ELECTRO-OPTICAL PRODUCTS DIV ROANOKE VA
FIBER OPTIC COUPLERS.(U)

F/G 20/6

JUL 79 G W BICKEL; L E FOLTZER; G A RINES

F33615-78-C-1448

UNCLASSIFIED

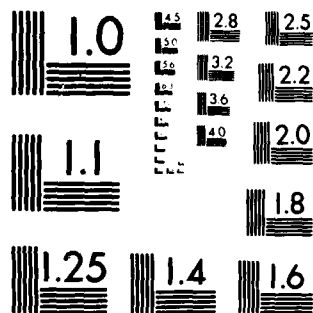
AFAL-TR-79-1149

NL

23

23

23



MICROCOPY RESOLUTION TEST CHART
NATIONAL BUREAU OF STANDARDS 1963 A

Table 12

Three dB "T" Performance.

All Loss Measurements in Decibels

<u>Package ID</u>	<u>Coupler Type</u>	<u>Injected Port</u>	<u>Output Port</u>	<u>Output Port</u>	<u>Total Excess Loss</u>
#GHJ	3 dB	G	-13.06 (H)	-14.15 (J)	-10.56
		H	-13.61 (G)	-14.45 (J)	-11.00
		J	-14.87 (G)	-15.02 (H)	-11.94

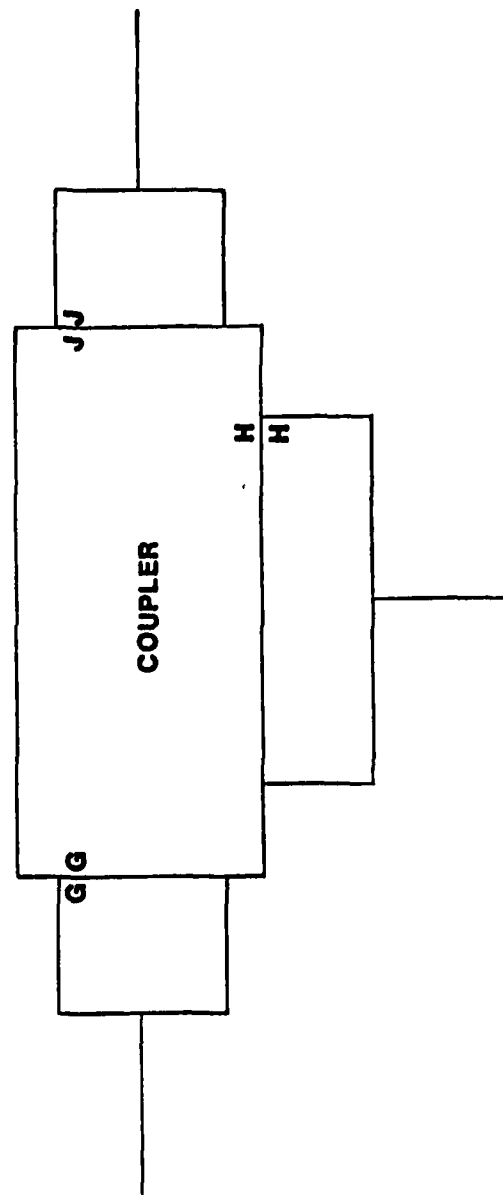


Table 13

Five dB "T" Performance.

All Loss Measurements in Decibels

<u>Package ID</u>	<u>Coupler Type</u>	<u>Injected Port</u>	<u>Output Port</u>	<u>Output Port</u>	<u>Total Excess Loss</u>
#DEF	S dB	D	-14.3 (F)	-17.2 (E)	-12.5
		F	-14.2 (D)	-20.0 (E)	-13.2

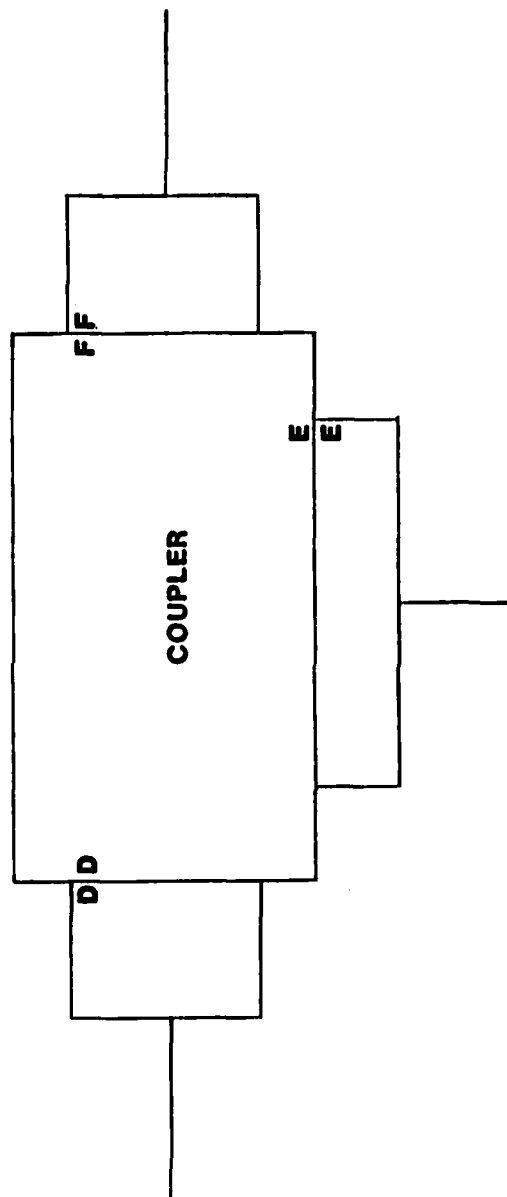
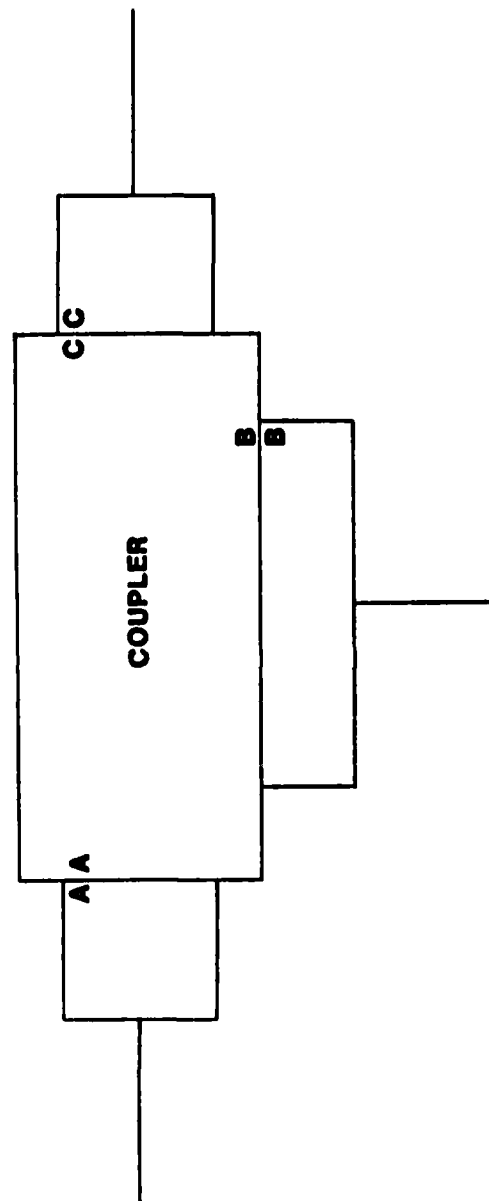


Table 14

Ten dB "T" Performance.

All Loss Measurements in Decibels

<u>Package ID</u>	<u>Coupler Type</u>	<u>Injected Port</u>	<u>Output Port</u>	<u>Output Port</u>	<u>Total Excess Loss</u>
#ABC	10 dB	A	-4.82 (C)	-22.6 (B)	-4.74
		C	-5.61 (A)	-26.1 (B)	-5.57



SECTION VIII

TRANSMISSION STAR COUPLERS

This section is devoted to the discussion of the 7- and 19-port transmission stars fabricated during this program. The integral connector concept for stars using silicon V-groove alignment is dealt with in detail in Section V. The determination of the multiway connector to be used on the external package of the star couplers is also discussed in Section V. This discussion deals with coupler performance improvements, the processing unique to the star coupler fabrication, and finally the actual termination of the pigtails and external package design.

1.0 Fusion Technique Improvement

The elongation of the transition region of the couplers has been described for directional and "T" couplers. The same principle applies to star coupler fabrication. After a good uniform circular fusion is obtained in the central coupler region, attention is given to the transition region. The coupler is heated just enough to allow elongation in the transition area. The goal is to taper the fibers in this area slightly to create a gentle interface angle for each optical core as it joins

the fused mixer region. The total increase in length for a completed star coupler resulting from the elongation of the transition regions was on the order of 4 mm. The amount of elongation was determined by a combination of visual inspection and by observing and maximizing the optical throughput level during fabrication.

This active monitoring of coupler performance was a major improvement in the fabrication procedure. To achieve this active monitoring a light emitting diode (LED) source and two PIN photodiodes were used. The detector outputs were connected to a dual trace oscilloscope to allow simultaneous viewing of the throughput values of the injected fiber and one of the other fibers.

One input port was chosen to be injected with the LED source and the throughput of this unfused fiber was recorded. As the fusion began, the output of the injected fiber would drop, and the other ports would rise in output as the mixer region was created. The remaining output fibers could be checked by placing them one by one in one of the detectors and a calculation of uniformity and excess loss could be made

at any point in the fabrication procedure. This technique provided immediate feedback and made it possible to understand the correlation between coupler performance and the geometry of the coupler fusion and transition areas.

Some of the seven-port star couplers made in this program were laboratory models to demonstrate the coupler performance achievable by these techniques. No strain relief or special packaging was used on the coupler; therefore, the loss seen is due solely to the coupling process which takes place in fusion and transition areas. The data obtained for a representative device of this type is shown in Table 15.

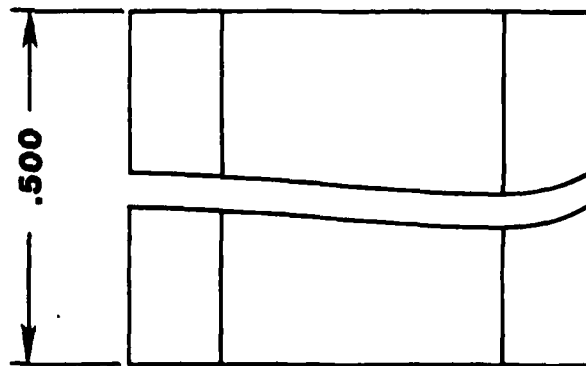
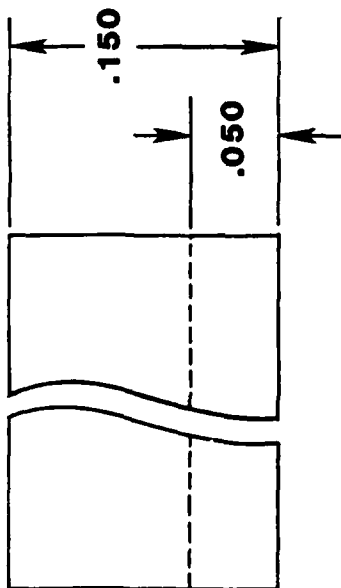
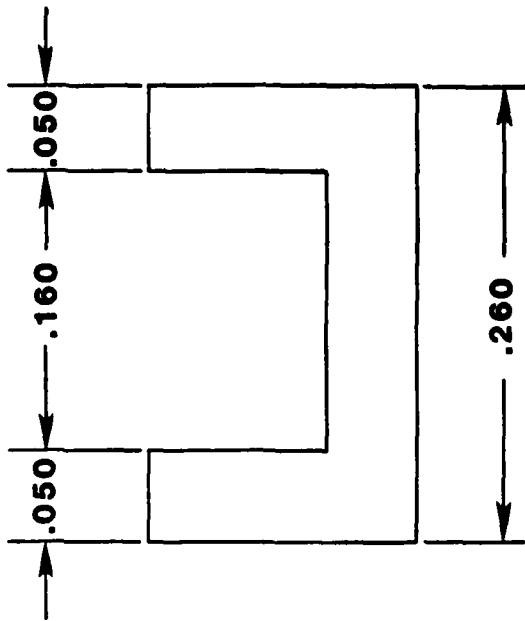
2.0 Star Coupler Fabrication Procedure

Once the final decision was made with respect to the star coupler package a definite fabrication procedure was established. The final package design consisted of an Invar internal package of sound environmental design, housed in a die-cast aluminum box which contained the Hughes multiway fiber optic connectors.

Figures 18, 19, and 20 are illustrations of the components that comprise the internal package. The processing steps

Table 15
Elongated Seven-port Star Coupler Data.

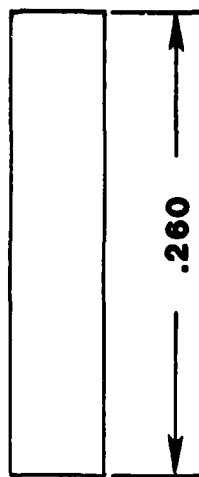
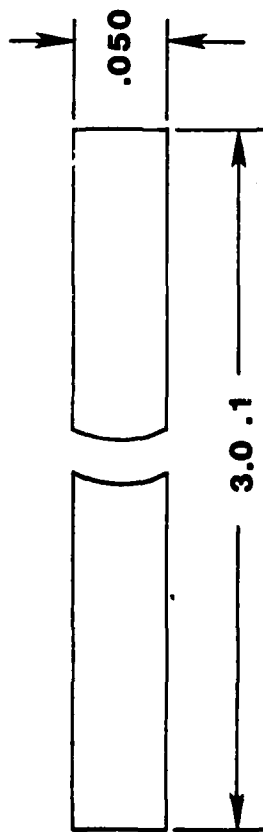
Throughput to Output Ports (dB)							Excess Loss (dB)
1	2	3	4	5	6	7	
-10.00	-9.89	-10.55	-10.21	-10.43	-10.21	-10.00	-1.73



ALL DIMENSIONS INCHES
ALL TOLERANCES $\pm .002$
MATERIAL: INVAR

302 12166

Figure 18. Stacking Block for Star Couplers.



**DIMENSION IN INCHES
TOLERANCE $\pm .002$
MATERIAL: INVAR**

3 0 2 1 2 1 6 4 3

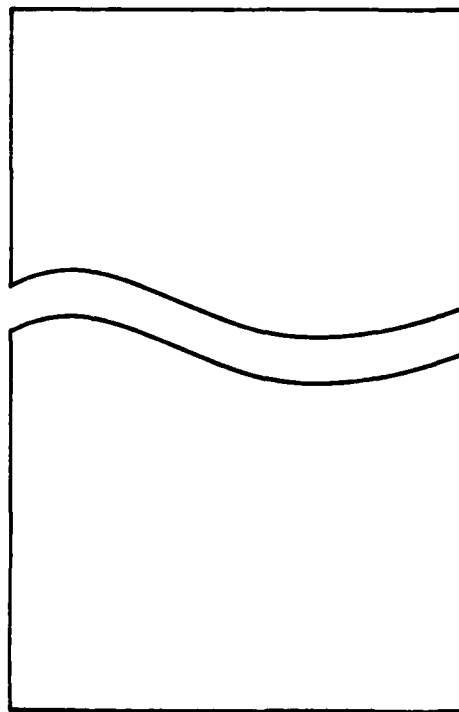
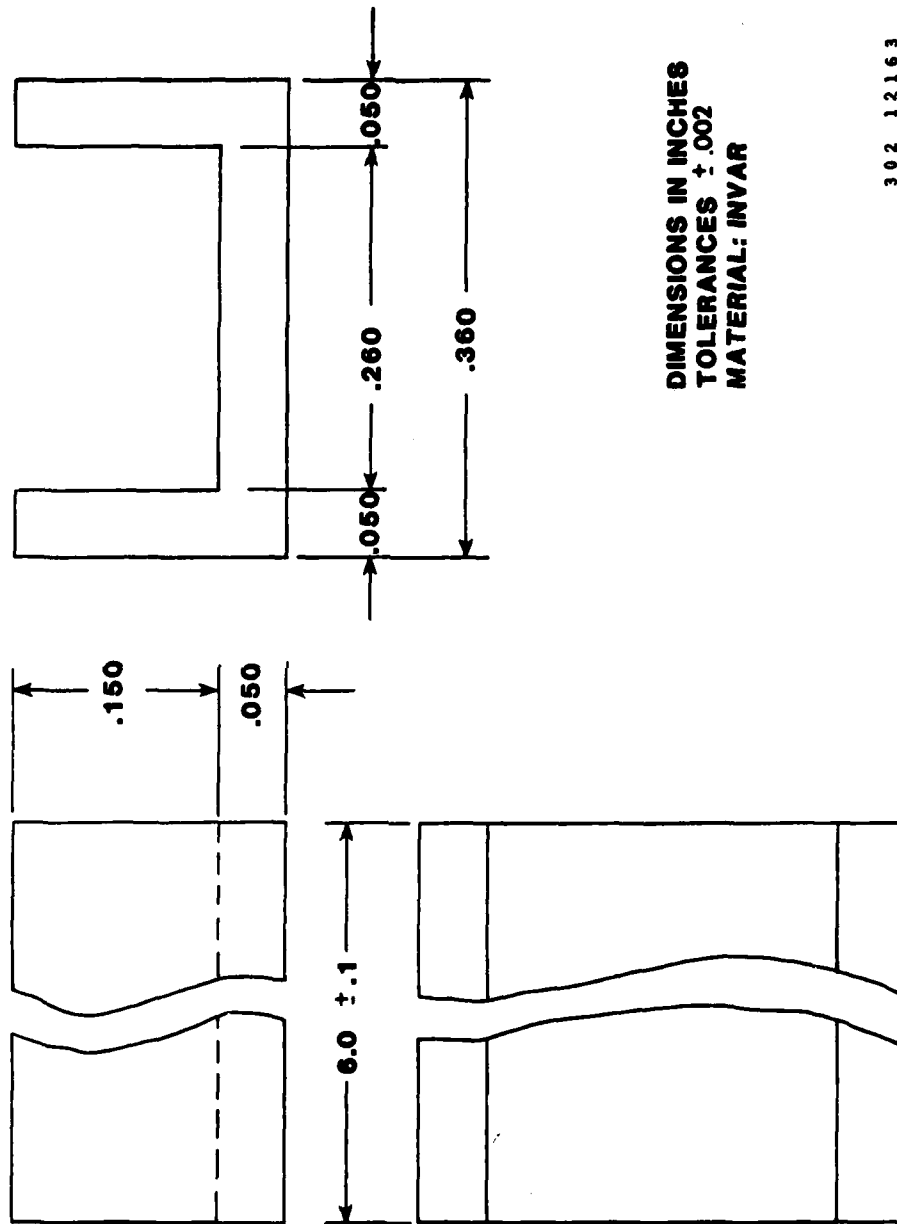


Figure 19. Lid for Star Couplers.



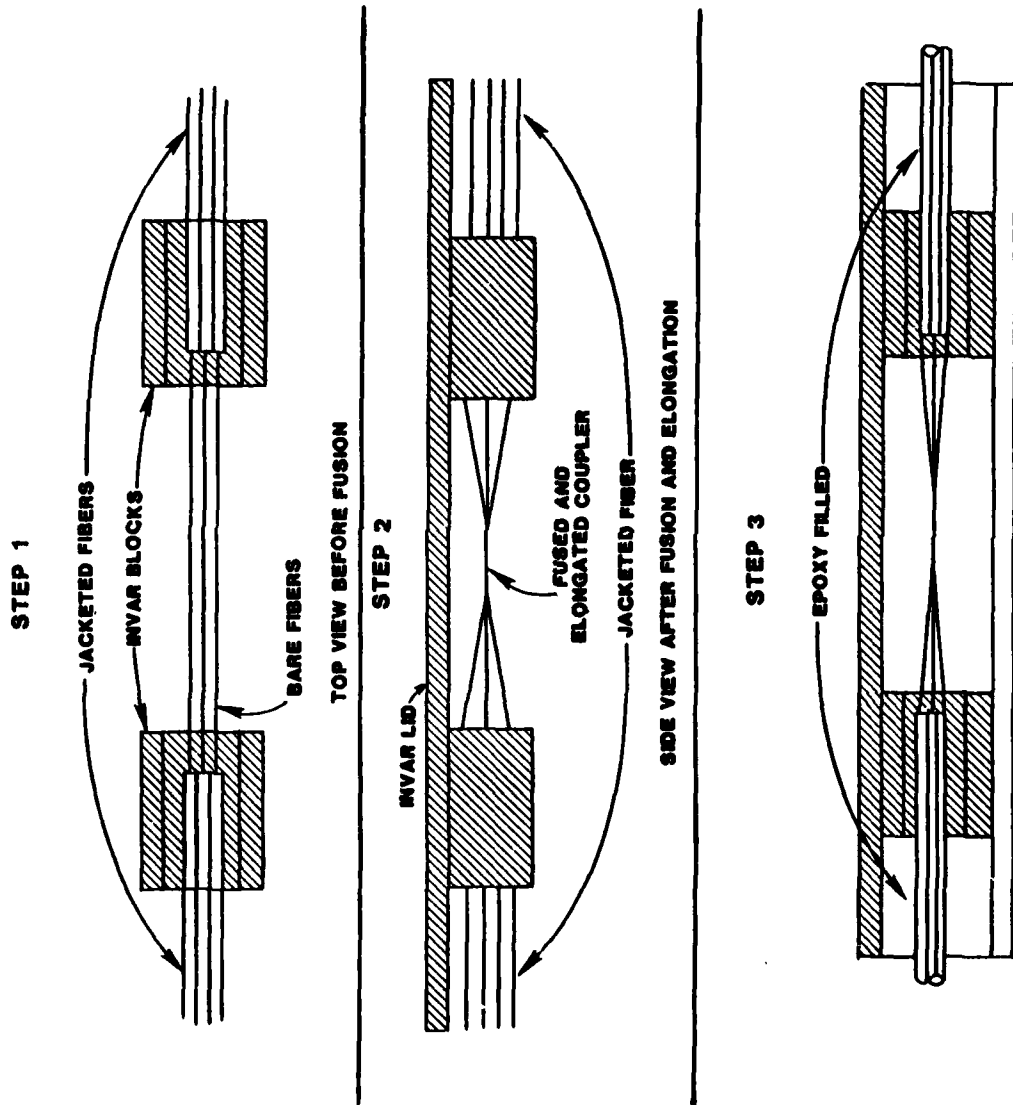
302 12163

Figure 20. Main Channel of Internal Star Coupler Package.

involved in the actual fabrication of the couplers are outlined in Figure 21 and are described in detail in the following paragraphs.

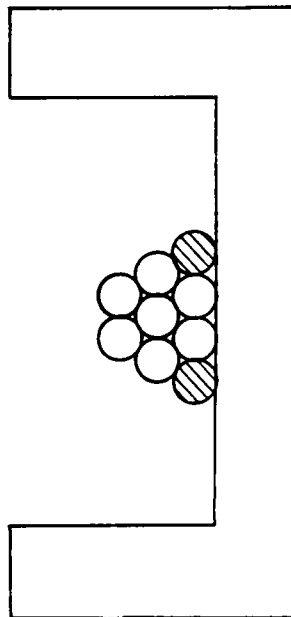
The first step in fabrication is to prepare the appropriate number of fibers for silver plating in the center of 3-4 m fiber lengths. The details of fiber preparation and silver plating are described in Appendix A. Once the fibers are silvered in this central region, they are stacked in Invar blocks as shown in step 1 of Figure 21. Cross-sectional views of the unique arrangements for 7- and 19-port couplers are shown in Figure 22.

The fibers were positioned one by one and permabonded in place. As each layer was completed a thin fillet of Torr-seal epoxy was placed over the jacketed portion of the fibers to ensure a lasting bond between the jackets and the Invar. Also, a length of approximately 1 millimeter of the silvered core material was covered with a small amount of Torr-seal epoxy bonding the fiber cores to the Invar blocks. This provided the strain relief needed for environmental stability.

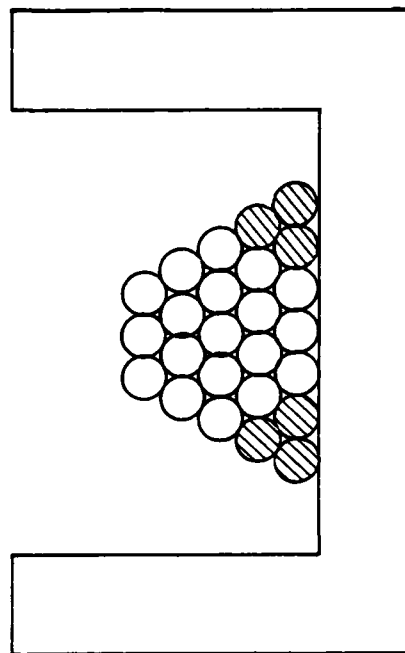


302 12161

Figure 21. Star Coupler Fabrication Steps.



**SEVEN PORT
STACKING ARRANGEMENT**



**NINETEEN PORT
STACKING ARRANGEMENT**

○ OPTICAL ACTIVE FIBERS

▨ "DUMMY" FIBERS FOR STACKING ONLY

3 0 2 1 2 1 6 2

Figure 22. Cross-sectional View of Fiber Stacks.

After curing each layer, another layer of the stack was added in the same manner. Once a complete stack was generated and cured, the etching and cleaning of the region to be fused began. The techniques of etching and cleaning explored are described in detail in Section V.2.0. A clean fiber surface was a prerequisite to beginning the tying and fusing step.

The two Invar blocks containing the stacked array of fibers were aligned on translation stages such that the surfaces were parallel and the distance between them matched the prepared fiber lengths appropriately before the stacking began. Therefore, the completed stacks did not need to be moved prior to fusing the coupler.

The fibers were brought into intimate contact by tying them at four points in the coupler region with cotton thread. The fused mixer region was created using a Water Welder[®] torch as has been described previously. The active monitoring described in the first part of this section was employed to optimize the fusion and elongation of the coupler in terms of optical performance.

When a satisfactory coupler was produced, the Invar lid was epoxied to the two Invar blocks to prevent any relative movement between the blocks that could cause coupler breakage. This lid also provides a means by which to move the coupler as a unit for installation in the long Invar channel of Figure 20. Step 2 of Figure 21 shows the package at the point of the lid attachment, and step 3 shows the general layout of the completed internal package after the "step 2 package" has been epoxied into the long Invar channel.

The fiber pigtails are epoxied to the long Invar channel in the region between the stacking blocks and the end of the channel as shown in step 3 of Figure 21.

This procedure yields the completed internal coupler package. At this point further measurements of optical performance were made and candidates for deliverable brass-board models were chosen.

3.0 External Packaging

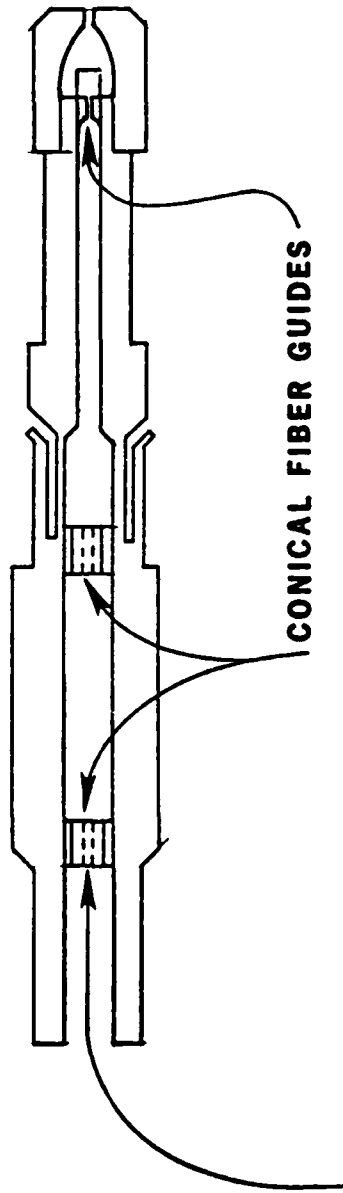
The candidates chosen for delivery were terminated using Hughes fiber optic contacts and were mounted in die-cast

aluminum boxes. The Hughes 20-pin multiway connector was mounted in the wall of the external package.

In order to terminate PCS fibers in the Hughes ferrule it was necessary to drill out the ferrule to allow the jacketed fiber to pass up to the head of the ferrule. The silver plated region of the bare fiber must be kept as short as possible. Figure 23 shows a cross-sectional view of the ferrules and points out the conical fiber guides that had to be drilled out.

The primary approach for termination was to silver plate the fibers and epoxy them into the ferrules; however, an additional step was explored which proved to be very beneficial in the termination procedure.

The plastic material Kynar[®], mentioned in Section V.3.0, was applied as a very thin coating over the silver plating. This served two purposes. It provided abrasion protection to the silver coating, and it filled any pores in the silver coating creating an interface far superior to the epoxy interface that would be introduced otherwise.



302 12130

Figure 23. Hughes Ferrule Modification.

The Kynar[®] was diluted with acetone to the point where a dip coating would apply a thin coating. The plastic was then heated briefly with a heat gun to cure the material properly.

The fiber ends so prepared were then placed in the ferrules with a small bead of epoxy being carried to the ferrule head on the fiber end. Tra-bond 2135B was used for this purpose, and the ferrules were cured at 75°C to prevent modification of the Kynar[®].

After termination, the couplers were mounted in the external package, and ferrules were inserted into the multiway connector using an appropriate insertion tool. The packaged couplers are pictured in Figure 24.

4.0 Brassboard Models

One brassboard model of each design of transmission star coupler was delivered at the end of this program. The devices delivered are pictured in Figure 24, and the measured optical performance of the devices is given in Tables 16, 17, and 18.

Table 18 contains the backscatter data compiled for the 7-port coupler. In all cases, the backscattered level was



Figure 24. Photograph of Completed Star Couplers.

Table 16
Seven-port Star Coupler Performance. Output Ports.

Injected Port	1	2	3	4	5	6	7	Total Excess Loss
1	-16.60	-16.40	-17.16	-16.44	-17.25	-16.83	-16.59	-8.30
2	-15.82	-15.40	-16.02	-15.82	-15.95	-15.01	-15.82	-7.23
3	-16.16	-15.46	-13.86	-15.70	-16.30	-15.58	-15.82	-7.03
4	-17.34	-17.43	-18.47	-19.10	-17.07	-18.02	-17.52	-9.35
5	-20.40	-20.55	-21.77	-22.22	-20.69	-20.97	-21.53	-12.66
6	-16.59	-15.95	-17.52	-17.34	-16.30	-16.83	-17.52	-8.37
7	-20.10	-21.25	-24.37	-23.78	-20.21	-20.65	-23.22	-13.18

Measurement through entire connected device

All loss measurements in decibels.

Excess loss as monitored during fusion of coupler: -5.9 dB

Table 17
Nineteen-port Star Coupler Performance.

A*		B**		A*		B**	
Input port P-P Loss	1.000	Input port P-P Loss	1.00	Input Port P-P Loss	2.00	Input Port P-P Loss	2.00
I	1.000	I	1.00	I	1.00	I	1.00
	-21.130		-22.58		-26.02		-27.04
I	2.000	I	2.00	I	2.00	I	2.00
	-24.260		-26.40		-25.05		-26.21
I	3.000	I	3.00	I	3.00	I	3.00
	-22.188		-24.91		-22.92		-24.14
I	4.000	I	4.00	I	4.00	I	4.00
	-24.638		-27.27		-27.04		-29.41
I	5.000	I	5.00	I	5.00	I	5.00
	-28.062		-31.37		-29.92		-32.04
I	6.000	I	6.00	I	6.00	I	6.00
	-22.041		-23.80		-25.84		-27.27
I	7.000	I	7.00	I	7.00	I	7.00
	-25.051		-26.60		-24.26		-25.67
I	8.000	I	8.00	I	8.00	I	8.00
	-23.010		-25.51		-25.05		-26.40
I	9.000	I	9.00	I	9.00	I	9.00
	-27.035		-28.68		-30.28		-32.04
I	10.000	I	10.00	I	10.00	I	10.00
	-26.812		-27.04		-25.67		-27.27
I	11.000	I	11.00	I	11.00	I	11.00
	-22.747		-23.80		-26.60		-28.36
I	12.000	I	12.00	I	12.00	I	12.00
	-27.270		-28.06		-23.80		-26.60
I	13.000	I	13.00	I	13.00	I	13.00
	-24.025		-25.67		-27.78		-30.28
I	14.000	I	14.00	I	14.00	I	14.00
	-22.264		-24.26		-24.38		-27.27
I	15.000	I	15.00	I	15.00	I	15.00
	-22.041		-24.14		-24.91		-27.78
I	16.000	I	16.00	I	16.00	I	16.00
	-21.829		-23.49		-27.27		-29.41
I	17.000	I	17.00	I	17.00	I	17.00
	-26.205		-29.03		-26.81		-29.03
I	18.000	I	18.00	I	18.00	I	18.00
	-23.590		-24.38		-25.84		-27.52
I	19.000	I	19.00	I	19.00	I	19.00
	-29.823		-31.37		-28.06		-30.28
Excess Loss		Excess Loss		Excess Loss		Excess Loss	
	-11.043		-12.82		-13.02		-14.87

*Losses through coupler plus two silver terminations in ferrules
 **Losses through entire connector device

Table 17
Nineteen-port Star Coupler Performance (Continued).

A*		B**		A*		B**	
Input port	12.00	Input port	12.00	Input port	17.00	Input port	17.00
P-P Loss		P-P Loss		P-P Loss		P-P Loss	
I	1.00	I	1.00	I	1.00	I	1.00
	-25.80		-24.91		-24.77		-26.21
I	2.00	I	2.00	I	2.00	I	2.00
	-27.52		-29.05		-29.03		-30.79
I	3.00	I	3.00	I	3.00	I	3.00
	-24.14		-25.84		-23.59		-25.05
I	4.00	I	4.00	I	4.00	I	4.00
	-28.06		-29.82		-26.60		-28.36
I	5.00	I	5.00	I	5.00	I	5.00
	-25.84		-28.06		-27.52		-29.82
I	6.00	I	6.00	I	6.00	I	6.00
	-24.91		-27.52		-23.36		-30.28
I	7.00	I	7.00	I	7.00	I	7.00
	-26.40		-28.36		-25.67		-27.27
I	8.00	I	8.00	I	8.00	I	8.00
	-33.80		-35.05		-26.40		-27.78
I	9.00	I	9.00	I	9.00	I	9.00
	-30.28		-32.04		-30.79		-32.04
I	10.00	I	10.00	I	10.00	I	10.00
	-24.91		-26.31		-28.06		-29.41
I	11.00	I	11.00	I	11.00	I	11.00
	-27.78		-29.82		-27.52		-28.68
I	12.00	I	12.00	I	12.00	I	12.00
	-26.21		-27.52		-25.20		-27.27
I	13.00	I	13.00	I	13.00	I	13.00
	-28.36		-29.41		-30.28		-32.04
I	14.00	I	14.00	I	14.00	I	14.00
	-23.91		-25.51		-26.02		-28.06
I	15.00	I	15.00	I	15.00	I	15.00
	-24.38		-25.67		-26.21		-28.68
I	16.00	I	16.00	I	16.00	I	16.00
	-24.91		-26.40		-27.78		-29.82
I	17.00	I	17.00	I	17.00	I	17.00
	-27.78		-29.82		-27.27		-29.82
I	18.00	I	18.00	I	18.00	I	18.00
	-24.91		-27.52		-28.68		-30.79
I	19.00	I	19.00	I	19.00	I	19.00
	-29.82		-32.04		-29.82		-32.83
Excess Loss	-13.35	Excess Loss	-15.07	Excess Loss	-14.16	Excess Loss	-15.97

*Losses through coupler plus two silver terminations in ferrules
 **Losses through entire connector device

**THIS PAGE IS BEST QUALITY PRACTICABLE
 FROM COPY FURNISHED TO BDC**

Table 17
Nineteen-port Star Coupler Performance (Continued).

A*		B**		A*		B**	
Input port P-P Loss	5.00	Input port P-P Loss	5.00	Input port P-P Loss	8.00	Input port P-P Loss	8.00
I	1.00	I	1.00	I	1.00	I	1.00
	-26.60		-29.03		-26.21		-28.06
I	2.00	I	2.00	I	2.00	I	2.00
	-26.21		-27.27		-27.27		-29.03
I	3.00	I	3.00	I	3.00	I	3.00
	-24.91		-27.27		-25.67		-27.78
I	4.00	I	4.00	I	4.00	I	4.00
	-27.52		-30.79		-28.36		-29.41
I	5.00	I	5.00	I	5.00	I	5.00
	-33.80		-35.05		-27.04		-28.68
I	6.00	I	6.00	I	6.00	I	6.00
	-27.27		-28.68		-29.03		-32.04
I	7.00	I	7.00	I	7.00	I	7.00
	-28.36		-30.79		-24.51		-26.40
I	8.00	I	8.00	I	8.00	I	8.00
	-24.38		-26.81		-35.05		-36.81
I	9.00	I	9.00	I	9.00	I	9.00
	-29.41		-30.79		-30.79		-32.83
I	10.00	I	10.00	I	10.00	I	10.00
	-26.60		-28.68		-27.04		-28.68
I	11.00	I	11.00	I	11.00	I	11.00
	-24.91		-26.81		-27.78		-29.41
I	12.00	I	12.00	I	12.00	I	12.00
	-28.36		-30.28		-25.05		-26.81
I	13.00	I	13.00	I	13.00	I	13.00
	-26.60		-28.06		-26.40		-27.78
I	14.00	I	14.00	I	14.00	I	14.00
	-24.77		-26.60		-24.26		-26.02
I	15.00	I	15.00	I	15.00	I	15.00
	-26.81		-27.78		-25.51		-26.60
I	16.00	I	16.00	I	16.00	I	16.00
	-20.79		-27.78		-24.91		-26.81
I	17.00	I	17.00	I	17.00	I	17.00
	-30.28		-32.83		-29.82		-32.04
I	18.00	I	18.00	I	18.00	I	18.00
	-27.52		-29.82		-27.27		-29.41
I	19.00	I	19.00	I	19.00	I	19.00
	-29.03		-30.28		-29.03		-30.28
Excess Loss	-13.48	Excess Loss	-15.98	Excess Loss	-14.05	Excess Loss	-15.79

*Losses through coupler plus two silver terminations in ferrules
 **Losses through entire connector device

Table 18
Backscatter Data. Seven-port Star (Delivered Device).

INJECTED PORT	OTHER INPUT PORTS						
	1	2	3	4	5	6	7
1	-	-37.2	-38.1	-41.1	-41.1	-44.1	0
2	-39.4	-	-38.1	-41.1	-44.1	-41.1	-44.1
3	-41.1	-44.1	-39.4	-	0	-44.1	0

Above measurements taken with dry fiber ends on output fibers. When ends were submersed in index matching fluid the backscatter was beyond the dynamic range of the measurement equipment (i.e., greater than -50 dB)

greater than 37 dB below the injected level. For some ports the level was beyond the dynamic range of the measurement equipment which was about 50 dB below the injection level.

SECTION IX

ACTIVE COUPLERS

As part of this task's work, a number of potential techniques for multimode fiber active coupler applications were identified. The following is a list of the potential candidate methods that was compiled on the basis of very preliminary considerations and was intended as the starting point for more thorough technique study.

Acousto-optic Effect

- o Bulk
- o Saw

Electro-optic Effect

Electro-absorption Effect

- o Franz-Keldysh Effect

Liquid Crystal

Electro-chromism

Nonlinear Absorption

Of these six potential techniques, three were isolated for further study on an experimental basis. These were (1) Electro-absorption (Franz-Keldysh Effect), (2) Acousto-optic Interaction, and (3) the Electro-optic Effect.

Experiments were performed for both the Acousto-optic Effect and the Franz-Keldysh Effect. The Electro-optic Effect was examined in theory only.

The results of the Acousto-optic investigation were moderately successful, and this technique has good potential for certain applications. This topic is covered in detail in Section IX.1.0.

The investigation of the Electro-absorption Effect, in general, was not very successful, although its potential for single mode use appears good. This subject is covered in detail in Section IX.2.0.

1.0 Acousto-optic Interaction

The acousto-optic interaction between light and acoustic waves in a photoelastic medium is well understood and has been used extensively in the recent past for switching, scanning, and mode-locking laser beams. Efforts in the field to date have resulted in the successful development of several new acousto-optic materials to extend operation of devices to high speeds. In view of the tremendous progress that has been made in fiber optics recently and the constant improvement in acousto-optic device performance, it is natural to explore the problem of switching light emitted from optical fibers.

1.1 Theory

Sound waves traveling in a photoelastic medium create periodic strains which produce periodic changes in the index of refraction of the medium via the photoelastic constants. If light is passed through the medium, these periodic refractive index changes perturb the motion of light producing changes in both its frequency and momentum. Since, in the acousto optic interaction both energy and momentum are conserved, the light beam and acoustic wave can interact only if the following relations are satisfied:

$$\omega_s = \omega_i \pm \Omega \quad \text{conservation of energy}$$

$$k_s = k_i \pm K \quad \text{conservation of momentum}$$

where K and Ω are the acoustic wavevector and angular frequency and k_i and ω_i are the optical wavevector and angular frequency for the incident and scattered optical waves.

Assuming the medium is isotropic, the above relations are satisfied when the incident optical wavevector makes an angle θ_β (called the Bragg angle) with the acoustic wavefront where

$$\sin \theta_\beta = 1/2 \frac{|\underline{\vec{k}}|}{|\underline{\vec{K}}|}$$

In this case, the scattered optical wave makes an angle $-\theta_\beta$ with the acoustic wavefront, the total angle through which the light is scattered being $2\theta_\beta$. Since θ_β is normally small, we have for the angle outside the deflector

$$\theta_\beta = 1/2 \frac{\lambda_0}{V} f$$

where V is the acoustic velocity, f the acoustic frequency and λ_0 the wavelength of light in air.

Figure 25 shows the geometry of the input and output beams relative to the acoustic column for isotropic materials, such as lead molybdate, glass, and tellurium dioxide, which are commonly used in modulators¹. When the Bragg condition is satisfied, the angle of incidence and the angle of diffraction are identical, and the direction of acoustic energy flow exactly bisects the incidence and exit angles.

The intensity of the first order beam is given by the equation¹

$$\frac{I_1}{I_0} = \rho \left(\sin^2 \frac{\pi}{\lambda} \sqrt{\frac{M_2 L P_a}{2H}} \right) \left(\text{sinc}^2 \frac{\pi L \alpha}{\lambda} \right) \quad (2-1)$$

where:

I_1 = Intensity of first order beam

I_0 = Intensity of zeroth order beam when the acoustic energy in the medium is zero

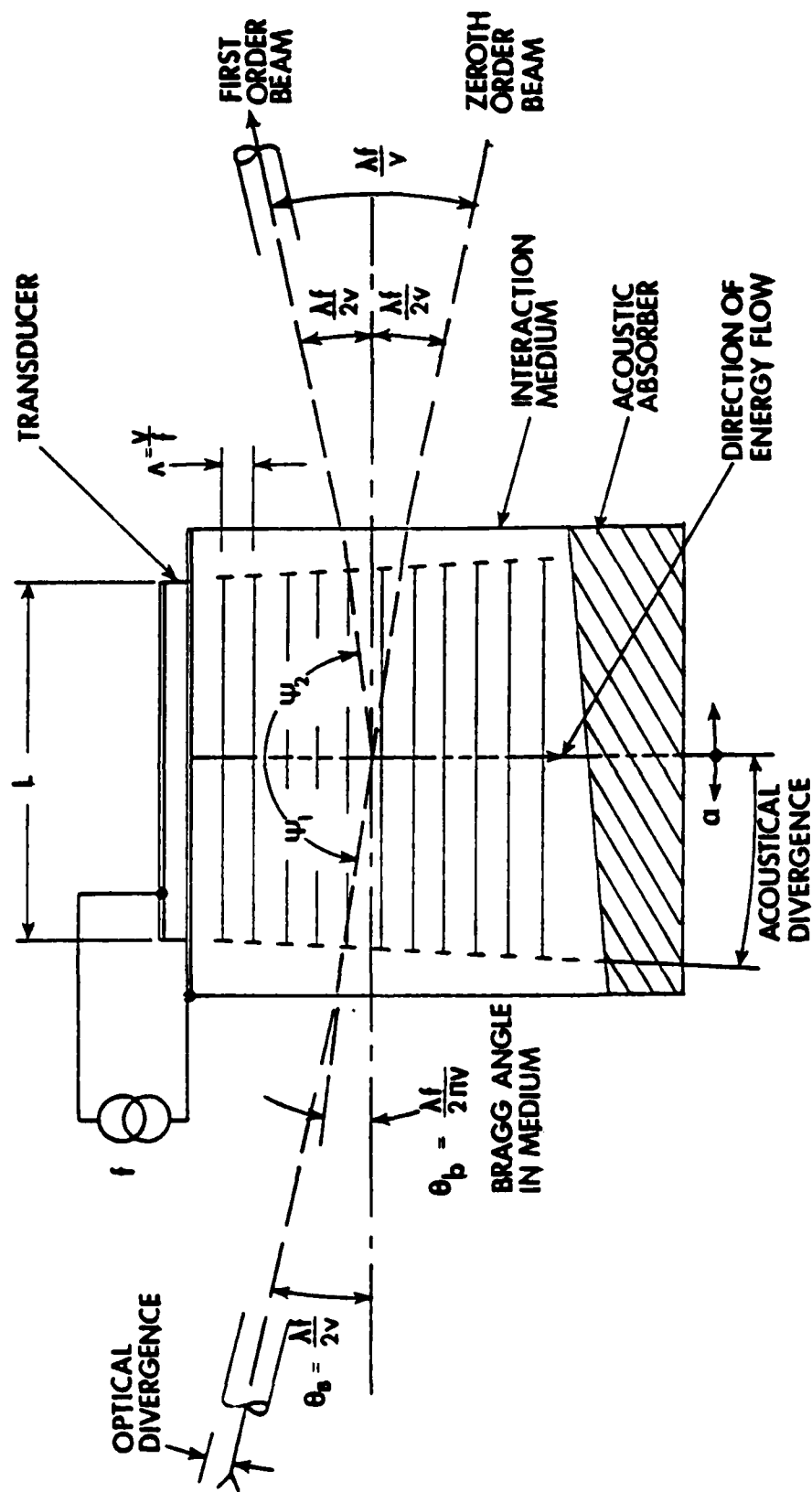
ρ = A variable <1 which is related to the acousto-optic Q of the Bragg cell and to the ratio of the optical beam divergence to the acoustic column divergence

λ = Laser wavelength in free space

M_2 = Elasto-optic figure of merit of the interaction medium ($= 36.3 \times 10^{-15} M^2/w$ for lead molybdate)

P_a = Acoustic power in the interaction medium = a constant times the electrical input power to transducer

¹ Application Note AN 772A, Isomet Corporation, 5263 Port Royal Road, Springfield, VA 22151



302 11000

Figure 25. Geometry of Input and Output of Acoustic-optic (A-O) Device.

L = Interaction length

Λ = Acoustic wavelength in medium = $v \div f$ =
acoustic velocity \div acoustic frequency

α = Bragg angle error

The portion of the light, ρ , diffracted into the first order is a complicated function of β , where

$$\beta = \frac{\pi}{2} \frac{\theta_o}{\theta_a},$$

and

θ_o = optical divergence in medium

θ_a = acoustical divergence in medium.

A plot of this factor is shown in Figure 26. Typically, for a modulator used with a laser beam (~1 mm diameter) more than 90% of the incident light can be diffracted into the first order beam.

The second factor in the equation for I_1/I_0 gives the diffracted intensity as a function of modulator drive power P_a . When $P_a = \lambda^2 H / 2M_2 L$, the diffracted power is a maximum relative to the first and third factors of the equation. Note the dependence on λ^2 which does imply some penalty for operation at longer wavelengths.

The third factor in the equation adjusts the result for Bragg angle error, α , due to beam divergence or misalignment. It

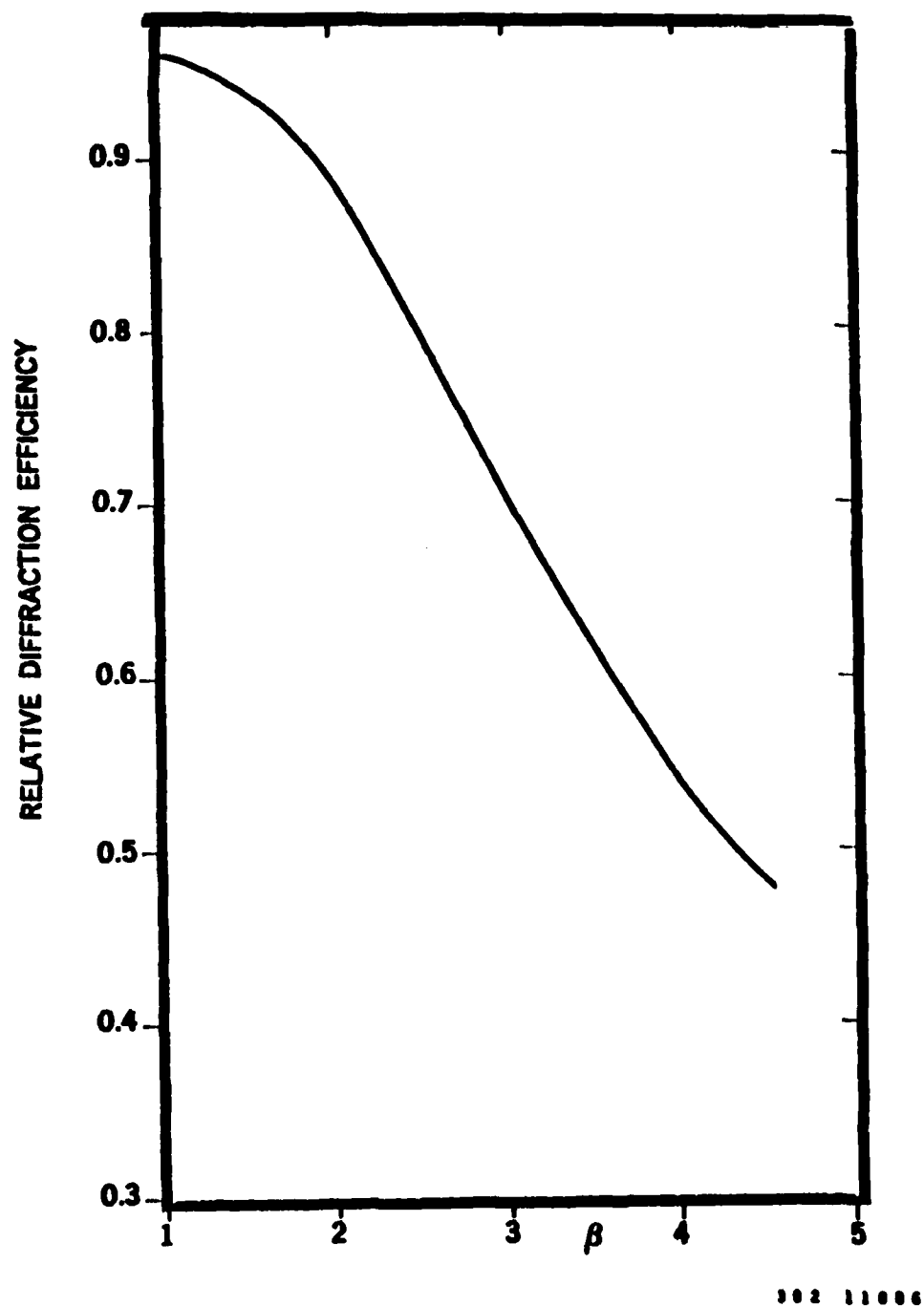


Figure 26. Variation of Intensity in A-O Modulator.

is this factor that is important when dealing with radiation from a nonlaser source that has a divergence larger than the diffraction limit. In Figure 27, this factor is plotted as a function of L/L_0 , where $L_0 = (n/\lambda) (v/f_0)^2$ is a characteristic interaction length, and δ/θ_β , where $\delta = \alpha \cdot n$ and n is the index of refraction of the medium.

1.2 Predicted Performance

In this section, the expected performance of the fiber acoustic switch will be evaluated based upon the theory outlined above. The configuration of the switch or modulator is as shown in Figure 28. The light from the input multimode fiber is collimated by a graded index (GRIN) lens. After traversing the acousto-optic switch, the light is then recaptured and focused onto one of two output fibers by a single GRIN output lens. The fibers have a core diameter of approximately 50 μm , a numerical aperture (NA) of .25 or .50, and propagate many thousands of modes. Although standard bulk lenses could be used, GRIN lenses were epoxied to the fibers in order to eliminate Fresnel reflections and because the GRIN lenses are compact and convenient to use. After collimation by the lens, the beam emitted by a 50 μm core,

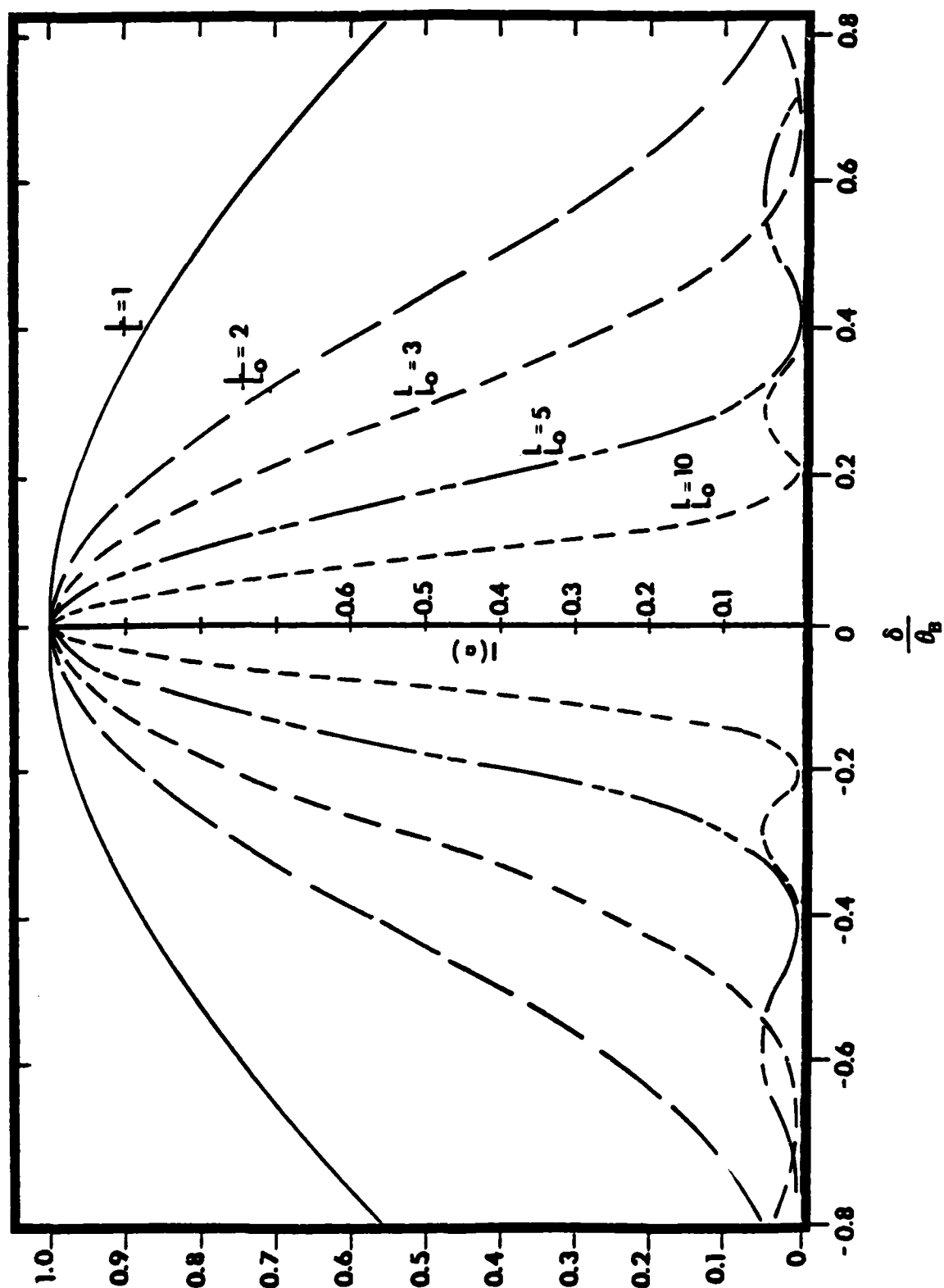
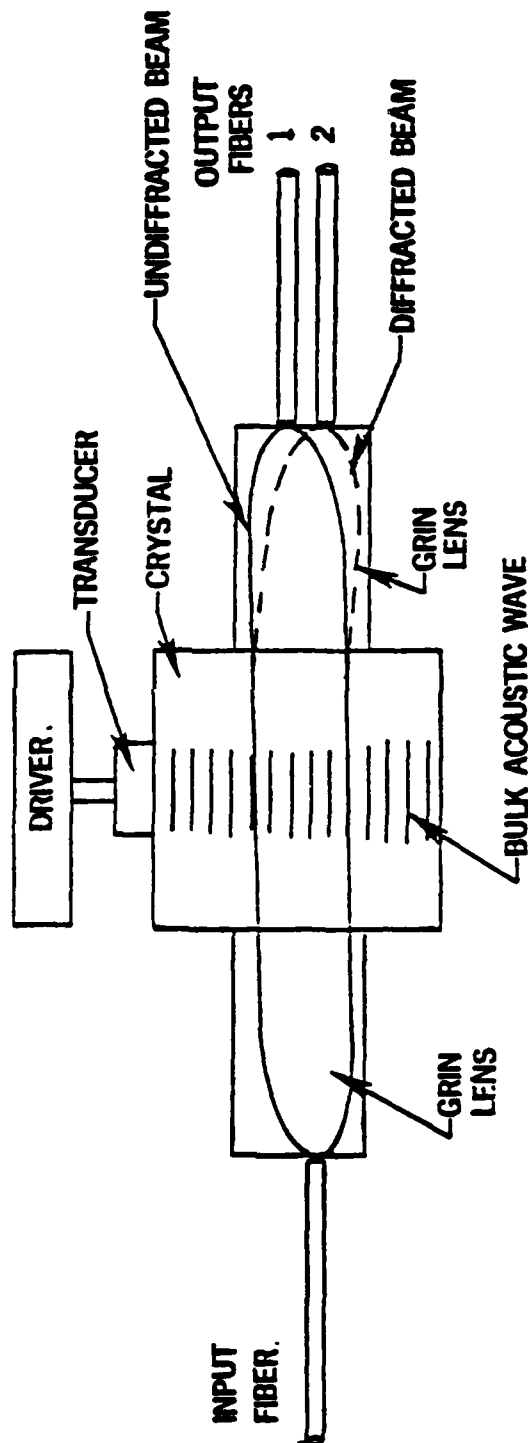


Figure 27. Intensity Variation vs Bragg Angle Error.

302 11000



302 11001

Figure 28. Configuration of Switch or Modulator.

.25 NA fiber will be about 1 mm wide and $\pm .75^\circ$ in divergence in air.

The modulator used in the experiments was purchased from Isomet Corporation¹ (Model No. 1206-1). The device interaction medium is lead molybdate (PbMoO_4). Specification for this switch when used with a He-Ne laser beam include 1 mm active aperture, 30 dB contrast ratio, 1.6 watts drive power for 85% deflection efficiency, only 3% static insertion loss, and a bandwidth (for a 1 mm beam) of 2 MHz. The complete 1206 specification sheet is reproduced in Table 19. In addition, a Model 223-2 digital driver was also purchased to provide the required 110 MHz drive frequency and 1.6 watts of power. The driver requires 450 mA at 28 Vdc and a transistor-transistor logic (TTL) signal.

Clearly, the acousto-optic interaction is highly effective as a laser beam modulator or switch as indicated by the above specifications. The performance is significantly

Table 19

Model 1206-1 Specification Sheet.

SPECIFICATIONS

Spectral Range:	440-633 nm, others on special order
Interaction Medium:	Lead Molybdate (PbMoO_4)
Acoustic Velocity:	3.63 mm/ μs
Active Aperture:	1 mm
Center Frequency, C.F.:	110 MHz
RF Bandwidth, Δf :	46 MHz
Input Impedance:	50 Ω nominal
VSWR:	<1.5:1 @ 110 MHz
Optical Power Density:	250w/mm ² focussed
Contrast Ratio, DC:	>1000:1

PERFORMANCE VS. WAVELENGTH

Wavelength (nm):	442	515	633
RF Drive Power (w):	0.8	1.0	1.6
Bragg Angle (mr):	6.7	7.8	9.6
Beam Separation (mr):	13.4	15.6	19.2
Static Insertion Loss (%)*:	10	3	3

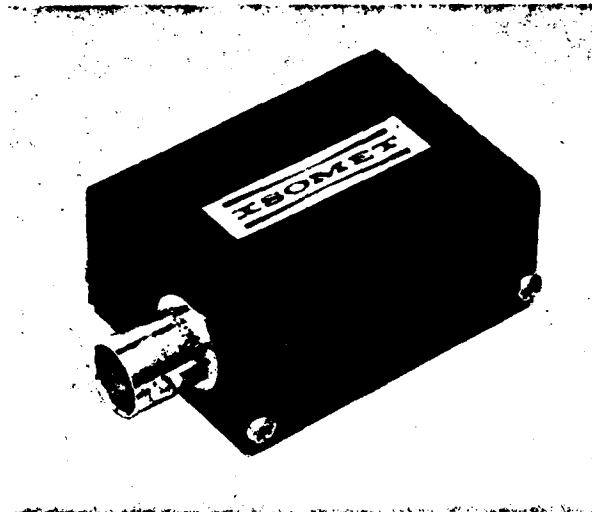
PERFORMANCE VS. BEAM DIAMETER

Beam Dia. (mm):	1.0	0.34	0.2	0.084
Video Rise Time (ns):	180	60	35	15
Video Bandwidth (MHz):	2	6	10	25
Deflection Eff. (%):	85	85	80	60

*On special order, narrow band V-coat can be supplied with reduced insertion loss at specified wavelength.

Table 19

Model 1206-1 Specification Sheet (Continued).



APPLICATIONS

- Wideband Modulator
- Frequency Shifter

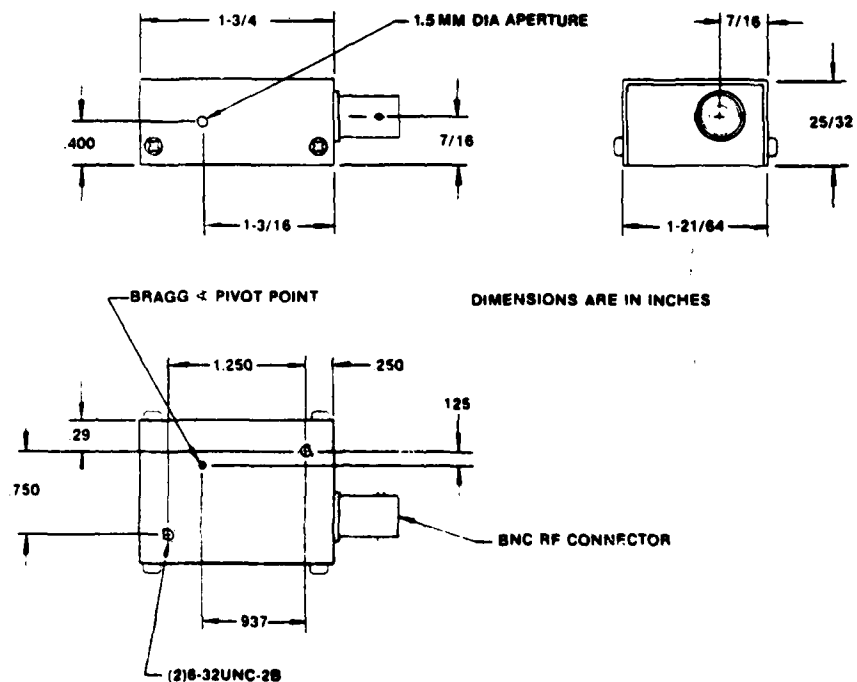
FEATURES

- 25 MHz Video Bandwidth
- Low Drive Power
- Small Size
- Good Temperature Stability

EXPLANATION OF MODEL NUMBER

BASE MODEL 1206 - 1
WAVELENGTH
-1, 440-633 nm

OUTLINE DRAWING



modified, however, when using a collimated fiber beam with the relatively large divergence of $\pm .75^\circ$.

1.2.1 Static Insertion Loss

Insertion loss contributions in the passive unswitched state may arise from three principal sources:

- a. Attenuation in the crystal itself
- b. Loss in reflections at interfaces between fibers, lenses, and crystal
- c. Loss due to fiber coupling with lenses

The first factor will not make a significant contribution to the loss, since the optical transmission of lead molybdate (PbMoO_4) has an attenuation of less than a few percent per centimeter over a wavelength range of $.4 \mu\text{m}$ to $5.5 \mu\text{m}$.

The second factor, reflection loss, may be nearly eliminated by using antireflection (AR) coatings. This is particularly true if graded index lenses are used, since the glass/air and PbMoO_4 /air interfaces are eliminated, and only the glass/ PbMoO_4 interface must be addressed. Since the index of PbMoO_4 is 2.37, a one layer coating with index 1.89 will eliminate this reflection. Without this coating the total reflection loss is .5 dB.

The third factor, coupling of multimode fibers with lenses, is somewhat more complicated than the first two. Losses may arise from inherent diffraction loss, lens aberrations, or imperfections in the lens surface or body. Simple lens defects will not be a significant source of loss for commercial high quality aspheric lenses, but somewhat less is known about the quality of graded index lenses. In particular, some preliminary measurements with graded index lenses at EOPD indicate that the length of the lens is not always cut and polished to a high accuracy. This problem may be corrected with tighter control on purchased parts or by polishing to the correct length at EOPD.

Also at this moment, the theory of diffraction losses from multimode fibers using graded index lenses is not well understood, and less is known about aberrations relative to bulk lenses. Researchers in Japan have reported fiber to fiber coupling losses of well under 1 dB using Selfoc[®] lenses. These results have not been reproduced at EOPD and 2 dB is a safe assumption for the fiber to fiber coupling loss, with an additional .5 dB of loss due to the acoustic-optic (A-O) crystal.

1.2.2 Loss in Switched State

The diffraction efficiency of the A-O switch is given by the product of the three factors in Equation (2-1). The first factor, ρ , is related to the ratio of the optical divergence to the acoustical divergence. From Figure 26, it can be seen that about 90% of the light will be deflected if the optical divergence is about the same as the acoustic divergence. For most practical modulators, the acoustic divergence is of the order of tenths of a degree. For a typical single mode laser beam, approximately 500 μm diameter, the divergence will be approximately $.1$ to $.2^\circ$ and ρ will be approximately 90%. However, using a multimode fiber with a standard 2 mm diameter, .5 NA GRIN lens results in a beam divergence of about $\pm .3^\circ$ in the crystal. This divergence is larger than that of the acoustic beam and part of the light will be poorly deflected. From Figure 26, the loss will be approximately 1.5 dB.

The second factor in Equation (2-1) can be 100% if the acoustic power is adequate, and this in turn is related to the wavelength and interaction length. For standard modulators operating at $.633 \mu\text{m}$, the power requirement, 1.6 watts, is easily obtained for full 100% deflection.

Note, however, that this required power does increase with λ^2 so that long wavelength operation is somewhat more difficult.

The third factor in Equation 2.1 is again related to the divergence angle of the optical beam. Assuming that the alignment of the beams can be accomplished accurately, then the variation from the exact Bragg angle is given by the divergence of the collimated optical beam. With GRIN lenses and a $.3^\circ$ divergence in the crystal and $\theta_\beta = .6^\circ$ as is typical, then δ/θ_β in Figure 27 is .5. For an interaction length of $L/L_0 = 2$, then 80% of the optical power will be deflected, as estimated from Figure 27.

Combining the loss from the three factors gives 1.5 dB from part 1, 0 dB from 2, and 1 dB from part 3 or a total of 2.5 dB loss due mainly to the divergence of the collimated optical beam. Another 2.5 dB of loss may be expected from the passive coupling, as described in the preceding section, for a total attenuation of 5.0 dB.

1.2.3 Contrast Ratio

The contrast ratio (or on/off ratio) is excellent for the switched output port when using a laser beam. Greater than 30 dB isolation is typical for an A-O device, limited only by the small amount of scattering in the high optical quality crystal. This contrast ratio may be severely degraded in the fiber optic switch if the divergence of the collimated beam is large and a portion of light incident on one port overlaps the other.

For the straight through or unswitched beam, the on/off ratio of an acousto-optic switch or modulator is much worse. Even for a laser beam, the best that can be expected is about 90% deflection efficiency or 10:1 on/off ratio. Since the deflection efficiency predicted for the multimode case is 2.5 dB or about 56%, the on/off ratio will be a little better than 2:1.

1.2.4 Speed

The speed of response of an A-O device is directly related to the width of the optical beam. This is due to the transit time of the acoustic wave across the optical beam. For PbMoO_4 with $V = 3.63 \text{ mm}/\mu\text{s}$, the rise time (or fall

time) for a 1.0 mm beam is 180 ns.

1.2.5 Operating Wavelength

PbMoO_4 is transparent and operable from .4 μm to 5.5 μm , but the required acoustic power is proportional to the square of the wavelength. For convenience, tests were run on the device at .6328 μm . However, longer wavelengths can be used and the only penalty will be increased radio frequency (rf) drive power.

1.2.6 Size

The volume occupied by the crystal, transducer, and the coupling optics is quite small. The entire device can be contained in a volume approximately 2 x 3 x 5 cm. The associated drive electronics is somewhat larger.

1.3 Experimental Results

Preliminary experiments were carried out using the Model 1206 modulator and a He-Ne laser. These tests verified the excellent switching performance expected for a highly collimated source. The results are presented in Table 20 and can be summarized as follows: deflection efficiency 91%, static insertion loss 10%, contrast ratio about 30 dB.

Table 20
Performance of Modulator with He-Ne Laser.

	<u>I_1 (μW)</u>	<u>I_2 (μW)</u>
V Off	950	<1
V On	80	800

Input = 1050 μ W

Fiber to fiber coupling was then used with the modulator using a single input and single output fiber with .25 NA, 55 μm core. The full NA of the fiber was injected with He-Ne by using two microscope objectives to generate a .30 NA incident beam. A 2 mm diameter GRIN lens with .50 NA was used to expand the fiber beam to about 1.2 mm and collimate to about $\pm .7^\circ$ in air, and an identical lens was epoxied to the output fiber. Initial adjustment of the modulator was made by projecting the collimated beam on the wall and orienting the crystal to obtain the best switching action. Then the output fiber and lens were scanned across the output face of the crystal to measure the deflected and undeflected intensities with and without applied voltage.

Lowest attenuation was obtained for the undeflected beam, as expected, with 6 dB insertion loss and 54% deflection efficiency. The deflection efficiency is in good agreement with estimates made in the previous section. However, the fiber coupling loss is considerably higher than predicted and is due to two additional factors not included before: spreading of the collimated beam and PbMoO_4 /air reflection losses. Although the lensed beam is collimated, the $\pm .3^\circ$

spread in the crystal causes the beam to widen as it traverses the 2-3 cm distance between fibers. The larger beam diameter is completely captured by the output GRIN lens and focused on the output fiber face. However, the portion of the beam wider than the original collimated beam will be incident on the fiber at an angle larger than the fiber NA and not captured.. This results in a loss estimated at about 1 dB. The other factor, Fresnel reflections, adds another 2 dB to the total loss, although in an actual switch this loss could be almost entirely eliminated. Thus, these two factors alone account for 3 of the 6 dB observed loss. The remaining 3 dB is due to lensed coupling losses and a small amount of attenuation in the crystal. The output fiber was traversed across the end of the crystal to measure the deflected beam intensity. However, due to the spreading of the optical beam and the small angle of diffraction, it was difficult to detect another distinct maximum that represented the deflected beam. Instead, the intensity gradually decreases as the fiber is moved from the undeflected maximum. However, the on/off ratio does become a maximum at a particular position which can be called the deflected beam. At this point, the throughput loss was 12 dB and the on/off ratio was 23:1 or 13.5 dB. The loss of the deflected beam is considerably

larger than predicted and is due to the changed angle of the deflected beam. Again, the entire beam is captured by the output lens, but the incident light now exceeds the fiber NA. This can be corrected, in theory, by properly angling the receiver fiber. However, this would be difficult to construct in the actual switch and was not done during these experiments. The on/off ratio of 13.5 dB is also less than the 30 dB that might be expected and is due to leakage of light, due to the lensing process, from the undeflected position into the deflected output position.

These preliminary experiments failed to demonstrate the optimum performance that is possible using acousto-optics with multimode fibers. One of the main problems is the incident light not being at the proper angle for capture by the limited NA of the fiber. This can be corrected for the deflected beam by angling the output fiber. Also, a smaller interaction region and therefore a lesser distance between GRIN lenses would limit the loss due to NA expansion for both the undeflected and deflected beams. Finally, a device with a larger Bragg angle would allow greater physical separation of the two output beams and much better

cross talk isolation. Operation at longer wavelengths would be beneficial in this respect since the Bragg angle does increase directly with wavelength. It was not possible to obtain a second iteration on the device design and angling of one fiber with respect to the other is a more difficult procedure than planned for these preliminary investigations. However, it was possible to eliminate most of the loss associated with the angular expansion and deflection of the collimated beams by using large NA fibers on the output, i.e., 50 μ m core, .50 NA, high loss fibers. This proved to be very successful at reducing throughput losses. For the undeflected beam, total fiber to fiber loss was 3 dB with 56% modulation depth. Of that 3 dB loss, 1 dB is due to the diameter mismatch on the input and output and about .5 dB is from Fresnel reflections ($n = 1.5$ index fluid was used between lenses and crystal). For the deflected position, which is not well defined due to the small Bragg angle and beam overlap, the loss was 6 dB with 90% modulation depth (10:1 on/off ratio). The loss of 6 dB arises from the 3 dB passive loss and 50% deflection efficiency.

In order to better simulate action as a switch, it was desirable to use a dual fiber termination on the output, as opposed to scanning one fiber across the output of the crystal. This was not possible with the standard 125 μm outer diameter (od), 55 μm core fiber, since the core separation of these two fibers would be too large for the Bragg angle of the switch. These cores could have been placed closer together by etching the cladding, but it was easier to use the high loss fibers with 55 μm od and 50 μm core diameter and high NA. Two such fibers were epoxied and polished in a ferrule with the fibers adjacent to each other and the resulting dual fiber termination used on the output of the crystal. The maximum performance was obtained by positioning the fibers through trial and error. Loss of 6 dB for each port was obtained simultaneously with 2.5:1 and 10:1 on/off ratio for the undeflected and deflected beams, respectively.

The results from all of the fiber coupling experiments are summarized in Table 21. Although the performance is not as good as could be expected with all parameters optimized, reasonably good switching has been obtained. Additional work in this area to optimize the switch by decreasing the

Table 21

Results of A-O Device.

Input: 55 μ m core, .25 NA
Output: 55 μ m core, .25 NA single fiber
Results: Position 1 - 6 dB loss 54% modulation depth
Position 2 - 12 dB loss 90% modulation depth

Input: 55 μ m core, .25 NA
Output: 50 μ m core, .50 NA single fiber
Results: Position 1 - 3 dB loss 56% modulation depth
Position 2 - 6 dB loss 90% modulation depth

Input: 55 μ m core, .25 NA
Output: 50 μ m core, .50 NA dual fiber
Results: Port 1 - 6 dB loss 60% modulation depth
(2.5:1 on/off)
Port 2 - 6 dB loss 90% modulation depth
(10:1 on/off)

length of the interaction region and increasing the Bragg angle and to improve the fiber coupling by angling the fibers and decreasing passive lensed coupling losses could result in a low loss, relatively high efficiency switch or modulator. Ultimate performance may be less than 2 dB loss in the passive state and 4 dB for the deflected beam. Isolation of 20 to 30 dB between the beams should also be possible.

2.0 Franz-Keldysh Effect

2.1 Theory

The Franz-Keldysh effect refers to the shift in the absorption band edge of a semiconductor or insulator due to an applied electric field¹. Application of an electric field to the material can result in an increase or decrease in the carrier energy state with the result that the photon energy required for an interband transition is decreased. All insulators and semiconductors experience this effect,

¹N. Bottka. Optical Engineering. 17, 530 (1978).

but only direct band gap materials are useful as modulators. Table 22 illustrates the broadening of the band edge for GaAs¹.

A typical device configuration consists of a direct band gap material, such as GaAs, and a narrow band optical source, preferably a laser, with a center wavelength close to the absorption edge of the modulator. Application of an electric field to the modulator causes the absorption edge to shift to longer wavelengths, and the laser emission which was previously transmitted is now attenuated. Thus, a Franz-Keldysh device does require careful matching of the source and the modulator. Another drawback of the Franz-Keldysh effect is that it is only possible to produce a modulator. There is no feasible switch configuration.

An advantage of the Franz-Keldysh effect is that the device may function in a data bus both as a detector and

Table 22
Broadening of GaAs Band Edge.

<u>Field (V/μm)</u>	<u>Band Edge Broadening (\AA)</u>
.01	1.3
.10	6.1
1.00	28.00
10.00	132.00

a modulator. Photons absorbed in the material generate hole electron pairs which then migrate to electrodes, forming a photogenerated current. In fact, with the rather high electric fields used with the Franz-Keldysh effect, avalanche photodetection is easily possible.

A modulator that may also function as a detector would be extremely useful in a "bit-deletion" data bus, shown in Figure 29. For this type of data bus there is one optical source that continuously sends a stream of data bits along the bus. Individual terminals modulate this data stream in order to send information. Using a Franz-Keldysh detector/modulator would eliminate the need for a data bus tap to a separate detector. For a bit deletion data bus with Franz-Keldysh modulator/detector, an entire optical send receive terminal with source, detector, and optical "T" couplers would be replaced by one in-line semiconductor device and probably simpler electronics.

There are two main electric field configurations possible for the Franz-Keldysh modulator: field parallel to the light propagation and field perpendicular to the light propagation direction. For the field parallel to the

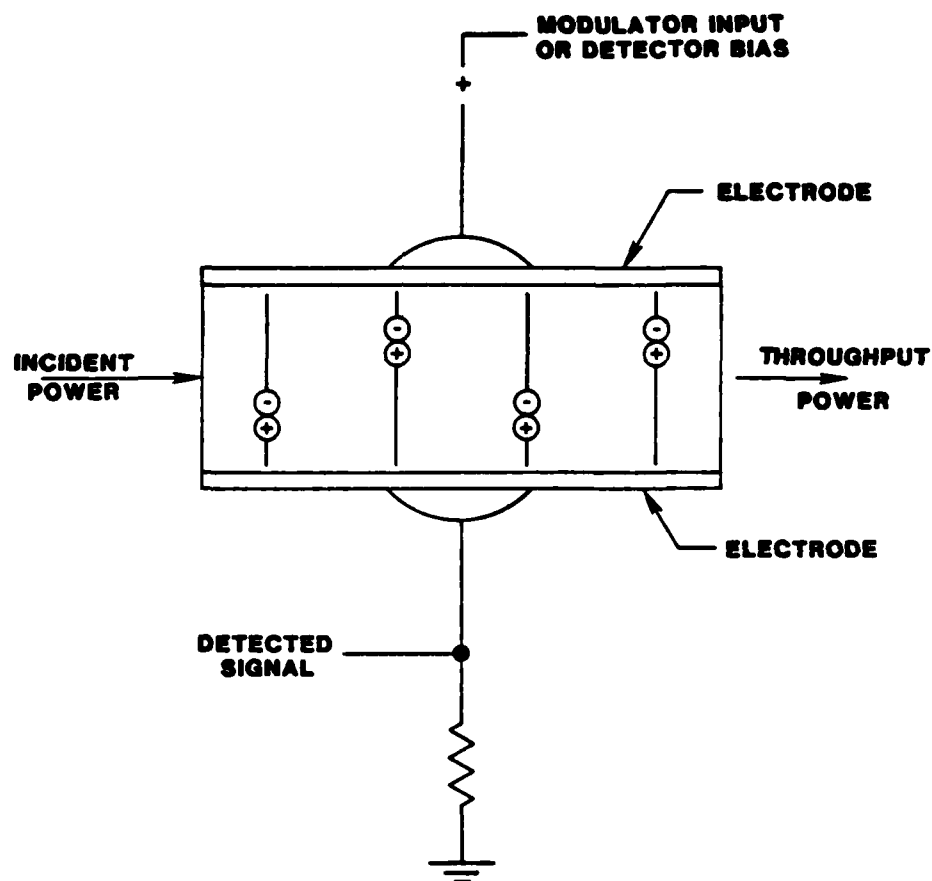


Figure 29. Modulator/detector For
"Bit Deletion" Data Bus.

propagation direction, the electrodes must be transparent and, in general, larger voltages are required since the voltage must be applied across the entire path of light travel in the crystal. This is not a preferred orientation when using an insulator, unless the diameter of the light spot is very large. Otherwise, the waveguide configuration (field perpendicular to the propagation direction) is more natural. In this case, the light is confined by the material (or focused to a small spot size as it traverses the material), so that the thickness and hence voltage is kept small for a given electric field. The interaction length of the light and the insulator can then be made as long as desired, consistent with passive absorption loss and construction difficulties.

However, other complications arise when a low resistivity semiconductor is used. In this case, it is difficult to generate a large electric field in the material due to the mobile charge. With conducting electrodes, a relatively uniform field is generated across the material, but a substantial current flows, which limits the voltage that can be applied. With blocking electrodes, a space charge region forms blocking the penetration of the field into

the crystal, so that only a small thickness of the material has a substantial electric field, depending on the carrier concentration. This blocking effect can be lessened by using intrinsic semiconductor material and operating at high frequencies, above the corresponding relaxation time for the carriers in the crystal. However, this severely limits the usefulness of the device, especially as a detector, and this mode of operation will not be considered further here.

Much previous work has been done on Franz-Keldysh modulators for fiber optics using semiconductor positive-negative (p-n) junctions as the active modulator region.^{2,3} At the p-n junction, a very strong electric field can be generated without electronic conduction. The field can be varied from dc up to high frequency and to voltage up to the crystal breakdown. These modulators use light propagation down the p-n junction region (field perpendicular to propagation) and have had strong modulation effects, for example, 30 dB extinction at a particular wavelength with only a few volts

²J. C. Dymant and F. P. Kapron. J. Appl. Phys. 47, 1523 (1976).

³J. C. Campbell, J. D. DeWinter, M. A. Pollack, R. E. Nahory. Appl. Phys. Lett. 32, 471 (1977)

applied. Guiding of the light occurs along the junction due to the index difference of the adjacent semiconductor layers. Unfortunately, such devices are generally limited to narrow active regions due to the same considerations of charge rearrangement discussed above. These devices, however, show excellent promise for use with single mode systems and should be developed further.

Another possible technique for using semiconductors is to compensate the material with a dopant to create a very high resistivity crystal. This can be done with GaAs, for example, by doping with Cr, and resistivity as high as 10^7 ohm-cm is available. However, such doping creates other problems, such as high optical absorption in the zero field state so that the insertion loss of the device is high. Also, this doping tends to lessen the sharpness of the transition from transmissive to absorptive state and the modulation is not as strong.¹

Thus, for successful implementation of a semiconductor Franz-Keldysh modulator, the most promising technique is

either single mode transmission along a p-n junction or a multimode device using intrinsic material in a field-parallel-to-light-propagation configuration. The performance of the multimode device will not be as good as that obtained with the p-n junction single mode modulator, but this is true in general of single mode versus multimode devices. Theoretical calculations¹ show that large depths of modulation can be obtained for this multimode configuration, but the voltages required are higher, e.g., of the order of 100 volts or more.

2.2 Experimental Results

Some experiments of a preliminary nature were carried out in order to explore the use of bulk GaAs (as opposed to a p-n junction) in a multimode Franz-Keldysh modulator. The approach used Cr compensated material with greater than 10^6 ohm·cm resistivity from Laser Diode Labs. High resistivity material was used in order to be able to apply an electric field across the crystal for use in a waveguide arrangement. For this purpose, a crystal was lapped and polished to a thickness of approximately 50 μ m and evaporated on both sides with aluminum electrodes. Three different crystal lengths were used - 1 cm, 2 cm and 3 cm - in order to test absorption versus length as well as voltage.

The edges of the crystal were polished so that light could be coupled into the crystal with a multimode fiber. Unfortunately, the optical attenuation of the crystal, even at wavelengths out to $1.0\text{ }\mu\text{m}$, far above the band edge, was much too large for making useful measurements. The increased absorption with doping was predictable. However, the 20 dB/cm magnitude of the effect made it impossible to obtain data since the input white light source had to be filtered by a monochromator and hence was weak to begin with. After coupling to a fiber and then adding the GaAs losses, the signal was not strong enough to observe any effects with voltage. Of course with this large absorption loss, the crystal would not be usable as a modulator even if there had been a noticeable effect.

Another experiment was carried out using the same material in the configuration of electric field parallel to the light propagation direction. The crystal was approximately $250\text{ }\mu\text{m}$ thick and had $80\text{ }\text{\AA}$ thick aluminum electrodes which added about 5 dB of throughput loss to the normal 3 dB GaAs reflection loss for two air surfaces. Better transparent electrodes could be fabricated from a doped semiconductor with a wider bandgap or a conductive oxide layer if this were required.

The results plotted in Figure 30 give the attenuation in dB relative to the zero voltage state for four different applied voltages: 300, 500, 700 and 1000 V. The largest effect occurs between 8400 and 8500 Å and is limited to about 2.5 dB for 1000 V. However, this absorption is at a wavelength where the crystal is already highly absorbing (15 dB bulk loss for 250 μm), so that device operation is not possible in this region. Farther in the infrared where the zero field loss is less, the modulation depth varies between 5 and 20% for voltages of 300 V to 1000 V.

Improvement in this performance cannot be obtained by making the crystal thinner in order to yield a higher electric field for a given voltage. If it is assumed that the compensated semiconductor behaves as an insulator, then the full electric field falls across the crystal and a thinner crystal will have a higher electric field for the same applied voltage. However, the amount of absorbing crystal that is traversed will also decrease so that these two effects will tend to cancel. On the other hand, if the crystal behaves like a semiconductor and the electric field is screened in the crystal, then the entire voltage drop falls only along a portion of thickness of the crystal. In

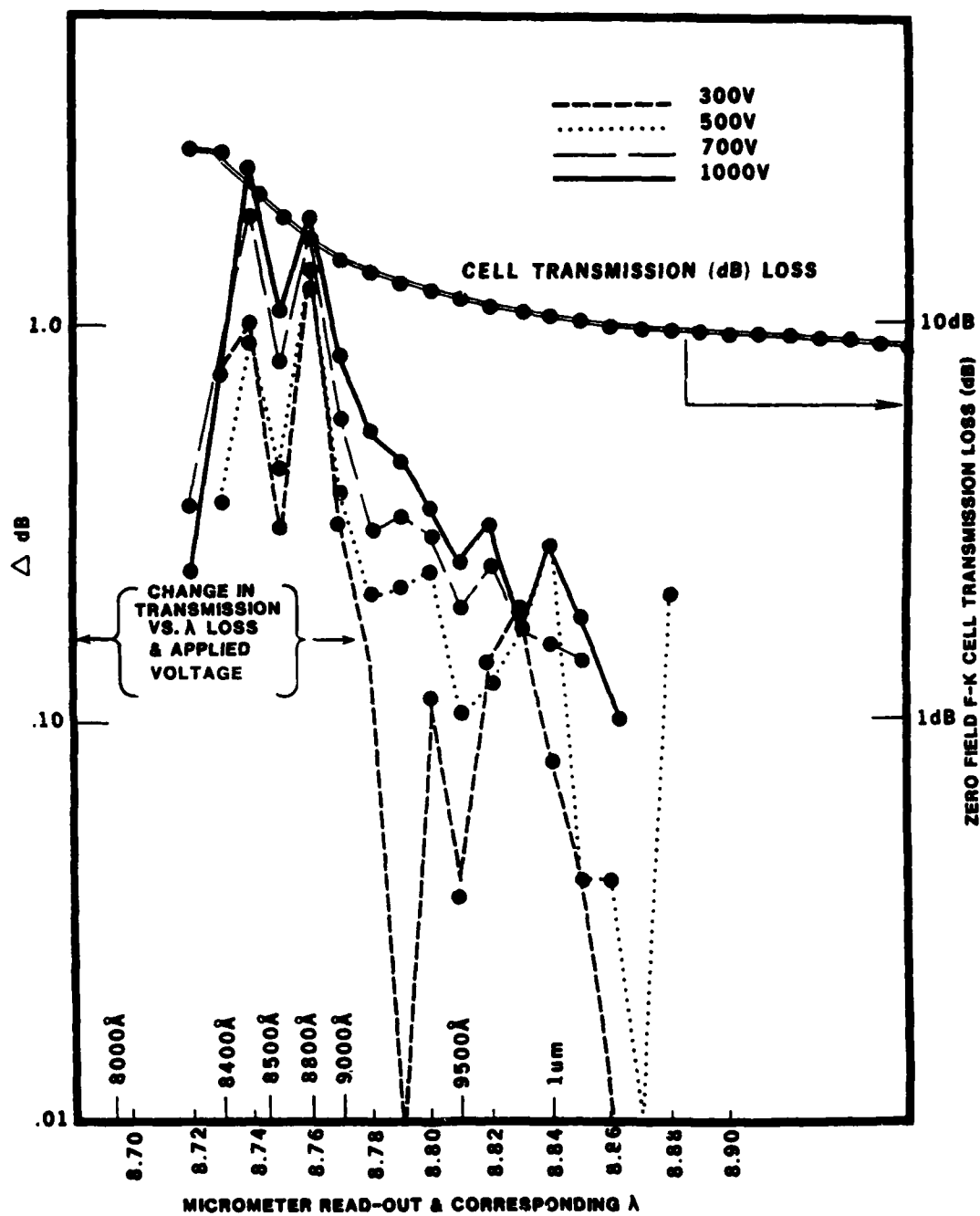


Figure 30. Franz-Keldysh Results.

that case, making the crystal thinner also has no effect on the modulation, since only the region of the crystal near the electrodes has any effect at all.

Two other factors may have played a role in the results presented here. As previously mentioned, the Franz-Keldysh effect requires a narrow band source for optimum operation, since the shift in band edge is less than 100 Å even for high voltages. The results in Figure 30 were obtained with a prism monochromator that had a relatively wide wavelength window. Thus, these measurements tend to smear the sharp drop in transmission that should occur and do not give the full modulation depth that may exist at one precise wavelength. Secondly, it is not known to what extent the Cr doping modifies the behavior of the GaAs. Such doping does cause a broadening of the absorption band with zero applied field. Since the observed transmission curve of the GaAs with $V = 0$ does not show the sharp drop predicted by theory, these effects have definitely played a role in the measurements. Additional experiments with intrinsic material and a narrower wavelength source are required to better determine the potential of this type of modulator.

3.0 Electro-optic Devices

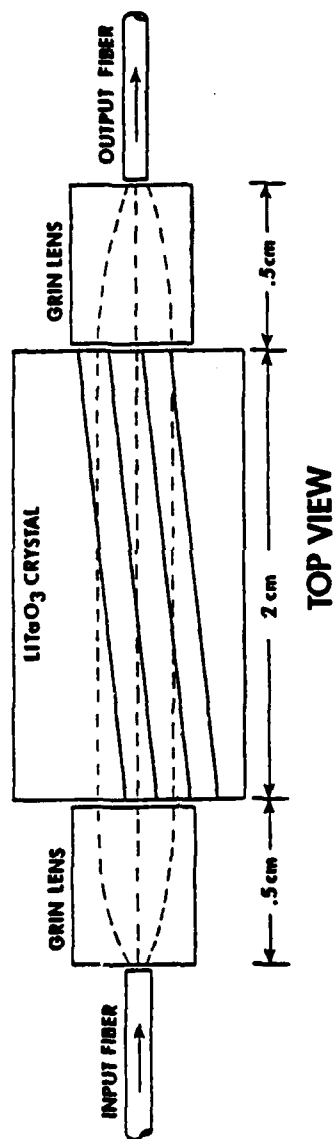
Most of the past effort in fiber optic switching has been centered on the electro-optic Pockels effect in semiconductors, such as GaAs, or ferroelectrics such as LiTaO_3 or LiNbO_3 . This work has been fairly successful in developing devices that are suitable for use with single mode systems, although low loss coupling into and out of the device is still a problem. Some research has also been performed on electro-optic devices for multimode switching and modulation using LiTaO_3 . In this case the fiber coupling tolerances are eased, but total insertion losses have still been fairly high.

In the course of this research, the emphasis has been on couplers with low insertion loss, since this has been the most important failing of previous efforts. Thus, the acousto-optic, which should be capable of very low intrinsic loss, has received the most attention. The Franz-Keldysh effect also appeared to be capable of very low throughput loss at the beginning of this study. For the electro-optic effect, past efforts have not been as encouraging due to losses encountered from polarization effects and crystal losses. However, some attention is warranted, and a small study effort was included for this technique.

3.1 Electro-optic Coupler No. 1

Two versions of electro-optic couplers are described in this section. Both can be fabricated with LiTaO_3 , a readily available electro-optic material with excellent properties, and both designs can switch multimode, unpolarized light. However, two entirely different principles are represented: diversion of the light by total internal reflection at electro-optically induced index barriers and transmission or reflection of light in a Fabry-Perot cavity due to phase changes induced in the active medium.

The first device is shown schematically in Figure 31. The input multimode fiber is butt coupled to a graded index lens which in turn is directly butt coupled to an electro-optic crystal, such as LiTaO_3 . The output from the crystal is then refocused on the output fiber with another graded index lens. The crystal and graded index lenses are flat plates with the same thickness as the fiber diameter. The light beam is guided in the direction perpendicular to the crystal and collimated in the plane of the crystal, so that a non-diverging beam is created and nearly all of the input light is collected by the output fiber.



002 11002

Figure 31. Electro-optic Coupler No. 1.

Modulation and/or deflection electrodes for the switch are created by evaporating a series of deflection electrodes on top and bottom of the crystal. A voltage applied across the thickness of the electro-optic crystal changes the index of refraction and creates an index barrier that can totally internally reflect the light incident on the barrier. For operation of the device as a two-port modulator, it is only necessary to deflect the light by an amount such that it will not be refocused by the output graded index lens onto the output fiber. For use as a three-port tap-off device, the deflected light must miss the main fiber lens entirely and be incident on another graded index lens to be focused onto a receiver fiber, and a larger deflection angle or longer crystal is required.

Some numerical calculations will demonstrate the feasibility of this coupler. A step index fiber with .25 NA is assumed and the crystal is LiTaO_3 . A commercial graded index lens is available that will collimate and expand the light from the fiber by a factor of 40 while the index difference between the LiTaO_3 ($n = 2.2$) and the glass ($n = 1.5$) will provide an additional collimation of 1.5. The light cone in the glass fiber is $\pm 9.4^\circ$ which becomes $\pm .16^\circ$ in the LiTaO_3 after this collimation. As a modulator, it can be shown that it

is only necessary to deflect the light beam by $.3^\circ$, so that it will not be refocused by the output lens into the fiber. This can be done by a total internal reflection barrier oriented at $.2^\circ$ to the light beam in the crystal. The index change required for total internal reflection at an incidence angle θ is given approximately by:

$$\Delta n/n \approx \theta^2$$

and we obtain $\Delta n/n = 10^{-5}$ for $\theta = .2^\circ$. Using the material parameters for LiTaO_3 , 4 V is required for the transverse magnetic (TM) modes and 16 V for the transverse electric (TE) modes for this index change. Thus, only 16 V is sufficient to completely deflect 100% of both polarizations.

We may summarize the performance of the coupler as follows. The spreading loss in the crystal is only 2% so that the total throughput losses will be quite low (<1 dB) if AR coatings are used on the crystal edges. The capacitance is about 50 pF which will allow operation at 100 MHz or higher if the device is positioned close to the switch. The figure of merit, $1/2CV^2$, is $6.4 \mu\text{W}/\text{MHz}$, which is quite reasonable considering the number of modes in the fiber. The on/off ratio or modulation depth is limited by

imperfections in the crystal, since the deflection is theoretically 100%. In practice, it should be fairly easy to obtain a ratio of 10 dB. Construction of similar devices has already been performed, so that all of the fabrication steps involved are quite feasible.

3.2 Electro-optic Coupler No. 2

The second potential electro-optic device is shown schematically in Figure 32. This approach also uses two graded index lenses for collimation and focusing, but the construction of the electro-optic switch is different. A reflective coating is placed on both ends of the LiTaO_3 so that the crystal is a cavity with total reflection r and transmission t given by:

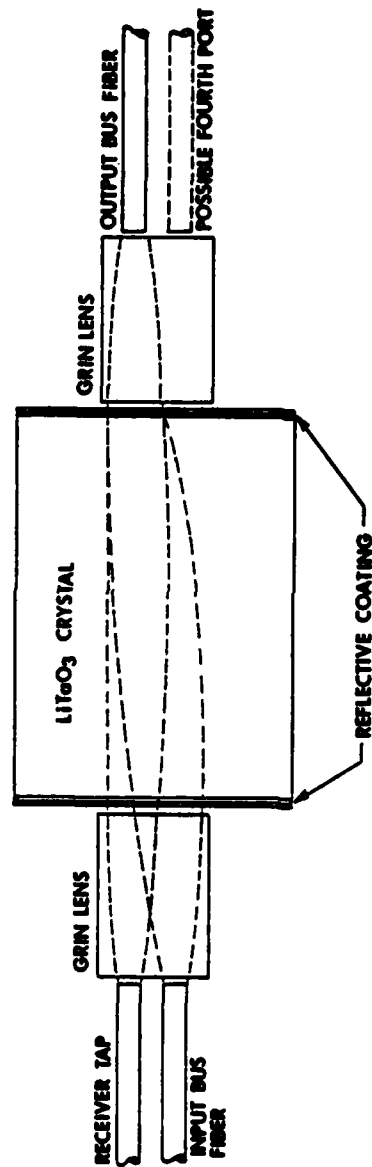
$$r = \frac{4R \sin^2 (\delta/2)}{(1-R)^2 + 4R \sin^2 (\delta/2)}$$

$$t = \frac{(1-R)^2}{(1-R)^2 + 4R \sin^2 (\delta/2)}$$

where R = intensity reflection coefficient of reflective coating

$$\delta = 4\pi n l \cos \theta / \lambda_0$$

n = index of refraction of transparent material



002 11000

Figure 32. Electro-optic Coupler No. 2.

l = thickness of transparent material

θ = incidence angle between a ray and reflective coatings

λ_0 = wavelength of light in free space
or normal incidence, unity transmission occurs when

$$l = m\lambda_0/2n$$

where m = any positive integer.

The maximum reflection is $4R/(1+R)^2$ hence a reflection coefficient of 0.8 produces a maximum reflection of .987 or an extinction coefficient of -19 dB.

The switch is operated by applying a voltage to change n , thereby varying the transmission between a maximum and minimum. If the device length is 10^4 wavelengths long (≈ 1 cm), then an index change $\Delta n/n$ of less than 10^{-4} will be sufficient to activate the switch. This index change can be obtained across a thin wafer ($\approx 100 \mu\text{m}$) of the crystal with about 100 volts, but there is a problem with applying the voltage in this direction, since the TE and TM modes will be affected differently. There are two possible solutions: propagating the beam at an angle to a major crystal axis so as to adjust n and Δn

separately for the TE and TM modes or applying the voltage across the length of the crystal.

The second electro-optic approach has some drawbacks in higher operating voltages, especially if the voltage is applied in the direction of the light flow. However, it has the potential for much more versatile operation as a switch. In particular, if two input fibers are placed at one end of the switch, and two output fibers connected at the other end, the device can operate as a four-port reversing switch, which in turn can be used as a very versatile building block for much more complicated switching networks. The other parameters, such as size, speed and signal to cross talk ratio, are similar to the first electro-optic device.

Additional study of either of these techniques is not required. The next logical step would be construction and test of experimental models.

SECTION X

CONCLUSIONS AND RECOMMENDATIONS

This program was directed toward the development of passive and active coupler components for use in fiber optic data bus systems. Specifically, passive coupler elements (directional, "T", and transmission stars) suitable for class II airborne environments as defined in MIL-E-5400 were developed and tested for optical and environmental performance. Techniques suitable for active coupling (switching, modulation, demodulation) in multimode fiber data bus systems were evaluated theoretically; one technique was implemented in developmental model form, and a second was investigated experimentally. The conclusions drawn from this effort are discussed in the following sections, and recommendations are made where appropriate.

1.0 Passive Couplers - Conclusions

The passive couplers developed under this program use the technique of direct fusion of uncladded plastic

clad silica fibers (PCS) to form the couplers. This technique was developed for a variety of couplers under a previous program. The main thrust of the current program was to develop suitable packages and associated processes to overcome susceptibility of the couplers to catastrophic failure due to a variety of environmental conditions. The primary results of the program can be summarized as follows:

- a. Packaged couplers using direct fusion of PCS fibers meet the thermal and vibrational requirements of MIL-E-5400
- b. Techniques for connector termination of PCS fibers, meeting mechanical and optical performance requirements, were significantly improved
- c. A complex materials and processing compatibility problem significantly limited the optical performance achieved in the couplers
- d. Optical performance of packaged directional and star couplers can be improved by application of techniques developed late in the program

The package concepts that were generated for this program were designed to protect the coupler elements from

catastrophic degradation due to mechanical shock, thermal expansion of the package and stress applied externally through the fiber pigtail leads. All three of these objectives were satisfied and the devices passed tests as specified in MIL-E-5400, without a single failure.

It should be noted that:

- o These packaging techniques have been successfully applied to fused biconical taper couplers using glass-glass fiber types with excellent optical performance.

In the final packaging stage for the star couplers delivered under this program 104 single-fiber connector terminations were made with less than 10% rework required. The optical performance of these connected fibers was excellent, and the mechanical performance achieved in one earlier technique was maintained. This was achieved by using a combination of techniques that had been used separately before. The first technique, initially developed under the previous program and using a chemically deposited silver coating, had high mechanical integrity against fiber pull-out from the connector ferrule under

tension, but was subject to varying degrees of optical performance degradation through abrasion of the coating during handling. A technique developed elsewhere using a Kynar[®] copolymer typically achieved good optical performance, but was subject to fiber pull-out because of relatively thick plastic layers. This technique was modified to provide an extremely thin (on the order of one micron) coating over the silver coating, thereby preserving the optical integrity of that coating, and improving the mechanical integrity of the copolymer.

A variety of complex materials and processing problems occurred over the course of the program in the fabrication of optical couplers into the environmental protection packages. These problems were largely manifested in degradation of the coupler optical performance from successive processes required to preserve the coupler mechanical integrity. Although a number of approaches to the problem were investigated within the time allotted to technique and process improvement, none of these were

particularly successful in reducing the optical loss from packaging. Consequently, the couplers which were fabricated for environmental testing and as final deliverables had degraded optical performance as compared to couplers delivered under the previous contract.

However, the techniques used in terminating fibers in the final packages were developed after the test and deliverable couplers were fabricated. It presently appears that this technique is suitable for solving the optical degradation problem. Thus, at least in the case of the directional and transmission star couplers, it appears that both optical and environmental integrity can be achieved in a single package. Since the "T" coupler's optical performance is at present limited by basic coupler fabrication technique, rather than advanced processing problems, it is not expected to be significantly improved.

2.0 Passive Couplers - Recommendations

In order for this technology to be further pursued, it appears desirable to conduct a serious, detailed materials

processing and compatibility program. Further, a program aimed toward the development of a hard, low refractive index adhesive material, if successful, would substantially improve the optical characteristics of the devices, reduce the number of processing steps and increase device yield resulting in lower unit cost. Alternatively, a small-scale program to incorporate the particular technique used in connector termination at the end of the current program into the coupler fabrication and packaging processes may be beneficial. Such a program would be applicable to the directional and transmission star couplers.

Because of the basic fabrication problems with the "T" couplers, it appears that further pursuit of current techniques is not advisable. If true "T" couplers are an important component for data bus implementation, then further effort should be along the following lines:

- a. Investigation of new, innovative approaches to achieve true "T" couplers with high optical performance
- b. Selection of high performance directional couplers to be packaged together in a "T" coupler configuration

3.0 Active Couplers - Conclusions

In the active coupler portion of this program, a preliminary survey identified a number of techniques which could potentially be used for active coupler applications in multimode optical fiber data buses. Of these, four were chosen for further investigation. There were (1) the creation of a waveguide region in thin crystal and modulation of the waveguiding region by the electro-optic effect, (2) the modulation of a Fabrey-Perot cavity by the electro-optic effect, (3) acousto-optic deflection, and (4) material absorption modulation through an applied electric field (Franz-Keldysh effect). A further detailed study resulted in the decision to implement the acousto-optic coupler and to conduct further experimental evaluation of the Franz-Keldysh effect.

The results of this effort can be summarized as follows:

- a. The bulk acousto-optic effect and the E-O waveguide approach can be currently used to implement moderate performance active couplers for multimode fiber applications

- b. The E-O Fabry-Perot cavity modulation approach can probably be successively implemented, but because of high voltage requirements and potential performance limitations has no significant advantage
- c. The Franz-Keldysh effect is difficult to implement in a viable form compatible with multimode optical fibers

The E-O waveguide approach has been successfully developed by other laboratories, and has demonstrated usable switching and modulation characteristics, but with a relatively high insertion loss. It is this latter problem which may limit this approach to applications requiring moderate performance characteristics.

Experimental verification and evaluation of the E-O Fabry-Perot approach is required before its performance limitations can be fully assessed. It may be expected, however, to suffer the same limited optical performance characteristics that appear to occur in all other active couplers for multimode fibers.

The experimental evaluation of the bulk acousto-optic effect by implementation of both modulator and switch configurations shows that moderate performance levels can be achieved at relatively low insertion loss. Acousto-optic crystals and driver electronics suitable for use in multimode fiber couplers are available off-the-shelf. In the multimode configuration, switching rates are limited to about 5 Mb/s.

The Franz-Keldysh effect has been previously investigated as a technique compatible with single mode fiber transmission. The experiments in the current program were designed to evaluate the effect for compatibility with multimode fibers. In the latter case, a bulk effect is required whereas previous effort was directed toward effects in a p-n junction. Although a bulk effect was observed, the magnitude achievable with reasonable voltage levels was unsuitable for modulation applications, and occurred only over a very narrow wavelength band. In addition, there was substantial inherent (zero voltage) absorption within the

wavelength region where the effect was significant. However, some of the difficulties encountered with the materials available for this experimental effort may be surmountable. Thus, it is not at present totally clear that the Franz-Keldysh is unusable in an active coupler configuration for multimode fibers.

4.0 Active Couplers - Recommendations

Based on the foregoing discussion, it is clear that a moderate performance active coupler can be implemented for multimode fibers with minor additional development.

On the other hand, a high performance active switching technique for multimode configurations continues to be elusive. It appears that such a coupler will require new, innovative techniques. Assuming the continuing requirement for multimode active couplers of high performance, it appears that effort should be directed toward these innovative approaches.

APPENDIX A

MODIFIED FIBER SILVERING PROCESS

APPENDIX A

MODIFIED FIBER SILVERING PROCESS

I. FIBER PREPARATION

The fibers used for this program were in actuality coated with two jackets. The first is Sylgard 184[®], followed by a protective outer jacket of Hytrel[®]. The mechanical stripping of the Hytrel[®] jacket and silicone RTV cladding material is accomplished by the following technique.

The fiber to be stripped is placed in a groove, such that the silica fiber within the jacket and cladding lies below the top surface of the block containing the groove. See Figure A-1. A razor blade is brought down in contact with the block, cutting edge perpendicular to fiber axis, and the fiber is rotated about its axis. This makes a single cut around the periphery of the fiber without actually contacting the fiber. Without lifting the blade, the blade angle of attack is now adjusted to be almost horizontal, and the fiber is drawn under the blade which cuts off a slice of the jacket from one side of the fiber over the desired length. Using finger cots, the jacket and in some cases the cladding can be peeled away from

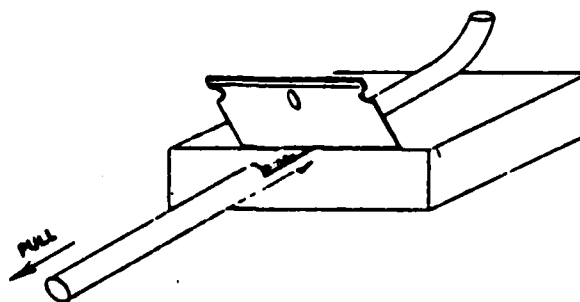
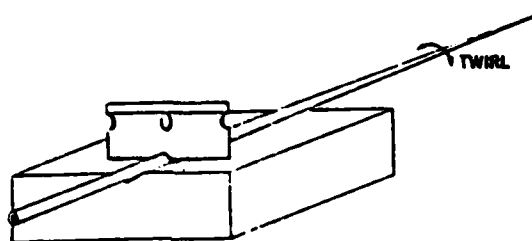
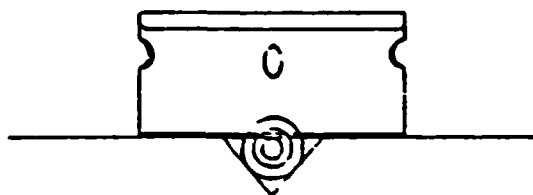


Figure A-1. Fiber Jacket Removal.

the fiber. At this point, the bare fiber is cleaned and the remaining RTV removed by pulling the fiber through a Kimwipe[®] tissue "soaked" with a 50-50 mixture of Isopropyl Alcohol and Freon TF[®].

When preparing fibers for the fabrication of transmission star couplers, the cutting of the Hytrel[®] and silicone jacket is performed at two locations in the center of a length of fiber. A second cut is made at the desired distance from first cut and the jacket is carefully sliced at the top from the second cut toward the first. The same peeling and solvent cleaning procedures described above complete the preparation of the fiber for use in the fabrication of a transmission star coupler.

II. SILVER ELECTROLESS PLATING PROCESS

A procedure was developed for applying silver directly to the fibers by a chemical reduction process. This procedure, a modified Brashear¹ process, is used widely by mirror manufacturers, amateur and professional astronomers alike.

The modifications to the basic process are that of using pure, reagent grade materials and fiber cleaning procedures to yield uniform and dense silver films.

In the sections to follow, the fiber preparation procedures, chemical preparation and use procedures are discussed.

1. Chemical Preparation (Stock Solutions)

The following stock solution can be prepared in stock quantities for multiple uses (~10 silverings).

¹Amateur Telescope Making, Book One, pp. 158-159.
Albert G. Ingalls, Editor, Scientific American, 1970.

- a. Reagent grade potassium hydroxide (KOH) and distilled or deionized (DI) water (H_2O) 10 g KOH + 100 ml H_2O
- b. Reagent grade dextrose ($HOCH_2CH(CHOH)_4O$) and distilled or DI water (H_2O) 15 g dextrose + 150 ml H_2O
- c. Final fiber cleaning solution. Three parts, by volume of KOH stock solution and one part reagent grade ammonium hydroxide (NH_4OH). A total quantity of ~100 ml is usually sufficient for use. Keep tightly stopped when not in use to prevent dissociation of NH_4OH

2. Fiber Preparation for Silvering

The three (3) step cleaning procedures to follow should be performed just prior to initiation of the silvering procedure to minimize surface contamination. The last step in the cleaning procedure will take place during the final chemical preparation phase prior to silvering.

Step 1 - Squeeze the fiber between folds of a Kimwipe[®] tissue "soaked" with a 50-50 mixture of isopropyl alcohol and Freon TF[®]. Draw the fiber through the tissue. This step should be repeated until the bare

fiber appears to remain "wetted" by the solvent solution over the entire length of the bare fiber. A back and forth scrubbing motion near the bare fiber-jacketed fiber area will ensure cleaning of this area.

Step 2 - Submerge the bare fiber and approximately 1/4" of the jacketed fiber in a 25% HF solution for 20-30 seconds or in an ammonium bifluoride solution for 60-90 seconds. (Mixture ratio of 10 g $\text{NH}_4\cdot\text{HF}$ and 100 ml of DI H_2O .)

3. Final Chemical Preparation and Silver Plating Procedure

It should be noted that the prepared solution resulting from Steps 1 through 4 described below will, if allowed to age, result in the formation of silver fulminate, a potentially explosive substance, and should be prepared just prior to actual use only. Silver fulminate is known to spontaneously detonate at room temperature; however, this process has been used many times at ITT EOPD with no negative consequences.

The total preparation time and plating time involved is approximately ten (10) minutes. After the plating process is complete, the hazards are eliminated by dilution of the solution with water. No environmental problems exist with normal sink disposal.

The following procedures are to be performed on a cold (room temperature) stirring hot plate.

Step 1 - To 50 ml of distilled or deionized (DI) water add 2 mg of silver nitrate (AgNO_3). Stir until completely dissolved.

Step 2 - Add approximately (if fresh) 2 ml ammonium hydroxide (NH_4OH) to the solution prepared in Step 1 above. The solution will darken at first, add NH_4OH slowly until solution clears. If the NH_4OH has weakened slightly through disassociation, slightly greater quantities are required.

Step 3 - Slowly add 10 ml of potassium hydroxide (KOH) stock solution. Solution will again darken.

Step 4 - This step should be carried out slowly due to the fact that the precipitate formed in Step 3, which is responsible for the darkening of the solution, is not to be completely redissolved in this step. Add small quantities of ammonium hydroxide (NH_4OH) and stir for approximately one minute before more is added. The total quantity required is approximately 1 ml if NH_4OH is fresh and some color (weak tea) should remain to the solution.

Step 5 - To 50 ml of distilled or DI water, add 15 ml of stock dextrose solution.

The plating process is now ready to start.

The container holding the solution from Step 4 should now be placed in an ultrasonic cleaner with light to

moderate coupling to the sonic power. Pour the dextrose solution into the container holding the silver nitrate preparation and submerge the fibers to be plated. Plating is completed within three (3) minutes.

Rinse the fibers with running DI water for approximately 15 seconds. A second rinse is then applied by squirting or submerging in isopropyl alcohol to dry the film.

If the fiber cleaning procedures were performed adequately, the silver coating should be continuous not only on the bare fibers but also on the jacket material.

If multiple fibers are to be processed simultaneously, care should be taken to prevent direct contact during the plating process or voids may exist due to masking.

APPENDIX B

TERMINATION OF PCS FIBERS USING
PLASTIC CLADDING MATERIALS

AD-A082 360

ITT ELECTRO-OPTICAL PRODUCTS DIV ROANOKE VA
FIBER OPTIC COUPLERS.(U)

F/G 20/6

JUL 79 G W BICKEL, L E FOLTZER, G A RINES

F33615-78-C-1448

UNCLASSIFIED

AFAL-TR-79-1149

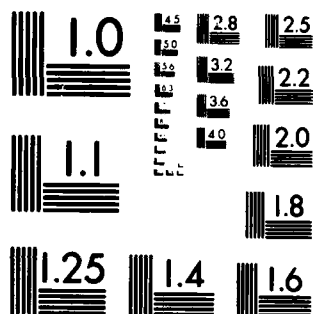
NL

3 3

01 000 000



END
DATE
FINISHED
4 80
DTIC



MICROCOPY RESOLUTION TEST CHART
NATIONAL BUREAU OF STANDARDS-1963-A

APPENDIX B
TERMINATION OF PCS FIBERS USING PLASTIC
CLADDING MATERIALS

Previous termination methods involved epoxy bonding the fibers, with the resilient cladding intact, into a connector, and polishing the ends of the exposed fibers. However, due to the resilient nature of the plastic cladding material, usually a silicone, four outstanding effects were observed. First, the faces of the fibers did not polish to optimum flatness. Second, the fiber edges had a tendency to chip. Third, the soft cladding allowed polishing material to become embedded between the cladding and the fiber core. Fourth, epoxies did not bond well to soft materials, and the fibers tended to pull back into the connector or push out from the connector when the cable was under stress. All of these effects contributed to degradation of the optical performance of the cable.

One possible method of avoiding these problems is to strip the cladding from the fiber in the termination area and re clad this area with a thin film of a less resilient, low refractive index material. This method was chosen as the most promising to provide an acceptable termination.

An investigation was initiated to establish a list of possible recladding materials. Since manufacturers do not often publish refractive indices of materials, the investigation was limited to classes of compounds known to have low refractive indices, i.e., highly fluorinated plastics and silicones. Samples of several materials were obtained and tested to determine the feasibility of each sample.

The published numeric aperture (NA) for plastic-clad, fused silica fibers generally falls in the range of .25 to .4. In order to keep the numeric aperture in this range, the new cladding must have an index of refraction less than 1.43

$$\text{since } NA = \sqrt{n_1^2 - n_2^2}$$

where n_1 = refractive index of the quartz core ($n_1 = 1.45$)

n_2 = refractive index of cladding

The refractive indices of the sample materials were measured with a Bausch and Lomb Abbe refractometer. Table B-1 presents the candidate materials and their respective refractive

Table B-1.
Possible Cladding Materials.

Item	Material	Source	Refractive Index (Visible Light)	Coating Solution	Cure Method
1	Kynar-TFE Copolymer	Optelecom Inc., Gaithersburg, Md.	1.40 film	35% Kynar-TFE 65% Acetone	Air Dry + 2-5 sec heat gun
2	Vydax TFE Dispersion	E.I. DuPont	1.35 film	As Supplied	Air Dry + 5-10 min @ 300°C
3	Methyltrimethoxy- Silane Z-6070	Dow Corning	1.37 liquid 1.40 film	10% Silane 2% Water .5% Acetic Acid 87.5% Methanol	Air Dry + 5-10 min @ 125°C
3	DC-40C Silicon Adhesive	Dow Corning	1.48 film	As Supplied	Air Dry + 1 hr @ 100°C
4	DC-840 Silicon Resin	Dow Corning	1.52 film	As Supplied	Air Dry + 1 hr @ 100°C
5	DC-991 Silicon Varnish	Dow Corning	1.54 film	As Supplied	Air Dry + 1 hr @ 100°C
6	Kynar 202 Dispersion	Penwalt Corp.	1.42	As Supplied	20 min @ 200°C 10 min @ 300°C
7	Kel-F 800	3M	1.416	35% by Weight in Acetone	Air Dry + 2-5 sec heat gun
8	Halar	Allied Chemical	Not Measured	No Film Achieved	

700000

indices along with the "as applied" formulation and the recommended cure schedule.

The Kynar-TFE copolymer was selected as the best overall recladding material. The index of refraction of this material limits the NA of fused silica fibers to .35. This material bonds well to the fiber core and provides a reasonable epoxy bond surface. When applied by dipping, the Kynar-TFE provided a continuous film with a uniform thickness of .0003 inch.

APPENDIX C

REFERENCES ON V-GROOVE ETCHING

Preferentially etched diffraction gratings in silicon*

Won-Tien Tsang and Shyh Wang

Department of Electrical Engineering and Computer Sciences and the Electronics Research Laboratory,
University of California, Berkeley, California 94720
(Received 30 December 1974)

Here, we describe the fabrication of diffraction gratings in the {100} surfaces of silicon by preferential etching. The gratings thus made have grooves with well-defined geometric shape and bounded by nearly perfect reflecting walls. Meanwhile, the importance of utilizing this technique in integrated optics is also discussed.

PACS numbers: 42.80.F, 85.40.C, 68.40.C

Anisotropic etching of single-crystal silicon^{1,2} and gallium arsenide (GaAs)^{3,4} by chemical reagents is a fabrication technique of growing importance and usefulness in integrated circuits, integrated optics, and other microfabrication areas. Its chief merit lies in the fact that excellent control of etched profiles and film thickness can be achieved by using this technique. In integrated circuits, its replacement of diffusion as a method of electrical isolation for devices on the same chip reduces parasitic capacitance and thereby offers improved performance.⁵ In integrated optics, its use in the fabrication of interconnections,⁶ thin-film prism mode separators,⁷ and optical waveguides⁸ on silicon wafers, and diffraction gratings⁹ on GaAs has been successfully demonstrated. In microfabrication areas, its use for making very thin silicon membrane used as x-ray masks in x-ray lithography,^{10,11} as substrate in generating ultrasmall patterns in electron lithography,¹² and as an insulating barrier in Josephson junctions¹³ is unique. In acoustics, it has also been used to fabricate ridged waveguides.¹⁴

Recently Comerford and Zory reported the use of preferential chemical etching in fabricating submicron gratings on GaAs for distributed feedback lasers.⁹ In our laboratory, we also have investigated the preferential etching technique as an alternative to ion-beam milling in our continued effort to seek ways of making high-quality gratings. Previously, we introduced the simultaneous exposure and development (SED) technique of making photoresist relief gratings¹⁵ and reported excellent results¹⁶ with the SED technique. In the present paper, we report our work on chemical etching of silicon substrates. The reason for choosing silicon in our initial experiment is twofold. Demonstrating the feasibility of using chemical etching techniques is only a first step. In order that we may eventually use the technique in integrated-optics device fabrication, we must have the chemical etching process under control. Silicon is well suited for such a study because of the extensive information about silicon gained from integrated-circuit technology. Any knowledge learned from chemical etching of silicon will be useful for similar processing of gallium arsenide. Second, a stable and smooth layer of SiO₂ can be grown on Si, which can be used as an insulating layer in a multilayer waveguide structure. We investigate the fabrication of diffraction gratings on silicon with the hope of using silicon as the basic substrate material for possible future integration of optical and electronic components.

Using the preferential etching technique, we have already fabricated waveguides⁷ and prism mode separators⁸ on Si. The possibility of making diffraction gratings will add to this list other passive components such as optical filters,¹⁷ couplers,¹⁸ and multiplexers.¹⁹ Furthermore, the diffraction gratings fabricated by the technique can also be used in spectroscopic applications when a metallic reflecting layer is coated on top of it. Comparing with the conventional ruling technique, this technique has the ability to produce high-quality diffraction gratings of submicrometer periods and with well-defined groove profiles bounded by reflecting smooth walls without involving a complicated mechanical process and long processing time, though the size of the gratings is limited at most to that of the silicon wafer.

Figure 1 shows two possible groove profiles that can be obtained when {100} faces of silicon are preferentially etched with the mask openings orientated along the {110} directions in the wafer using the KOH-H₂O-isopropyl alcohol system. This Si etchant is highly preferential with $R_{100} > R_{110} > R_{111}$, where R_{100} , R_{110} , and R_{111} denote the etching rates in the {100}, {110}, and {111} directions, respectively. Under optimum conditions, R_{100} can be 35 times greater than R_{111} . As a result, nearly perfect reflecting {111} planes are exposed as walls of the grooves. The V-shaped groove profile is essentially self-terminated when the bottom {100} plane disappears with the two {111} planes coming into intersection. After that, etching continues slowly in the {111} directions. The cup-shaped groove profile is obtained when the etching is stopped before the two bounding {111}

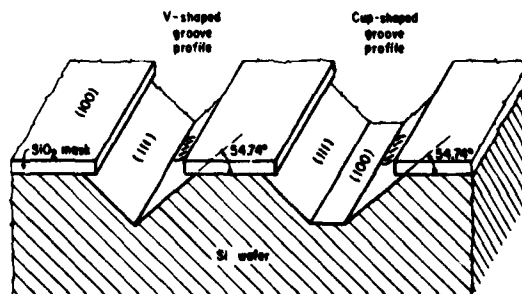
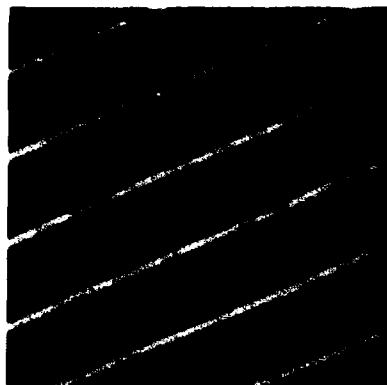


FIG. 1. Shows two of the possible groove profiles that can be obtained by preferential etching of the {100} surfaces of Si with mask openings orientated along the {110} directions.



(a)



(b)



(c)

FIG. 2. SEM photographs of a 0.95- μm -period diffraction grating fabricated by preferential etching of a {100} Si wafer; (a) and (b) show the tilted top view (45°); (c) shows the cross-sectional view (90°) of the grating.

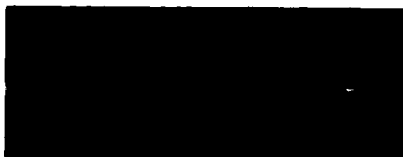
planes intersect. Thus, by controlling the etching time, either type of groove shape can be obtained. It is worth noting that since R_{111} is not zero, the width of the etched grooves will be slightly larger than that defined by the mask especially when deep grooves are etched as shown schematically in Fig. 1.

In the following discussion, we report our experimental procedures and results in the fabrication of diffraction gratings on silicon by preferential etching. Silicon wafers (one side polished, n -type 1–3 $\Omega\text{ cm}$, {100}) were cleaned and oxidized so as to grow a layer of SiO_2 film of about 1500 Å thick on top of the polished side, which was then spin coated at 4000 rpm with a solution of three parts Shipley AZ-thinner and one part

AZ-1350J.²⁰ After prebaking under a 2500-W ir lamp for approximately 15 min, relief gratings with grooves developed down to the SiO_2 surface and aligned parallel to the {110} direction were fabricated holographically using the SED technique.^{15,16} The photoresist relief gratings were then postbaked at a temperature of 120 °C for about 30 min in order to increase their adhesion to the SiO_2 film and their chemical resistance to the SiO_2 etchant. Regular commercial buffered HF was then used to etch away the exposed SiO_2 stripes until the Si surface was reached, thus transferring the grating patterns to the SiO_2 layer. The latter subsequently was used as the grating mask in the preferential etching process. Typical etching time was about 15 sec. Since the SiO_2 film used was very thin, the gratings became much weaker when the photoresist was removed with acetone or Remover 1112. With the SiO_2 gratings now acting as the protective mask, the silicon wafers were then etched with a preferential solution⁷ prepared by dissolving 4.5 g of KOH in a mixture of 15 ml deionized water and 25 ml isopropyl alcohol at 60 °C for typically 45 sec, depending on the width of the groove openings and the type of etched groove profile desired. During the etching process, the solution was kept under constant gentle agitation, and the samples were kept in the isopropyl alcohol-rich layer. After this etching process, since the groove depth increased and the groove shape was well defined with nearly perfect reflecting walls, the diffraction gratings became very strong again. Finally, the SiO_2 masks were etched away leaving high-quality diffraction gratings on the silicon wafers. For further applications of these gratings as couplers and filters in integrated optics and as diffraction gratings in spectrometers, a thick layer of SiO_2



(a)



(b)

FIG. 3. SEM photographs of a 0.95- μm -period diffraction grating showing the appearance of pits alongside the groove walls due to the rough edges of the SiO_2 grating mask.

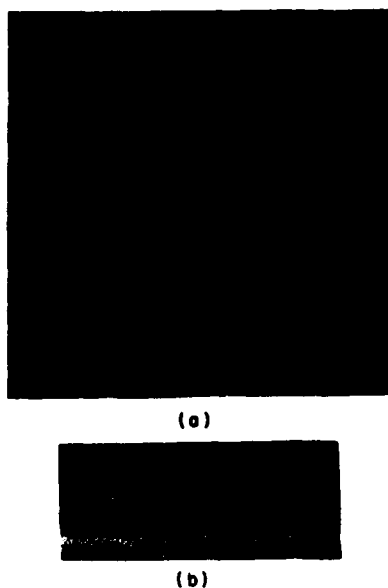


FIG. 4. (a) A SEM photograph showing the effect of postbaking a 0.8- μm -period photoresist grating. (b) shows the cross-sectional view of the same grating after preferential etching.

can be grown by oxidization without damaging the gratings so as to form an optical insulating layer.

Figures 2(a)–2(c) show the scanning electron micrographs taken with dynamic focusing of the tilted top and side views of a 0.95- μm -period grating made by the above-described technique. These micrographs clearly show the well-defined cup-shaped groove profiles, which have nearly perfect reflecting $\{111\}$ planes as side walls and $\{100\}$ planes as bottoms, as a result of preferential etching. Furthermore, the grating was perfectly clean, and no residues were left behind. The very slight unevenness of the side walls was due to small faults in the grating mask and imperfect alignment of the grating lines with the $\langle 110 \rangle$ direction of the wafer. From Fig. 2(c), it is seen that even though the grating ridges are very narrow (780 Å at the top, 2570 Å at bottom, and 1280 Å high) their shapes are very well defined and perfectly regular. A calculation of the inclination angle between the $\{111\}$ plane and the $\{100\}$ plane from these measured dimensions gives a value of 55° which agrees very well with 54.74° calculated crystallographically. From these micrographs, it is well expected that preferential etching in silicon can be used to produce high-quality gratings with period as small as 1000 Å. These micrographs also serve to demonstrate the ability of the SED technique in opening up wide stripes of photoresist grooves.

However, it is seen that, sometimes, irregular pits appeared along the sides of the groove walls as shown in Fig. 3(a) for a grating of the same period. Obvious-

ly, these pits arise as a result of rough edges in the SiO_2 grating mask when undercutting becomes serious in the chemical etching.¹⁸ However, their presence strongly indicates that the grating in the silicon wafer was formed by anisotropic etching. In Fig. 3(b), we show its cross-sectional view.

Since postbaking the photoresist gratings is important in the subsequent step of transferring the pattern to the SiO_2 film, we investigated its effect on the photoresist grating lines. Figure 4(a) shows a SEM photograph of a 0.8- μm -period photoresist grating after postbaking at 120°C for approximately 1 h. It is seen that the resist lines melt out and extend into the exposed grooves, thus reducing the width of the exposed strips (see Ref. 16 for a comparison between photoresist relief gratings before and after postbaking). Hence, if chemical etching is to be used, the exposed stripes must be wide. Otherwise, they will be covered up entirely after postbaking. In Fig. 4(b) we show the same sample after preferential etching. The wider grating ridges (1700 Å at top, 3390 Å at bottom, and 1210 Å high) in this sample shows very clearly the definite inclination between the $\{111\}$ and $\{100\}$ planes.

In conclusion, we have demonstrated the ability of preferential etching of single-crystal silicon in producing diffraction gratings of submicrometer period, which have well-defined geometrically shaped grooves and nearly perfect reflecting walls. In our experiments, the fact that two chemical etching processes, one for SiO_2 and the other for Si, were used demonstrates that submicrometer patterns can be fabricated without resorting to ion-beam machining, an etching technique generally used at present. From the experimental results we present here, it is well expected that such high-quality gratings can be fabricated with periods as small as 1000 Å when shorter-wavelength radiation sources, e.g., He-Cd laser, instead of Ar laser is used.

¹⁸R. M. Finne and D. L. Klein, *J. Electrochem. Soc.* **114**, 965 (1967).

¹⁹H. A. Waggener, R. C. Kragness, and A. L. Tyler, *Electronics* **40**, 274 (1967).

²⁰Y. Tami, Y. Komiya, and Y. Harada, *J. Electrochem. Soc.* **118**, 118 (1971).

²¹S. Iida and K. Ito, *J. Electrochem. Soc.* **118**, 768 (1971).

²²A. I. Stoller, *RCA Rev.* **31**, 271 (1970).

²³L. P. Bovin, *Appl. Opt.* **13**, 391 (1974).

²⁴Won-Tien Tsang, C. C. Tseng, and Shyh Wang, *Appl. Opt.* (to be published).

²⁵C. C. Tseng, Won-Tien Tsang, and Shyh Wang, *Opt. Commun.* (to be published).

²⁶L. Comerford and P. Zory, *Appl. Phys. Lett.* **25**, 208 (1974).

²⁷D. L. Spears, H. I. Smith, and E. Stern, in *Proceedings of the 5th International Conference on Electron and Ion Beam Science and Technology*, edited by R. Bakish (Electrochemical Society, New York, 1972).

²⁸R. A. Cohen, R. W. Mountain, H. I. Smith, M. A. Lema, D. L. Spears, and S. E. Bernacki, *MIT Lincoln Laboratory Technical Note No. 1973-38*, 1973 (unpublished).

²⁹T. O. Sedgwick, A. N. Broers, and B. J. Agule, *J. Electrochem. Soc.* **119**, 1769 (1972).

- ¹³C. L. Huang and T. Van Duzer, *Appl. Phys. Lett.* **25**, 753 (1974).
- ¹⁴R. C. Rosenfeld and K. Z. Bean, *Ultrasonics Symposium Proceedings* (IEEE, New York, 1972), p. 186.
- ¹⁵Won-Tien Tsang and Shyh Wang, *Appl. Phys. Lett.* **23**, 154 (1973).
- ¹⁶Won-Tien Tsang and Shyh Wang, *Appl. Phys. Lett.* **25**, 415 (1974).
- ¹⁷D. C. Flanders, H. Kogelnik, R. V. Schmidt, and C. V. Shank, *Appl. Phys. Lett.* **24**, 194 (1974).
- ¹⁸M. L. Dakas, L. Kuhn, P. F. Heidrich, and B. A. Scott, *Appl. Phys. Lett.* **16**, 523 (1970).
- ¹⁹K. S. Pennington and L. Kuhn, *Opt. Commun.* **3**, 357 (1971).
- ²⁰In these experiments AZ-1350J was used; however, for coating on SiO_2 film, AZ-111 gives better adhesion. Adhesion can also be improved by applying surfactant, e.g., hexamethyldisilazane, to the substrate prior to the resist coating.

Accurate Silicon Spacer Chips for an Optical-Fiber Cable Connector

By C. M. SCHROEDER

(Manuscript submitted July 1, 1977)

Assembled silicon array connectors have been fabricated with low splice loss. The silicon chips can be manufactured with submicrometer repeatability and accuracy. Improvements in chip thickness variations are anticipated which in turn should reduce the overall groove opening variations to a point where individual chip selection is not required.

I. INTRODUCTION

Low-loss multifiber splices have been obtained with the use of accurate silicon spacer chips. These spacer chips are used in a unique splicing technique developed by Bell Laboratories¹ and used in the Atlanta Fiberguide experiment. This multifiber cable splice is a stacked array consisting of two properly prepared cable connectors butted end to end.

A cable array connector is a laminate sandwich of silicon alignment chips with "V" grooves on both top and bottom surfaces interleaved with optical fibers epoxied to form a two-dimensional array (Fig. 1). A completed connector may consist of up to 144 optical fibers positioned by up to 13 alignment chips. Each fiber in the array must be positioned accurately to its counterpart in a mating array to obtain low splice loss. The transverse misalignment of the mating fibers should be no greater than one-tenth the core radius or typically 2.5 micrometers.^{2,3} This can only be obtained with alignment chips having high dimensional accuracy with respect to thickness, groove geometry, and position.

The feasibility of the multifiber splice was shown with alignment chips manufactured of aluminum. The aluminum chip, however, could not be manufactured repeatedly with the high dimensional accuracies required. An improved chip was developed, that met the above goals, using (100) oriented silicon⁴ and photolithographic techniques. This improved chip has demonstrated a significant reduction in the overall array splice loss.

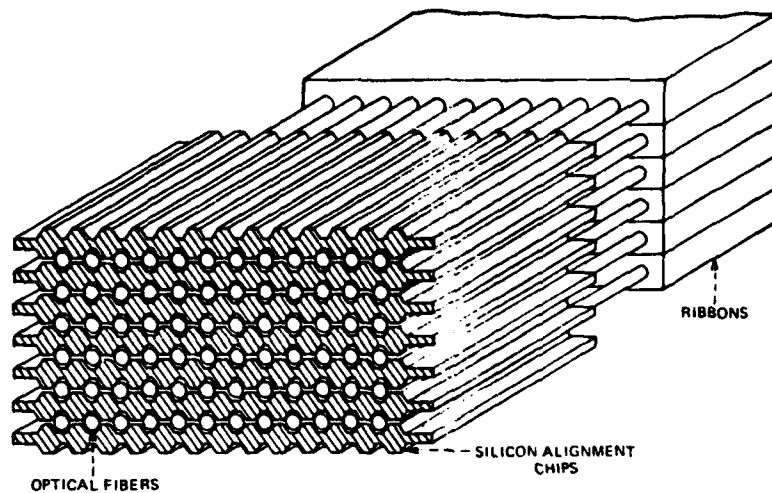


Fig. 1—Schematic of a multifiber array connector.

II. PHOTOLITHOGRAPHIC AND PROCESSING TECHNIQUES

The use of silicon for alignment chips offers several advantages. The material is readily available, it can be handled and processed relatively easily, and it can produce precise V grooves to photomask accuracy.

When a (100) surface slice of silicon covered by an oxide mask is submerged in a basic solution, the etch rate is much greater in the (100) direction than in the (111) direction (Fig. 2). This anisotropic etching of the silicon results in a precise V groove to an angle of 70.53° with the reaction self-stopping at the point where the (111) planes intersect. The groove opening is determined by the opening in the oxide mask. The (110) plane is used as a reference to align the photomask features parallel to the intersection of the (100), (111) planes.

The processing of the silicon first starts with the selection of a 5 cm diameter (100) surface oriented wafer polished on both surfaces to a thickness of 0.25 mm. Thickness variations and surface defects should

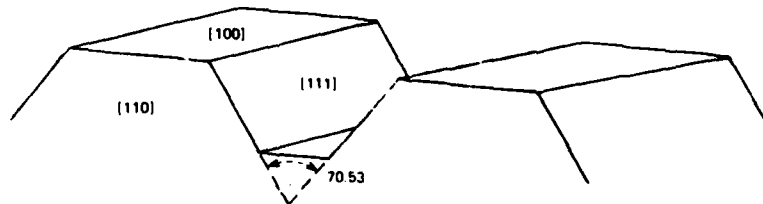


Fig. 2—Crystallographic planes used to manufacture alignment chips.

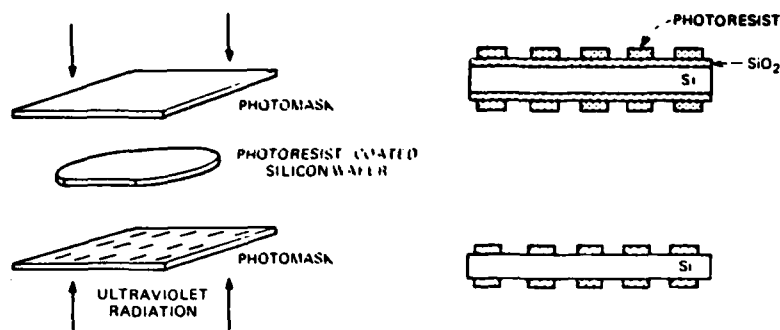


Fig. 3—Processing techniques.

be minimized for best results. The wafer is cleaned, then placed into a tube furnace for a 1-micrometer oxide growth. The wafer is then coated on both surfaces with a positive photoresist, placed between two prealigned photomasks and exposed to ultraviolet radiation (Fig. 3). The exposed wafer is removed, then developed leaving open windows of silicon oxide which are in turn etched in a buffered hydrofluoric acid solution. The remaining photoresist is removed leaving a silicon wafer covered by an oxide mask which is then placed into a potassium hydroxide solution for preferential etching⁵. A cross section of a typical silicon alignment chip is shown in Fig. 4.

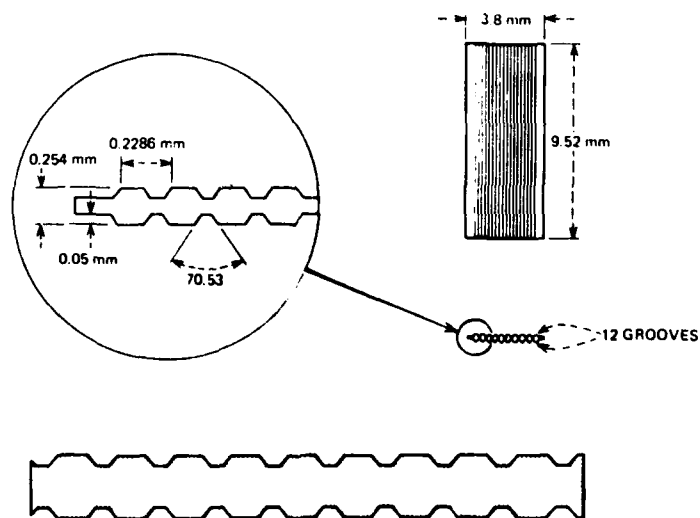


Fig. 4—Cross section of typical alignment chip with dimensions.

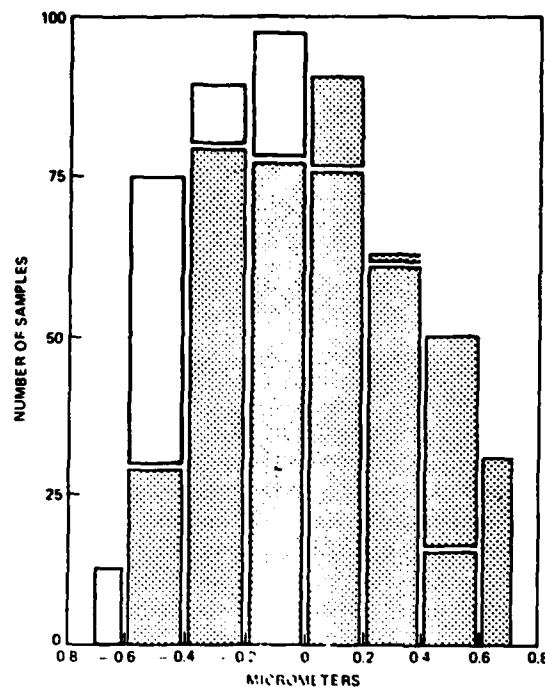


Fig. 5—Data on groove opening variations.

III. ALIGNMENT CHIP EVALUATION

A listing of variations that can cause splice loss in a multifiber connector in their present order of importance is as follows:

- (i) Alignment chip thickness variations
- (ii) Fiber diameter variations
- (iii) Groove opening variations
- (iv) Transverse misalignment of the top and bottom grooves
- (v) Aperiodic grooves

Excluding fiber diameter variations, the remaining list must be controlled by alignment chip accuracy.

Measurements on the photomask features and the chip profile were made with the use of a Hewlett Packard model 5526A laser interferometer. The object whose features are to be measured is placed onto a traversing stage under the cross hair of a microscope. A reflecting cube attached to the stage monitors the movement of one of the two paths of the interferometer. This movement is compared to a fixed length of the second path with the changes displayed on a monitor. The repeatability

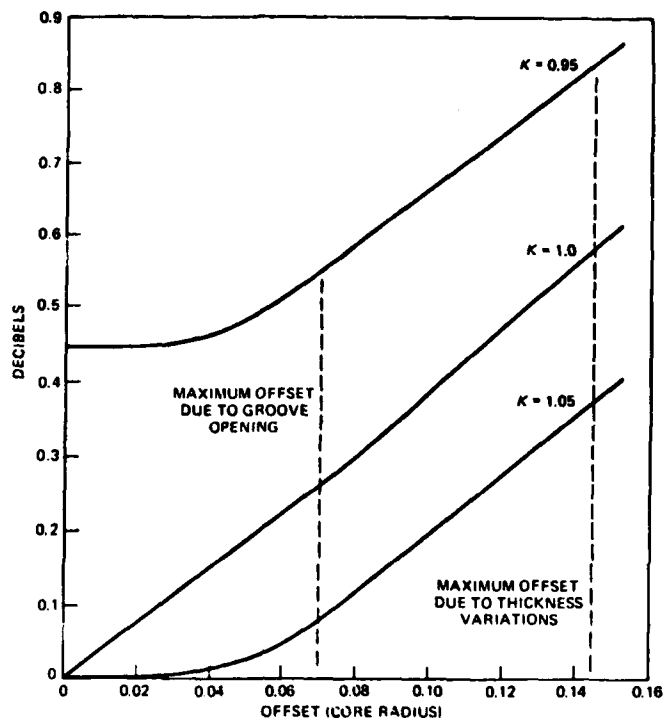


Fig. 6—Splice loss as a function of offset.

of the data was found to be 0.2 micrometer, limited chiefly by the vernier acuity of the eye.

Measurements on the photomask features indicate the required dimensions were well within the 1 micrometer stated accuracy for the masks with line-width variations not measurable across the mask face. Profile measurements on an etched silicon wafer indicate the groove periodicity of 228.6 micrometers was maintained within the measurement error. The transverse misalignment of the top and bottom grooves was held to 1 micrometer or less and the groove depth maintained at 50 micrometers. Variations of this type do not significantly add to the overall splice loss. The major contributors to array splice loss other than fiber diameter variations, was found to be chip thickness variations and groove opening variations.

The groove opening directly affects the vertical position of the optical fiber. The groove angle is constant but relatively steep with 1 unit of groove opening corresponding to 1.4 units of vertical drop in the optical fiber. The data on groove opening variations are shown in Fig. 5. These

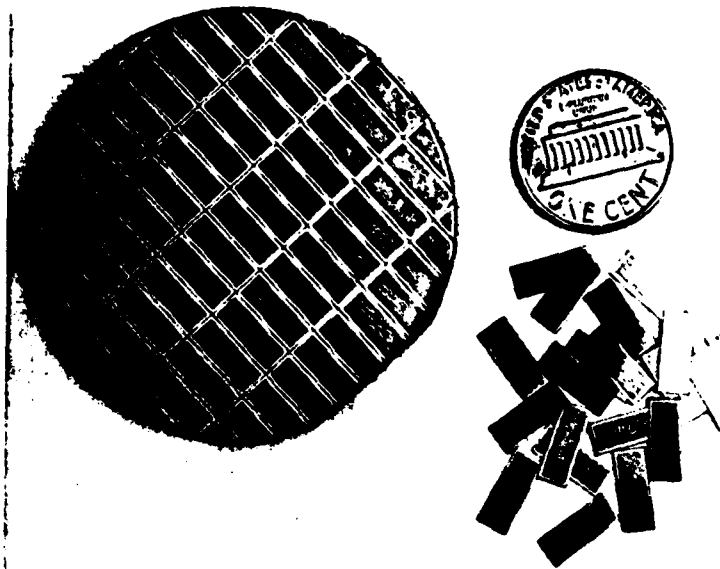


Fig. 7—Laser-scribed silicon wafer.

data were taken on both surfaces of one silicon wafer with the cross-hatched region being data from surface 1 superimposed onto data from surface 2. An overall shift in data of 0.2 micrometers can be observed when comparing the two surfaces. This shift was caused primarily by unequal exposure times. Maximum groove width variations were found to be ± 0.7 micrometers with a standard deviation of 0.23 micrometers. The maximum difference in groove width of 1.4 micrometers would cause vertical positioning errors of the optical fibers of 1.96 micrometers for a worst-case situation. While this deviation does not exceed the 0.1 core radius offset, it does point to a need to minimize groove width variations, which are probably caused by variations in wafer thickness with Fresnel diffraction playing a part in undercutting at the areas where the wafer and photomask did not contact. Thickness variations are at present the largest potential contributor to splice loss with total variations of 4 micrometers encountered on some wafers.

IV. LOSS DUE TO TRANSVERSE OFFSETS

Splice loss as a function of offset for small offsets of parabolic index fibers is shown in Fig. 6.³ K is the ratio of the radius of the receiving fiber to the radius of the transmitting fiber. The maximum offsets due to groove opening and thickness variations are displayed to indicate the

probable loss that could be expected in the worst-case situation. To avoid variations of this type an individual chip selection is required at present.

Splice loss data for 144-fiber array connectors using silicon alignment chips have been made with the results presented in a companion report by C. M. Miller.

V. SUMMARY AND CONCLUSION

A laser scribed silicon wafer is shown in Fig. 7. Each 5-cm diameter wafer yields 36 usable alignment chips 3.8×9.52 mm in size.

Assembled silicon array connectors have been fabricated with low splice loss. The silicon chips can be manufactured with submicrometer repeatability and accuracy. Improvements in chip thickness variations are anticipated which in turn should reduce the overall groove opening variations to a point where individual chip selection would not be required.

REFERENCES

1. C. M. Miller, "A Fiber-Optic Cable Connector," B.S.T.J., 54, No. 9 (November 1975), pp. 1547-1555.
2. D. L. Bisbee, "Measurements of Loss to Offsets," B.S.T.J., 50, No. 10 (December 1971), pp. 3159-3168.
3. C. M. Miller, "Loss vs. Transverse Offset for Parabolic Fiber Splices," B.S.T.J., 55, No. 7 (September 1976), pp. 917-927.
4. L. P. Boivin, "Thin-Film Laser-to-Fiber Coupler," Appl. Opt., 13, No. 2 (February 1974), pp. 391-395.
5. R. C. Kragness et al., "Etchant for Precision Etching of Semiconductors," Patent No. 3,506,509.

OPTICAL-FIBER CONNECTOR 97